MINISTRY OF EDUCATION

THE ANNALS OF "DUNAREA DE JOS" UNIVERSITY OF GALATI

Fascicle IX
METALLURGY AND MATERIALS SCIENCE

YEAR XLI (XLVI)
December 2023, no. 4

ISSN 2668-4748; e-ISSN 2668-4756

2023
GALATI UNIVERSITY PRESS

EDITORIAL BOARD

EDITOR-IN-CHIEF

Assist. Prof. Marius BODOR – "Dunarea de Jos" University of Galati, Romania

SCIENTIFIC ADVISORY COMMITTEE

Assist. Prof. Dragos-Cristian ACHITEI – "Gheorghe Asachi" Technical University Iasi, Romania
Assoc. Prof. Stefan BALTA – "Dunarea de Jos" University of Galati, Romania
Assist. Prof. Chenna Rao BORRA – Indian Institute of Technology, Republic of India
Prof. Acad. Ion BOSTAN – Technical University of Moldova, the Republic of Moldova
Researcher Mihai BOTAN – The National Institute of Aerospace Research, Romania
Prof. Vasile BRATU – Valahia University of Targoviste, Romania
Prof. Francisco Manuel BRAZ FERNANDES – New University of Lisbon Caparica, Portugal
Prof. Bart Van der BRUGGEN – Katholieke Universiteit Leuven, Belgium
Prof. Acad. Valeriu CANTSER – Academy of the Republic of Moldova
Prof. Valeriu DULGHERU – Technical University of Moldova, the Republic of Moldova
Prof. Gheorghe GURAU – "Dunarea de Jos" University of Galati, Romania
Assist. Prof. Gina Genoveva ISTRATE – "Dunarea de Jos" University of Galati, Romania
Assist. Prof. Nora JULLOK – Universiti Malaysia Perlis, Malaysia
Prof. Rodrigo MARTINS – NOVA University of Lisbon, Portugal
Prof. Strul MOISA – Ben Gurion University of the Negev, Israel
Assist. Prof. Priyanka MONDAL – CSIR-Central Glass and Ceramic Research Institute, India
Prof. Daniel MUNTEANU – "Transilvania" University of Brasov, Romania
Assoc. Prof. Alina MURESAN – "Dunarea de Jos" University of Galati, Romania
Prof. Maria NICOLAE – Politehnica University Bucuresti, Romania
Assist. Prof. Manuela-Cristina PERJU – "Gheorghe Asachi" Technical University Iasi, Romania
Prof. Cristian PREDESCU – Politehnica University of Bucuresti, Romania
Prof. Iulian RIPOSAN – Politehnica University of Bucuresti, Romania
Prof. Antonio de SAJA – University of Valladolid, Spain
Assist. Prof. Rafael M. SANTOS – University of Guelph, Canada
Prof. Ion SANDU – "Al. I. Cuza" University of Iasi, Romania
Prof. Mircea Horia TIEREAN – "Transilvania" University of Brasov, Romania
Prof. Ioan VIDA-SIMITI – Technical University of Cluj Napoca, Romania
Assoc. Prof. Petrica VIZUREANU – "Gheorghe Asachi" Technical University Iasi, Romania

EDITING SECRETARY

Assist. Prof. Marius BODOR – "Dunarea de Jos" University of Galati, Romania
Assist. Nicoleta BOGATU – "Dunarea de Jos" University of Galati, Romania
Assist. Prof. Eliza DANAILA – "Dunarea de Jos" University of Galati, Romania
Assist. Prof. Florin Bogdan MARIN – "Dunarea de Jos" University of Galati, Romania
Assist. Prof. Mihaela MARIN – "Dunarea de Jos" University of Galati, Romania

THE ANNALS OF "DUNAREA DE JOS" UNIVERSITY OF GALATI
FASCICLE IX. METALLURGY AND MATERIALS SCIENCE
Nº. 4 - 2023, ISSN 2668-4748; e-ISSN 2668-4756
Volume DOI: https://doi.org/10.35219/mms.2023.4

Table of Contents

THE ANNALS OF "DUNAREA DE JOS" UNIVERSITY OF GALATI
FASCICLE IX. METALLURGY AND MATERIALS SCIENCE
Nº. 4 - 2023, ISSN 2668-4748; e-ISSN 2668-4756
Volume DOI: https://doi.org/10.35219/mms.2023.4

THE ANNALS OF "DUNAREA DE JOS" UNIVERSITY OF GALATI
FASCICLE IX. METALLURGY AND MATERIALS SCIENCE
No. 4 - 2023, ISSN 2668-4748; e-ISSN 2668-4756
Article DOI: https://doi.org/10.35219/mms.2023.4.01

STUDIES AND RESEARCH REGARDING THE CREATION OF A DENTAL MODEL, THROUGH RAPID PROTOTYPING TECHNOLOGIES

Beatrice TUDOR, Claudiu GRIGORAS
"Dunarea de Jos" University of Galati, Romania
e-mail: beatrice.tudor@ugal.ro

ABSTRACT

The paper presents the creation of a dental bridge through two rapid prototyping technologies, SLA and FDM. The dental bridge model was made in a dental laboratory, being used later for 3D printing, through rapid prototyping, using the two technologies, FDM and SLA.

KEYWORDS: rapid prototyping, dental model, ceramic masses

1. Introduction

Rapid prototyping technologies can be used in: biomedicine and nanotechnology, supporting and developing the contribution of regenerative medicine. Engineering and medicine come together to improve the patients' life or even save their life.

Engineering has evolved a lot, through the application of top technologies, which help to easily create parts with increasingly complex geometries. In recent years, 3D printing technology has more and more applications in the medical field and is continuously developing. The 3D models made are widely used for various complex pathological studies, as well as in education.

Thanks to the advances in biomaterials used in 3D printing, and the research carried out, the range of applications of 3D printing has increased, in the manufacture of implants, prostheses, 3D scaffolds in tissue engineering, and regenerative medicine [1, 2].

2. Generalities, regarding the creation of models through rapid prototyping

The creation of the models includes the stage of creating the model with the help of a CAD software. In rapid prototyping technology, the STL format has been adopted. A three-dimensional scanner can also be used to digitize the object, but this method implies the existence of a previously created model.

Intraoral rapid scanning is used in the dental field. This procedure aims to produce images (3000 images/second). The configuration of the patient's teeth and jaw is rendered in 3D with very high accuracy.

The next stage is the modification of the CAD folder in STL format, which illustrates a three-dimensional surface of flat triangles. This file contains the coordinates of the vertices and the direction of the outward-facing normal of all triangles. Because STL files use planar elements, they will not accurately depict curved surfaces. By increasing the number of triangles, the accuracy improves significantly, but this increase in the number of triangles has the disadvantage of increasing the file size (Fig. 1).

For the next stage, a processing software is used, which is specialized, and which supports the construction of the STL (Standard Triangle Language) file in layers. Few programs exist, and most allow the user to modify the size, location, and orientation of the model.

Before processing, the software cuts the STL model after a certain number of layers of different thickness. The respective software can also generate an auxiliary structure, as a support for the piece, during manufacturing.

Next is the construction of the part itself, using a rapid prototyping technology.

The last stage is represented by the final processing (post processing). This includes removing the part from the prototyping machine, and removing the support brackets. Parts made of photosensitive materials must be treated before use [3, 4].

In the dental field, dental restoration materials have acquired a superior quality, being an increasingly used alternative in dental laboratories. Computer-aided design in the dental field is used for restorations or aesthetic work of dental models (Fig. 2).

THE ANNALS OF "DUNAREA DE JOS" UNIVERSITY OF GALATI
FASCICLE IX. METALLURGY AND MATERIALS SCIENCE
No. 4 - 2023, ISSN 2668-4748; e-ISSN 2668-4756
Article DOI: https://doi.org/10.35219/mms.2023.4.01

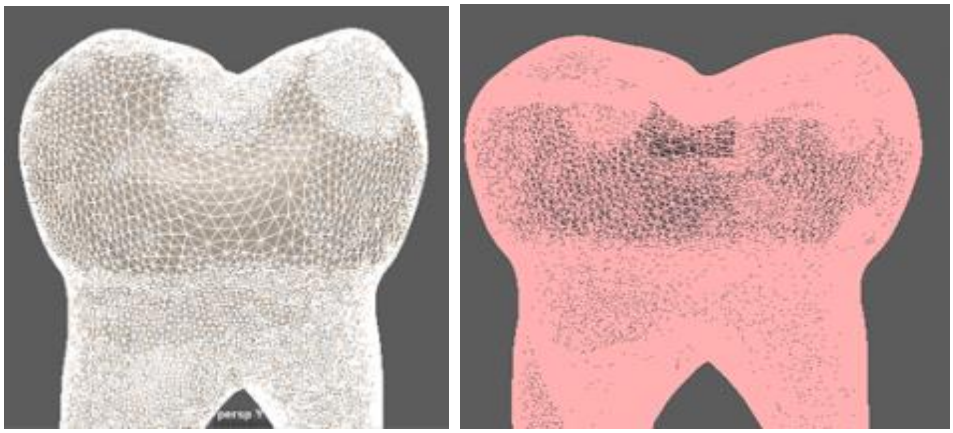

Fig. 1. *Different resolution files: left - fine resolution dental model; right - dental model with custom resolution*

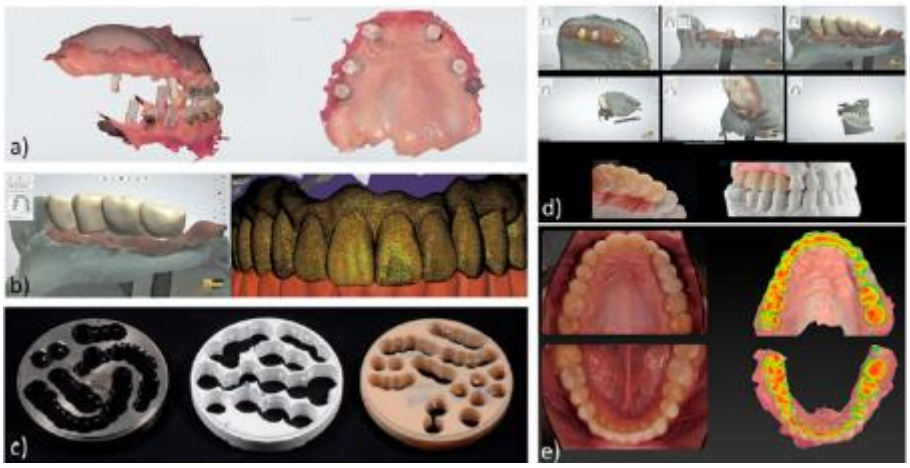

Fig. 2. *Representation of the steps of temporary restoration of dental models, made with the help of computer-aided design. a - 3D scan; b - dental prosthesis design; c - materials used (alloy, zirconium, polymer); d - design and final result of dental replicas; e - brief analysis*

3. Obtaining the dental bridge in a dental laboratory

Before making the dental bridge through the prototyping methods, we made the model in a dental laboratory.

The dental models were made in the dental technique laboratory, going through the following stages:

- the impression and the dental wax prosthesis are made by the dentist;
- the final impression renders with maximum precision, both the support area and the suction area. With the help of this final impression, the final model was obtained;
- the formwork follows, which consists of applying a strip of wax around the impression, then follows the preparation of the plaster paste;
- pouring the gypsum paste, and shaping the plinth;
- a pink wax base is made, (Fig. 3) and on this pink wax base, the acrylic teeth will be fixed;
- making the metal-ceramic dental bridge;
- casting and processing of the metal frame (Fig. 4);
- application of ceramic masses and glazing;

THE ANNALS OF "DUNAREA DE JOS" UNIVERSITY OF GALATI
FASCICLE IX. METALLURGY AND MATERIALS SCIENCE
No. 4 - 2023, ISSN 2668-4748; e-ISSN 2668-4756
Article DOI: https://doi.org/10.35219/mms.2023.4.01

Fig. 3. *Dental prosthesis made of dental wax*

Fig. 4. *Dental bridge with metal structure*

Fig. 5. *Dental bridge*

4. Making the dental bridge using FDM and SLA technologies

The dental model made in the dental laboratory was later used to make the dental bridge through prototyping.

The first stage in the creation of the dental bridge, through the FDM prototyping method, was represented by the execution of the part model, with the help of a software. Autodesk Maya (Maya) software was used. With the help of this software, it is possible to create numerous pieces from many fields such as medical, design, architecture, etc. The

THE ANNALS OF "DUNAREA DE JOS" UNIVERSITY OF GALATI
FASCICLE IX. METALLURGY AND MATERIALS SCIENCE
No. 4 - 2023, ISSN 2668-4748; e-ISSN 2668-4756
Article DOI: https://doi.org/10.35219/mms.2023.4.01

Autodesk Maya software has many uses such as, for example, making various 3D parts, animations, simulations, having numerous tools and functions. This 3D modeling software is one of the most popular, due to its performance, being chosen by many designers (Fig. 6).

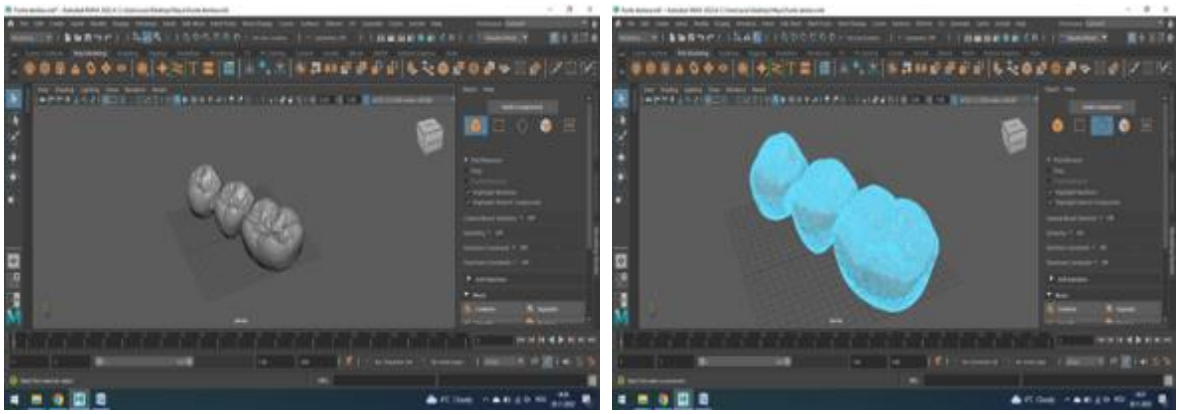

Fig. 6. *Creation of the 3D model of the dental bridge, made with the help of Autodesk Maya software*

After the model of the part was made, the next step was to modify the model in STL format [5].

After converting to STL format, the next step was to divide the model into thin transverse layers. To achieve this stage, another software was added, namely the PrusaSlicer software, to transform it into G-code. The transition from the STL format to the G-code, was made, because the printer used, does not recognize the STL format (Fig. 7).

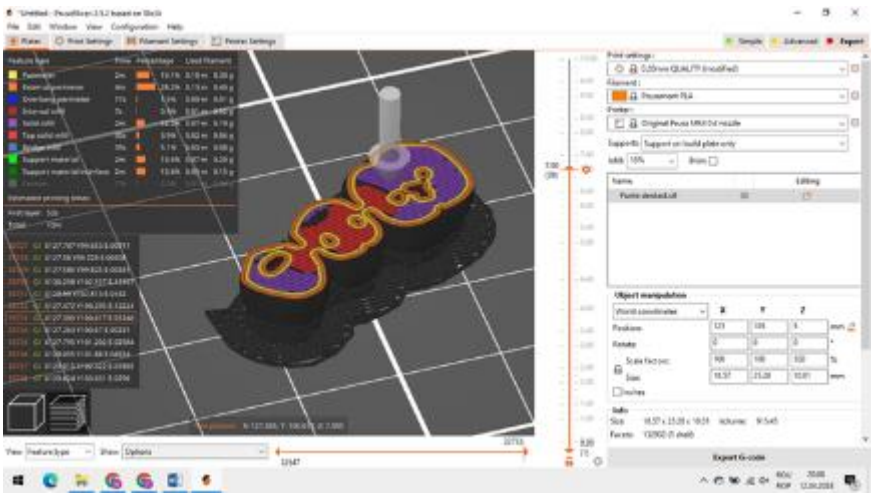

Fig. 7. *Representation of the dental model in layers, using the PrusaSlicer software*

The PrusaSlicer software, in addition to the role of "slicing" the 3D model in layers, also offers us the simulation of the 3D part, that is, the software shows me how it will be printed line by line, from bottom to top, layer by layer. The software also shows where the extrusion of the material will take place, the movements required for the table of the machine, and the extrusion head, and at what speeds they should move relative to each other [6].

The material used is PLA type plastic, and the temperature of making the model is 60 °C. After the 3D printing, the post-processing operation follows, representing the removal of impurities and the finishing of the part (Fig. 8).

The same dental bridge model was also made by SLA (stereolithography) technology. The material used for this technology is photopolymer resin. It was used the CHITUBOX software, as shown in Fig. 9.

The CHITUBOX software "slices" the 3D model into layers, but at the same time, shows how they will be printed, from bottom to top, layer by layer.

After creating the 3D model in the computer, and making the necessary adjustments, the speed and thickness of the layer, the actual printing followed.

THE ANNALS OF "DUNAREA DE JOS" UNIVERSITY OF GALATI
FASCICLE IX. METALLURGY AND MATERIALS SCIENCE
No. 4 - 2023, ISSN 2668-4748; e-ISSN 2668-4756
Article DOI: https://doi.org/10.35219/mms.2023.4.01

Fig. 8. *The final dental bridge model, made of PLA using FDM technology*

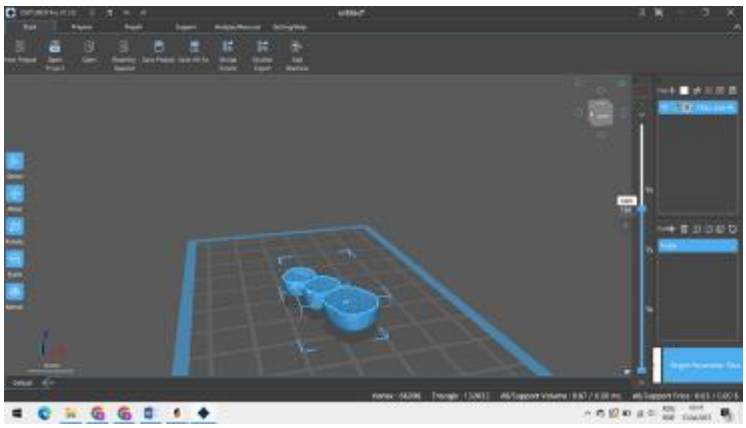

Fig. 9. *Representation of the dental model in layers, using the CHITUBOX software*

Fig. 10. *The final dental bridge model, made of photopolymer resin, using SLA technology*

5. Conclusions

The two models, made by FDM and SLA technologies, were compared, and we reached the following conclusions:

- the piece made with SLA technology has a high level of detail compared to the dental model made with FDM technology;

- the manufacturing time, for the dental bridge made with the help of SLA technology, was about 2 hours, and with FDM technology about 15 minutes;

- the dental model made with FDM technology is much more resistant than the SLA model;

- from the point of view of the resistance of the model, and the time for its realization, the study recommends the use of FDM technology for the creation of the dental bridge;

- the costs of making the dental bridge, through FDM technology, are lower, which recommends the use of this technology.

References

[1]. Cernica D., Márton E., Mester A., Chițu M., Benedek I., *Tehnica imprimării 3D în imagistică și aplicațiile medicale*, 2021.

[2]. Florea Gh., Chiriac Al., Marginean I., *Procedee performante de depunere în formă*, 1st ed. Galați: Editura Europlus, 2008.

[3]. Tsoulfas G., Bangeas P. I., Suri J. S., *3D printing: applications in medicine and surgery*, vol. 1.

[4]. Strub J. R., Rekow E. D., Witkowski S., Strub J. R., Rekow E. D., Witkowski S., *Computer aided design and fabrication of dental restorations: current systems and future possibilities*, J Am Dent Assoc, 137:1289-96, vol. 137, 2006.

[5]. Hesse H., Özcan M., *A review on current additive manufacturing technologies and materials used for fabrication of metal-ceramic fixed dental prosthesis*, J. Adhes. Sci. Technol., vol. 35, no. 23, p. 2529-2546, doi: 10.1080/01694243.2021.1899699, 2021.

[6]. Budak I., Kosec B., Sokovic M., *Application of contemporary engineering techniques and technologies in the field of dental prosthetics Analysis and modelling*, J. Achiev. Mater. Manuf. Eng., vol. 54, no. 2, p. 233-241, 2012.

THE ANNALS OF "DUNAREA DE JOS" UNIVERSITY OF GALATI
FASCICLE IX. METALLURGY AND MATERIALS SCIENCE
No. 4 - 2023, ISSN 2668-4748; e-ISSN 2668-4756
Article DOI: https://doi.org/10.35219/mms.2023.4.02

MATHEMATICAL MODELING OF THERMAL PROCESSING FOR AN AL-SI ALLOY

Marian-Iulian NEACȘU
"Dunarea de Jos" University of Galati, Romania
e-mail: marian.neacsu@ugal.ro

ABSTRACT

This paper presents the realization of a mathematical model of a heat treatment process of an Al-Si alloy, with the help of which the values of some mechanical properties are preached. The method of elaborating the mathematical model is a statistical method, namely the method of the active experiment.

With the help of the MATLAB software and based on the elaborated mathematical model, we created a graphic interface that allows the prediction of the values of three mechanical properties depending on the thermal processing conditions of the studied alloy.

KEYWORDS: aluminum alloy, thermal treatment, mathematical modeling, prediction of property values, graphic interface

1. Introduction

Non-ferrous alloys are a category of metal materials with special applications in the machine building industry and beyond, and aluminum and its alloys occupy an extremely important position in this category due to the wide range of potential applications [1, 2].

Aluminum alloys are used in the aerospace, chemical, electrical and electronic industries, consumer goods, automation and computer industry [3].

Although aluminum is the most abundant metal in the earth's crust, it has only recently become widely used in industry, as it is difficult to develop. The wide scope of aluminum and its alloys in the construction of landmarks by plastic deformation, casting or cutting is due to its excellent physical, chemical and mechanical properties, low density, excellent corrosion resistance but also excellent electrical and thermal conductivity [4].

The mechanical properties of these alloys can reach high values by applying appropriate heat treatments. Alloys change the properties of aluminum in a very wide range. Even small amounts of alloying elements have a great effect. Among the most important alloying elements we mention: silicon, copper, magnesium, zinc, nickel, titanium, etc. These alloying elements may dissolve in solid solution (although in small quantities) or may form soluble or insoluble compounds. The soluble material is particularly important because its presence in the structure indicates the possibility of applying a final heat treatment to increase hardness, mechanical strength, corrosion resistance, etc. [5, 6].

Today at European and global level it is possible to produce cheap and high quality in regulated environmental conditions, which means to consume as little energy and fuel as possible, ensure optimal working and living conditions for employees and ensure safety. We must not forget that it is necessary to offer safe products.

Mathematical modeling of processes is a useful basic tool both in the design phase and in the analysis of the operation of installations. By using specialized programs, we can determine an optimal metallurgical process of combining process modeling with computer use. The development of the specific mathematical apparatus and, in particular, of statistical methods has allowed the optimal decision issue to be addressed as a high technical and economic efficiency issue [7].

The mathematical models that can be used are an important source of information necessary for the optimal management of metallurgical processes.

The preliminary experiment clarifies the variation of process factors by performing a series of determinations based on programs (dispersion analysis, correlation analysis, etc.) which allows the selection of factors that significantly influence and highlights the links between factors as well as their contribution to the process [8].

THE ANNALS OF "DUNAREA DE JOS" UNIVERSITY OF GALATI
FASCICLE IX. METALLURGY AND MATERIALS SCIENCE
No. 4 - 2023, ISSN 2668-4748; e-ISSN 2668-4756
Article DOI: https://doi.org/10.35219/mms.2023.4.02

2. Experimental conditions

In the paper, the mathematical model of the heat treatment process applied to an aluminum alloy was performed, by statistical methods, namely the regression analysis by active experiment [8].

Experimental data were obtained from the artificial aging heat treatment applied to an aluminum alloy whose composition is shown in Table 1.

Table 1. *Materials for experimentation*

Al 7Si 0.3Mg	Si	Mg	Al
%	7	0.3	rest

The modeling methods by programming the experiment are different because the metallurgical processes are varied and complex. The most effective methods of programming the experiment is currently those of solving extreme problems, which involve determining the levels of independent sizes (input), u_2, ...u_k, for which the objective function [9]:

$$y = f(u_1, u_2, ..., u_k) \quad (1)$$

has extreme values (maximum or minimum), as well as the calculation of these values.

The method of the experiment programmed as opposed to the classical method of experimentation, provides for the realization of a number of four experiences near an arbitrarily chosen S1 point, aiming at determining the response surface, on a small area around that point, finding a linear equation of the form [10]:

$$y = b_0 + b_1x_1 + b_2x_2 + b_{12}x_1x_2 \quad (2)$$

which is a first approximation of the real equation of the process. To find out the extreme value of the Y parameter are necessary in case of its dependence on two factors, of $2^2 = 4$ experiences, so in total 4 experiences.

Experiment programming involves:

- establishing the necessary and sufficient number of experiences and the conditions for their realization;
- determination by statistical methods of the regression equation, which represents with a certain degree of approximation, calculable, the process model;
- determining the conditions for achieving the optimal value of the process performance (the parameter to be optimized).

The use of the active experiment, as a method of mathematical modeling, uses statistical methods in all stages of experimental research:

- before the experiment, by establishing the number of experiences and the conditions for their realization;
- during the experiences by processing the obtained results;
- after concluding the experiment with conclusions regarding the realization of future experiences [9].

We considered as main influencing factors (independent variables) the following technological parameters of heat treatment:

1 - artificial aging temperature – t, [°C];

2 - maintenance time at artificial aging temperature - τ, [hours].

The set of physico-mechanical properties is considered as parameters: Rm, $Rp_{0,2}$, A_5.

To establish the basic level and range of variation of influencing factors we used data from the literature on the nature of solid transformations and behavior in heating and cooling for treatment thermal alloys with aluminum base.

Given the studies and experimental results obtained by some authors on alloys with high-strength aluminum base, we established the conditions of experimentation as follows:

- for aging temperature:
  - basic level: u_{01} = 204 °C;
  - variation range: Δu_1 = 56;
- for aging:
  - basic level: u_{02} = 15 hours;
  - variation range: Δu_2 = 10 hours.

The following notations and symbols were used for the coded representation of the experiment:

Independent variables:

- x_1 - temperature;
- x_2 - time.

Dependent variables (optimization parameters):

Y1 - breaking strength, Rm, [MPa];

Y2 - flow limit, Rp_{02}, [MPa];

Y3 - elongation at break, A_5, [%].

There are the following differences between natural and coded values of xi factors [18]:

$$x_1 = \frac{t-t_0}{\Delta_t}; \qquad x_2 = \frac{\tau-\tau_0}{\Delta_\tau} \quad (3)$$

Yi values are expressed in natural units.

As the influence of the two factors on the performance of the process (Y) is studied, the 4 experiments according to the experimental matrix in Table 2 were performed.

Next, based on the matrix of the complete factorial experiment, the coefficients of the regression equation (the mathematical model) are calculated. Considering the Yi function as the analytical expression of the first order model, it is in the form [9]:

THE ANNALS OF "DUNAREA DE JOS" UNIVERSITY OF GALATI
FASCICLE IX. METALLURGY AND MATERIALS SCIENCE
No. 4 - 2023, ISSN 2668-4748; e-ISSN 2668-4756
Article DOI: https://doi.org/10.35219/mms.2023.4.02

$$Y_i = c_0 + \sum_{i=1}^{2} c_i \cdot x_i + \sum_{\substack{j=1 \\ i \neq j}}^{2} c_{ij}\, x_i x_j \quad (4)$$

Table 2. *Experimental matrix*

Nr. exp.	x_0	x_1	x_2	x_{12}	y_1	y_2	y_3
1	1	1	1	1	140	83	23
2	1	-1	1	-1	323	245	9.3
3	1	1	-1	-1	175	100	8
4	1	-1	-1	1	300	215	10

Following the ephaguation of the specific calculations, the values of the coefficients for the 3 equations that are presented in Table 3 resulted.

Table 3. *The values of the coefficients of the first order models*

b_i \ y_i	y_1	y_2	y_3
b_0	234.5	160.75	12.5
b_1	-77	-69.25	2.9
b_2	-3	3.25	3.5
b_{12}	-14.5	-11.75	3.9

Therefore, the equation of the mathematical model of order I (4), expressed in coded quantities, for each property, has the form:

$$y_1 = 234.5 - 77x_1 - 3x_2 - 14.5x_1x_2 \quad (5)$$

$$y_2 = 160.75 - 69.25x_1 + 3.25x_2 - 11.75x_1x_2 \quad (6)$$

$$y_3 = 12.5 + 2.9x_1 + 3.5x_2 + 3.9x_1x_2 \quad (7)$$

By replacing the x_i variables with the (3) relationships in the equations (5-7) (the final form of the mathematical model is obtained, expressed in natural quantities (treatment temperature and heat treatment time) for the three properties studied:

$$y_1 = 439.94 - 0.985 \cdot T + 5.004 \cdot \tau - 0.026 \cdot T \cdot \tau \quad (8)$$

$$y_2 = 350.42 - 0.93 \cdot T + 4.4 \cdot \tau - 0.02 \cdot T \cdot \tau \quad (9)$$

$$y_3 = 20.14 - 0.04 \cdot T - 1.18 \cdot \tau + 0.006 \cdot T \cdot \tau \quad (10)$$

With the help of the MATLAB program package and using the results of experimental research we have created a graphical interface that allows the simulation of the values of some mechanical properties for the alloy subjected to the thermal treatment of artificial aging.

For this simulation using MATLAB, the equations of the mathematical model were also used, the equations (8-10).

Through these simulations you can find the value of each property and the conditions (the value of the heat treatment parameters) thermal processing that lead to obtaining those values for each property.

Figure 1 shows under what conditions of temperature and time the value of 236 MPa is obtained for Rm.

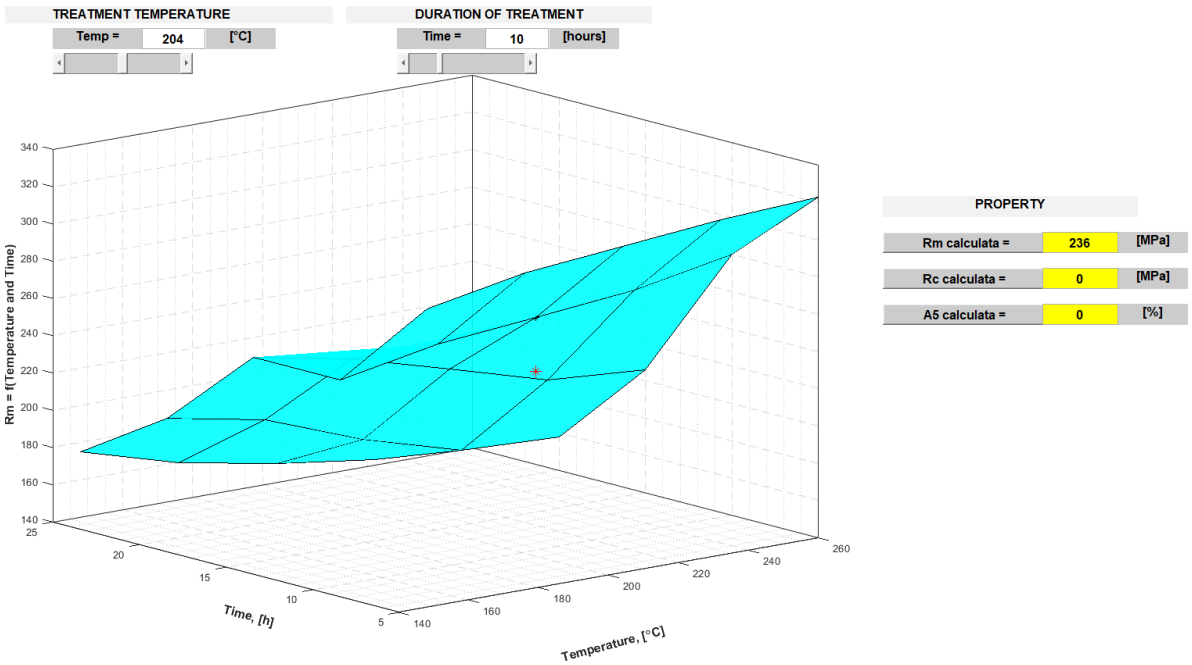

Fig. 1. *Simulation of Rm [MPa] when the artificial aging temperature is 204 °C and the thermal processing time is 10 hours*

THE ANNALS OF "DUNAREA DE JOS" UNIVERSITY OF GALATI
FASCICLE IX. METALLURGY AND MATERIALS SCIENCE
No. 4 - 2023, ISSN 2668-4748; e-ISSN 2668-4756
Article DOI: https://doi.org/10.35219/mms.2023.4.02

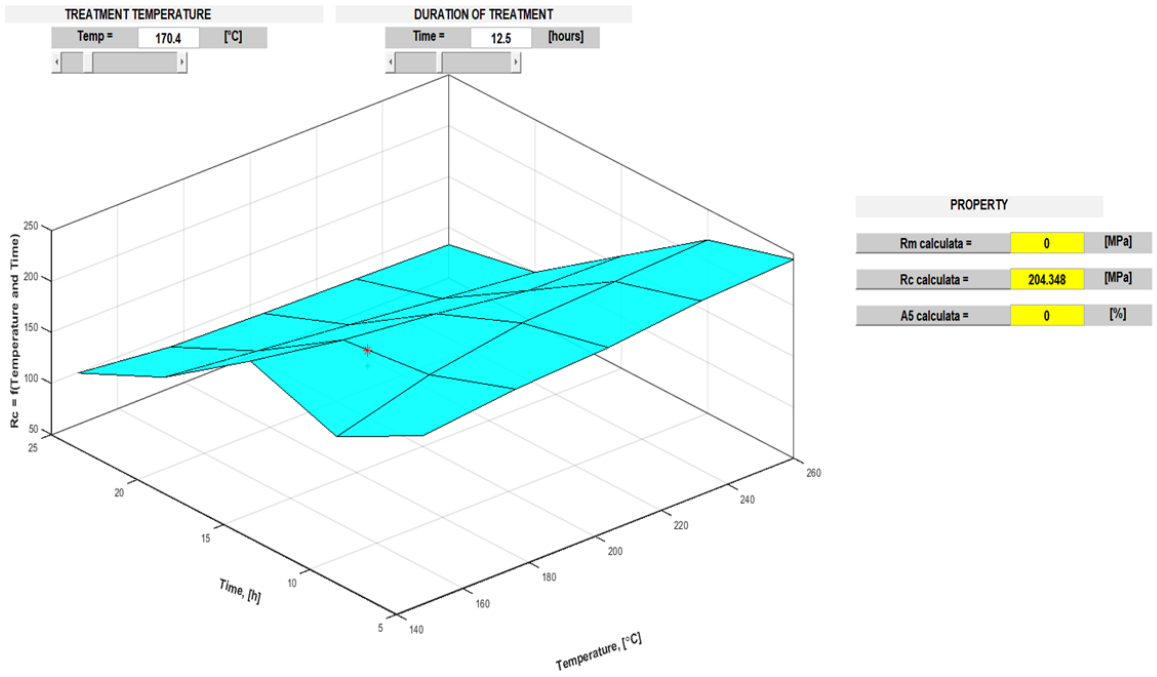

Fig. 2. *$Rp_{0.2}$ finding simulation [MPa] when the temperature is 170.4 °C and the time is 12.5 hours*

Figure 2 shows the simulation to obtain the value of 204.3 MPa for the flow limit as well as under what treatment conditions this value is obtained.

Figure 3 illustrates under what conditions of temperature and artificial aging time is obtained for elongation at break of 10.96 %.

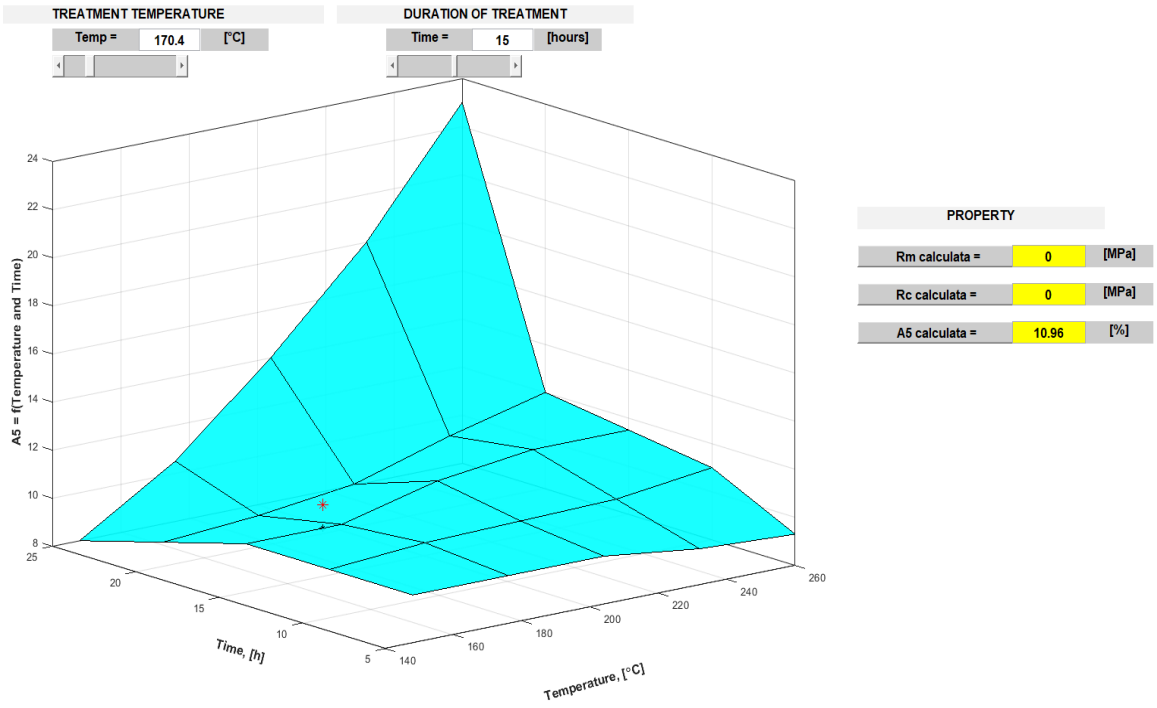

Fig. 3. *Simulation of A5 [%] when the artificial aging temperature is 170.4 °C and the artificial aging time is 15 hours*

THE ANNALS OF "DUNAREA DE JOS" UNIVERSITY OF GALATI
FASCICLE IX. METALLURGY AND MATERIALS SCIENCE
No. 4 - 2023, ISSN 2668-4748; e-ISSN 2668-4756
Article DOI: https://doi.org/10.35219/mms.2023.4.02

3. Conclusions

Following the elaboration of the mathematical model and the realization of the graphical interface with the help of the MATLAB in this paper, the following conclusions can be drawn:

• mathematical modeling of processes is a basic tool useful both in the design phase and in the analysis of the operation of installations.

• the values calculated for the optimized parameter Yi (i = 1... 3) are very close to the measured values, therefore the mathematical model performed allows the simulation of the heat treatment process, by varying the values of the technological parameters, within the experienced limits;

• the elaborated mathematical model allows the calculation simulation to find out the values of the studied mechanical properties;

• the graphical interface made with the help of MATLAB is based on the mathematical model made, for the prediction of the property values according to the two technological parameters of heat treatment, temperature and artificial aging time;

• the mathematical model presented, allows the calculation of optimizing the parameters of the heat treatment process, so as to obtain the optimal complex of the resistance and plasticity properties, with minimal costs.

References

[1]. Azarniya A., Taheri A. K., Taheri K. K., *Recent advances in ageing of 7xxx series aluminum alloys: A physical metallurgy perspective*, J. Alloy. Compd., 781, p. 945-983, 2019.

[2]. Rometsch P. A., Zhang Y., Knight S., *Heat treatment of 7xxx series aluminium alloys—Some recent developments*, T. Nonferr. Metal. Soc., 24 (7), p. 2003-2017, 2014.

[3]. Zhou B., Liu B., Zhang S., *The Advancement of 7XXX Series Aluminum Alloys for Aircraft Structures: A Review*, Metals., 11 (5), p. 718, 2021.

[4]. Dursun T., Soutis C., *Recent developments in advanced aircraft aluminium alloys*, Mater. Des., 56, p. 862-871, 2014.

[5]. Ranjan Kumar, Manjaiah M, Davidson M. J., *The effect of friction stir welding on the microstructure and mechanical properties of the dissimilar SS304 and Al7075-T6 alloy joints*, Welding International, vol. 37, issue 9, 2023.

[6]. Agus Sasmito, Mochammad Noer Ilman, Priyo Tri Iswanto, *Effects of rotational speed on the mechanical properties and performance of AA6061-T6 aluminium alloy in similar rotary friction welding*, Welding International, vol. 37, issue 9, 2023.

[7]. Ciucă I., Dumitriu S., *Modelarea şi Optimizarea Proceselor Metalurgice de Deformare Plastică şi Tratamente Termice*, Editura Didactică şi Pedagogică, Bucureşti, 1998.

[8]. Popescu D., Ionescu F., Dobrescu R., Ştefanoiu D., *Modelare în ingineria proceselor industriale*, Editura AGIR, Bucuresti, 2011.

[9]. Taloi D., *et al.*, *Optimizarea proceselor metalurgice*, Editura Didactică şi Pedagogică, Bucureşti, 1983.

[10]. Taloi D., *Optimizarea proceselor tehnologice – aplicaţii în metalurgie*, Editura Academiei, Bucureşti, 1987.

THE ANNALS OF "DUNAREA DE JOS" UNIVERSITY OF GALATI
FASCICLE IX. METALLURGY AND MATERIALS SCIENCE
No. 4 - 2023, ISSN 2668-4748; e-ISSN 2668-4756
Article DOI: https://doi.org/10.35219/mms.2023.4.03

COMPARATIVE STUDY OF SOME MATERIALS USED IN NAIL PLATE PROSTHESIS

Rodica MUȘALĂ, Vasile BRIA, Elena Emanuela HERBEI, Daniela-Laura BURUIANĂ, Viorica GHISMAN, Marius BODOR*
"Dunarea de Jos" University of Galati, Romania
*e-mail: marius.bodor@ugal.ro

ABSTRACT

Nails are involved in most everyday activities, whether physically for seemingly simple actions such, protection against external factors or roles with an aesthetic implication, for the integration of people into society. Often, any change at an aesthetic level is felt both from the point of view of the patient, who can be affected at a psychological level, feeling anxiety due to the lack of a part considered essential, and from the point of view of society that imposes a certain standard to be accepted in the community. Because of this societal standard, people with an untreatable nail deformity or disease can feel marginalized and excluded. Recently, an important number of studies have been carried out in this field, especially since the uses of polymeric materials have gained a wide field of applicability.

In this work, the comparison between three types of polymeric materials used in salon work was highlighted, for the aesthetic treatment of some diseases with a long healing time or even untreatable, by making prostheses for the affected nail plates of onycholysis. The mentioned materials were analysed microscopically, tested for roughness and hardness, and tested for compression and bending resistance, in order to understand how a nail prosthesis made of these materials behaves under different actions and external factors to which the nails are subjected to in daily activities. Finally, the method of making a nail prosthesis from one of the tested polymeric materials was presented and the importance of the functions of the nails, both aesthetic and medical, was highlighted.

KEYWORDS: nail plates, optical microscopy, hardness, roughness, mechanical testing, polymeric materials

1. Introduction

The nail is a semi-hard blade made up of several keratin cells that give it hardness [1]. A nail consists of several main elements, six in number: *The germinal matrix* - also called the root, is the most important part of the nail, because it produces onychoblast cells that over time develop and give rise to new cells, called onychocytes that migrate forward towards the distal nail fold. These onychocytes become harder keratin cells over time [1, 2]; *Lunula* - is the segment that shows the end of the germinal matrix. All nails have this area, but it is not visible on everyone equally [3]; *The nail bed* - is the area between the lunula and the hyponychium [4]; *Eponichium* - is located between the skin and the nail bed [5]. This structure provides the fingers with a superior barrier against microorganisms [6]; *Hyponychium* - It is the epithelial tissue between the nail plate and the tip of the finger, it is present between the free tip of the nail and the distal fold of the nail bed [7]. This epithelium is very rich in white and red blood cells and forms a seal against external microorganisms [5]; *Perionychium* - it is the tissue that covers the nail plate on the sides and has the same role as the hyponychium and eponychium [5, 7]. The nail plate is embedded in the folds or lateral folds of the finger. These being most often more prominent in the case of toenails [5]. If at birth, or during life this fold, together with the surrounding and protective layers of the matrix are damaged, there is a risk of a permanent defect of the nail [5]. The thickness of nails in a healthy adult varies from 0.5 mm to 0.75 mm, and in the case of toenails, greater than 1 mm. The rate of nail growth varies from 0.5 mm to 1.2 mm per week and the growth is continuous

THE ANNALS OF "DUNAREA DE JOS" UNIVERSITY OF GALATI
FASCICLE IX. METALLURGY AND MATERIALS SCIENCE
No. 4 - 2023, ISSN 2668-4748; e-ISSN 2668-4756
Article DOI: https://doi.org/10.35219/mms.2023.4.03

[8]. External factors, trauma, manicure, inflammation or infection can cause cuticle loss, this situation implies a difficulty of the proximal fold to protect the nail matrix [3, 9].

Due to external factors, nails are subject to a high risk of disease, being in the first line of contact with the external environment [9]. In this sense, the nails can suffer from a variety of diseases, depending on the cause, symptoms, but also on the way of formation. Nail conditions are not only aesthetic problems, but these problems can also indicate systemic diseases or show signs of infection in the body [10]. Some of the most common nail diseases are: onycholysis, onychomycosis, paronychia, pseudomonas, nail psoriasis, Beau's lines. These diseases have different causes: inflammatory, infectious, traumatic etc. [10].

There is the possibility that some of the nail diseases cannot be treated medically, due to the process of traumatizing the nail plate or the nail matrix. So, to improve the quality of life of patients, it was decided to solve aesthetic problems with the help of cosmetic products [11]. The most well-known materials used are nail varnishes, which are applied over a base layer, usually colourless, which has the role of fixing the next material and smoothing the irregularities of the nail plates, followed by the coloured layer and finally a protective, transparent layer which provides shine and prevents premature damage or chipping [11]. Most air-dry varnishes contain the following components:

- 15% film former, usually nitrocellulose which is a non-sensitizing, waterproof component that adheres to the nail plate;
- 7% thermoplastic resin (Toluene Sulphonamide Formaldehyde Resin - TSFR, which enables and strengthens the adhesion, hardness and flow of the material);
- 7% plasticizer, usually dibutyl phthalate and camphor, which improve flexibility and prevent shrinkage;
- 70% solvent-extender (toluene, butyl, or ethyl acetate and isopropyl alcohol, which allow the other components of the nail polish to remain liquid);
- 0-1% pigment;
- 1% suspending agent [11].

In the case of structural defects, such as Beau's lines, or trauma in the matrix area, polymer products have been developed that harden in contact with liquid monomers or ultraviolet radiation. There are two types, acrylic nails being the first type which is represented by a paste made of a liquid monomer, ethyl methacrylate and a powder polymer, polymethyl methacrylate that harden at room temperature with the help of an organic accelerator (benzoyl peroxide) forming a paste that is applied to the nails [11]. The second type, gel nails, are a mixture of ethyl cyanoacrylate and polymethyl methacrylate - the monomers are combined with the same powder polymer as the liquid acrylic nail which requires ultraviolet radiation to polymerize and harden [12].

The materials used in nail plate prosthetics, with the help of ultraviolet radiation, are composed of several substances, the main substance found in these products is methacrylate acid, a product with the following chemical formula: $CH_2=C(CH_3)COOH$ [13]. It is found in liquid or solid form but with a very low melting point. When in liquid form, it is colourless, and has a pungent odour [14]. In addition to the methacrylate acid, other components can be found, as for example: titanium dioxide – TiO_2, ethyl methacrylate - $C_2H_5O_2CC=CH_2$, trimethylolpropane triacrylate - $C_{15}H_{20}O_6$, polydimethylsiloxane - $CH_3[Si(CH_3)_2O]nSi(CH_3)_3$, methyl methacrylate - $CH_2=C(CH_3)COOCH_3$, hydroxyethyl methacrylate - $H_2C\backslash dC(CH_3)CO_2CH_2CH_2OH$, polyethylene terephthalate - $(C_{10}H_8O_4)_n$, 1-Hydroxycyclohexyl Phenyl Ketone - $C_{13}H_{16}O_2$, silicon dioxide – SiO_2 and wax, all of which having various functions.

The aim of the present work was to identify the best option for the restoration of a nail plate, choosing from three options, based on the results obtained from morphological testing, roughness, hardness, but also from a mechanical point of view using traction and compression testing.

2. Materials and methods

As part of the experimental part, 3 polymer materials used in nail plate prosthetics in manicure salons were chosen. These polymeric materials were inserted into straws of the same diameter, and length, to obtain the samples for the following analyses. After introducing the polymeric substance into the straws, they were placed in the 36 W UV lamp (λ = 356 nm) for 5 minutes (Figure 1), as this material becomes solid only in contact with ultraviolet rays. These polymer materials have in their composition photo initiating substances, which in contact with ultraviolet rays, produce heat and strengthen the polymer becoming solid.

Figure 1 shows the polymer material inserted into the straw under the UV lamp to polymerize the material and obtain the samples. After 5 minutes, the straws were removed and the samples were placed again under the UV lamp for another 2 minutes, to ensure the total polymerisation of the samples. At the end of polymerization, the samples were removed from the UV lamp and notated.

Figure 2 shows 2 samples of each polymer material used in the laboratory tests. The materials come from 3 different companies of polymer products: Kinetics, Gliterro and Macks, noted in the

THE ANNALS OF "DUNAREA DE JOS" UNIVERSITY OF GALATI
FASCICLE IX. METALLURGY AND MATERIALS SCIENCE
No. 4 - 2023, ISSN 2668-4748; e-ISSN 2668-4756
Article DOI: https://doi.org/10.35219/mms.2023.4.03

experiments with the letters K, G, M. From these samples, two sections with lengths between 12-14.5 mm were extracted, used later in the mechanical tests to observe their resistance to compression and bending, and a cylindrical section of 2 mm each for the microscopic analysis. All samples had an equal diameter of 5.85 mm (Fig. 3).

Fig. 1. *UV curing process of the samples*

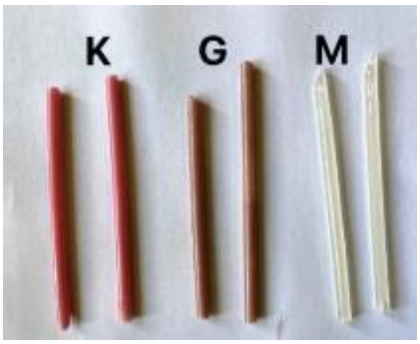

Fig. 2. *Obtained samples after UV-light curing*

Fig. 3. *The diameter of the specimens measured with a calliper*

After obtaining the samples, the microscopic analysis of the materials followed. For this analysis the inverted metallurgical microscope Kern OLM 171 was used. This microscope features a powerful and infinitely adjustable 50 W halogen incident light illumination, which ensures optimal illumination of the materials being analysed. This type of microscope is equipped with a trinocular tube, a simple polarizing unit consisting of an analyser and a polarizer, and a mechanical stage [15]. The microscope specifications offer magnification powers of 50x, 100x, 200x, and 500x. The interpupillary distance is 48-76 mm and the viewing position through the eyepiece is made at 30°. In the present case, a computer connected camera was used to capture images.

To analyse the roughness of the polymer materials used in nail plate prosthetics, an Insize ISR-C002 portable roughness meter was used. This roughness meter measures 21 roughness parameters. The obtained values are displayed on a digital screen

THE ANNALS OF "DUNAREA DE JOS" UNIVERSITY OF GALATI
FASCICLE IX. METALLURGY AND MATERIALS SCIENCE
No. 4 - 2023, ISSN 2668-4748; e-ISSN 2668-4756
Article DOI: https://doi.org/10.35219/mms.2023.4.03

for roughness, the profile and the curve and has the capacity to store 100 values. It can be connected via USB to a printer. As technical specifications, the Insize ISR-C002 roughness meter has an accuracy of +/- 10%. The material from which the probe is made is diamond and the probe is of inductive type. The roughness measurement force is 4 Nm. The number of interpenetrations is between 1 and 5. The device has two crossing speeds, namely: 0.5 mm/s and 1 mm/s [16].

For Vickers hardness testing, the Insize Micro-Vickers ISH-TDV1000A hardness tester was used. This device is used to measure the hardness of a small sample of material. Thanks to software based on Vickers hardness calculation, the obtained value can be converted, and the value of Rockwall hardness can be found. The device consists of a support table, mechanical, adjustable horizontally and vertically, two objectives that allow observing the sample before activating the indenter and after making the impression in the sample. The objectives have a magnification power of 10x or 40x and for the analysis carried out in this study, the 10x objective was chosen. The device also contains a camera connected to the eyepiece through which manually drawn axes are observed, according to the imprint of the indenter in the sample (Figure 4). The specifications of the durometer offer the possibility of changing the force, with the following options: 0.01, 0.025, 0.05, 0.1, 0.2, 0.3, 0.5 and 1 N. The charging time of the device varies between 5-60 s. For the Vickers hardness test, thin lamellae were obtained from each polymer materials used in this study.

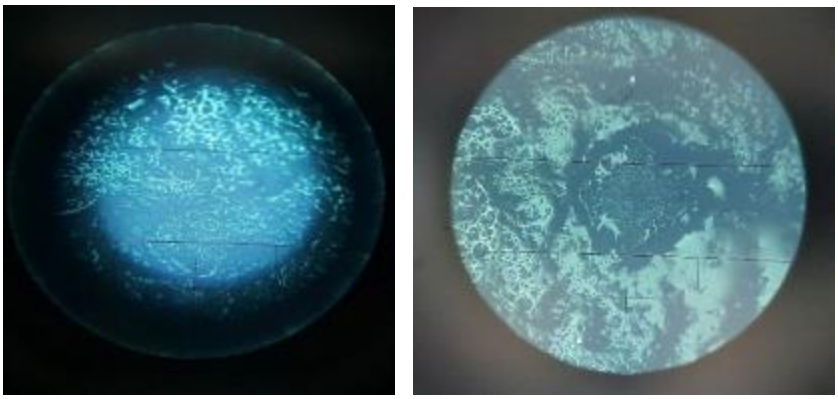

Fig. 4. *The surface of a K material sample before hardness testing – left image and a print in the same sample, framed by the measuring axes – right image*

Mechanical testing was performed using an Instron 8850 servo-hydraulic testing machine. The Instron 8850 series testing system is a dynamic, servo-hydraulic, floor-mounted, biaxial machine that provides axial torsional loading on the test specimens, in an integrated biaxial actuator. This instrument fulfils the material verification requirements with a wide testing range, biaxial static and dynamic [17]. The Instron 8850 system has a capacity of about 100 kN, and a torque capacity of about 1000 Nm, with an axial stroke of the actuator motor of 150 mm and a rotational stroke of 90° [18]. The first test of the polymeric materials used in this study, was the 3-poin bending test. For this purpose, the specimens were placed on the Instron 8850 system which had a support distance of 50 mm and the lowering speed of the action bar of 5 mm/minute. Two rounds of testing were performed for each polymer material. Fig. 5 offers three image captures showing an ongoing bending test for a sample made of the M material.

The next mechanical test was the compression testing, using the same test system, the Instron 8850 with a modified clamping system as seen in Figure 6.

The samples used for the compression testing were cut from the original samples and then polished to obtain flat surfaces. After the polishing, the samples lengths were measured with a calliper (Fig. 7) then tested using a descent of the upper platen of 1.3 mm/minute.

THE ANNALS OF "DUNAREA DE JOS" UNIVERSITY OF GALATI
FASCICLE IX. METALLURGY AND MATERIALS SCIENCE
No. 4 - 2023, ISSN 2668-4748; e-ISSN 2668-4756
Article DOI: https://doi.org/10.35219/mms.2023.4.03

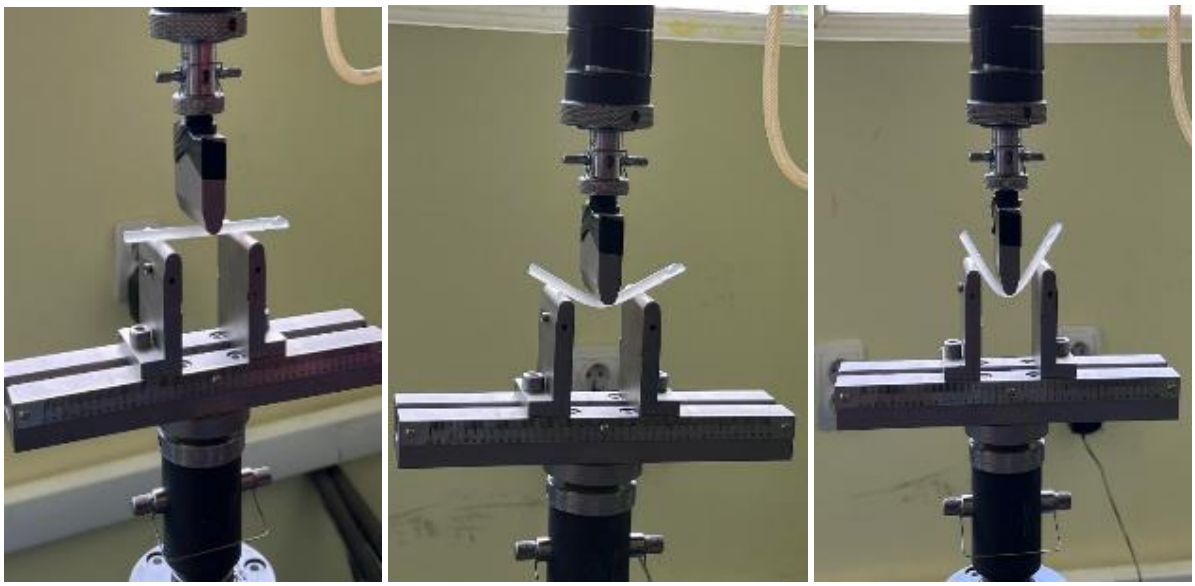

Fig. 5. *Image captures during the 3-point flexure test of a M material sample*

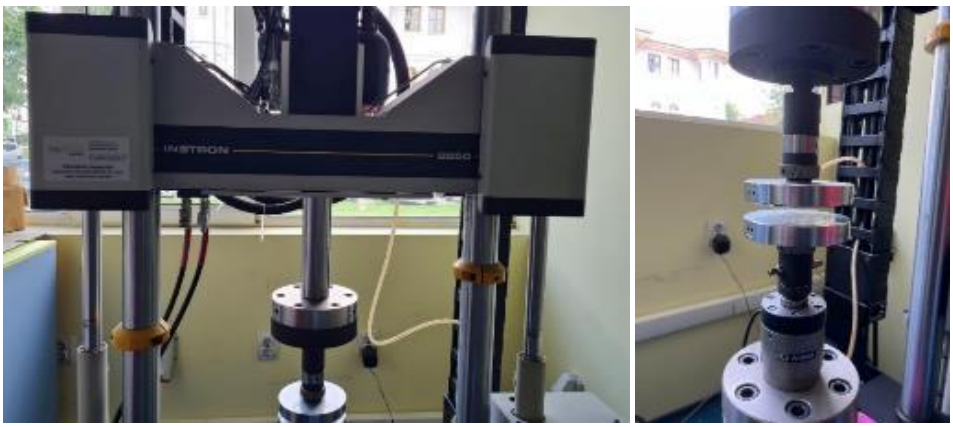

Fig. 6. *The Instron 8850 mechanical test system with a clamping architecture used for compression testing*

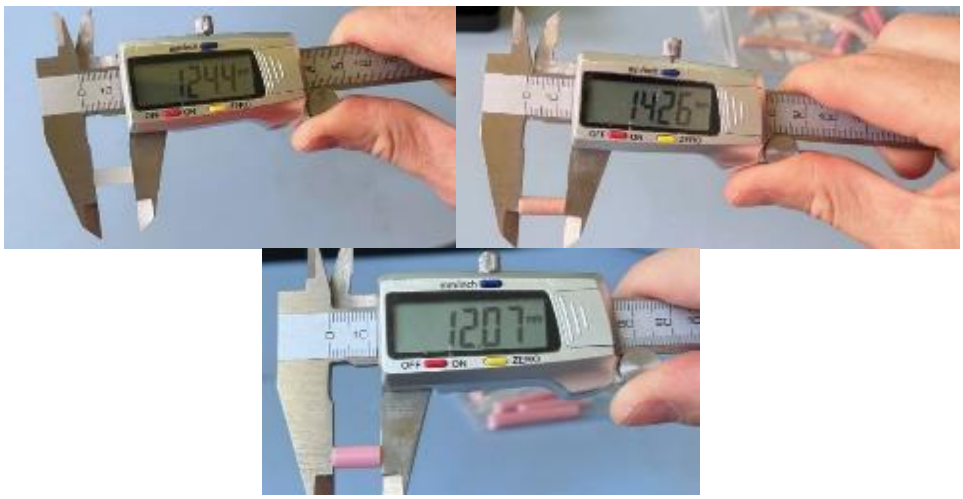

Fig. 7. *Measuring the length of test specimens for compressive strength testing*

THE ANNALS OF "DUNAREA DE JOS" UNIVERSITY OF GALATI
FASCICLE IX. METALLURGY AND MATERIALS SCIENCE
No. 4 - 2023, ISSN 2668-4748; e-ISSN 2668-4756
Article DOI: https://doi.org/10.35219/mms.2023.4.03

3. Results and discussions

3.1. Optical microscopy

Following the microscopic analysis performed with the Kern OLM 171 microscope, a magnified image of each tested sample was obtained. These images show the structure magnified at 50x (Figure 8).

The obtained images emphasize the first differences between the tested materials. Thus, the K material presents ramifications and perforations with a spongy appearance, while the M material presents a compact and more uniform structure, compared to the K material, but at the same time with many interspersed vesicles. Meanwhile, the G material stands out from the point of view of the microscopic image due to the lack of gaps and the reflections provided by the silicon dioxide. Thanks to the silicon dioxide, the quartz particles used for light diffusion and for aesthetic purposes are easily visible in this last tested material. In addition, this material, compared to the others, does not have perforations or a branched structure, but a uniform one.

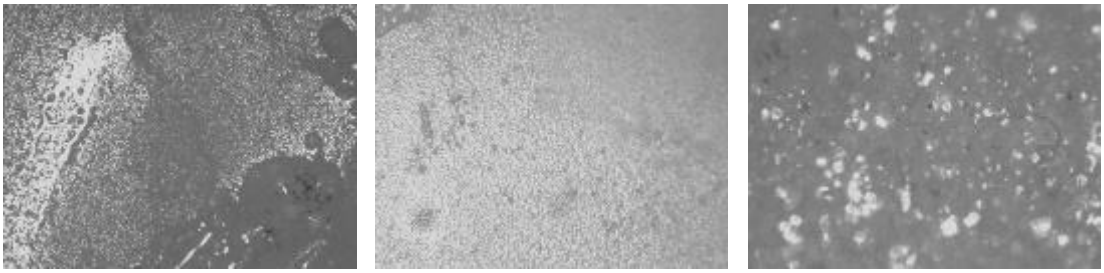

Fig. 8. *Microscopic images obtained using a 50x magnification for: K material sample – left image; M material sample – middle image; G material sample – right image*

3.2. Roughness testing

Following the laboratory tests of the roughness of the polymer materials using the Insize ISR-C002 roughness meter, different values of the roughness of the three samples were obtained. The value obtained and displayed on the device screen is the roughness value and is expressed in µm. The roughness value of the first tested polymeric K material is 0.629 µm (Figure 9 - left image).

Fig. 8. *Results of the roughness testing: K material sample – left image; M material sample – middle image; G material sample – right image*

The next material tested was the M material. In this case, the numerical value of the roughness is 0.802 µm (Fig. 8 – middle image). The last roughness test was performed on the sample made of the polymeric material G (Fig. 8 – right image). Its numerical value is: 0.434 µm. The three materials have different values, the lowest value belonging to the polymeric material G, followed by the K material and finally by the M material. From these values, it follows that the material with the roughest surface is the M material and the material with the smoothest surface is the G material. We can correlate the results obtained in the microscopic analysis with the results obtained in the case of the roughness analysis. The smoothest material from the point of view of roughness analysis is the material with the most uniform appearance, namely, material G. Considering the purpose of using these materials, we can deduce that the use of a material with a low roughness value, in our case, the G material, is the most desirable from an aesthetic point of view, since it imitates the smooth surface and thinness of the nail plate that requires prosthetics.

3.3. Hardness testing

Following the hardness tests carried out on the samples from the polymer materials, using the Insize ISH-TDV1000A device, the Vickers hardness value was found for each sample. The testing was carried out with preselected values of the apparatus, namely:

THE ANNALS OF "DUNAREA DE JOS" UNIVERSITY OF GALATI
FASCICLE IX. METALLURGY AND MATERIALS SCIENCE
No. 4 - 2023, ISSN 2668-4748; e-ISSN 2668-4756
Article DOI: https://doi.org/10.35219/mms.2023.4.03

the preset values of the indenter action force, the brightness with which the sample is observed, and the indenter loading time, to find out the Vickers hardness value of materials under equal conditions. For this purpose, a force of 0.5 kg was used, the loading and driving time of the indenter was 10 seconds, and the brightness level was set at 4. The first material tested was the K material, which presented a value of 5 HV (Figure 9 – left image).

Fig. 9. *Results of the hardness testing: K material sample – left image; M material sample – middle image; G material sample – right image*

The M material was the next one tested, and the recorder value was 2.4 HV (Figure 9 – middle image). The last specimen tested with the durometer was the G material. After testing, the Vickers hardness value was 3.5 HV (Figure 9 – right image). According to these results, in correlation with the purpose of use, we can deduce that the K material has the highest hardness when using these three polymeric materials. The harder the material used in the prosthesis, the greater the resistance of the prosthesis in the event of a shock.

3.4. Mechanical testing

The mechanical testing of the specimens provided an important insight into the mechanical properties of these polymeric materials. For bending strength testing, two specimens of the same material were used, resulting in different curves. The first three-point bending strength test was performed on polymer material K followed by M and G. Based on the data retrieved from the computer linked to the mechanical testing machine, a graph was obtained, with a comparative purpose of the displacement and the force to which all 6 samples were subjected. Based on the graph (Figure 10) a clear difference between the 3 types of materials is observed. The samples from the same material have very similar, almost identical results.

The first material subjected to the bending test was the polymeric material K. According to the graph, the flexural strength of this material from the point of view of displacement was the lowest, managing to yield in the shortest time to the load and break suddenly shortly after the action of 60 N. Also, is the material that recorded the highest withstanding force.

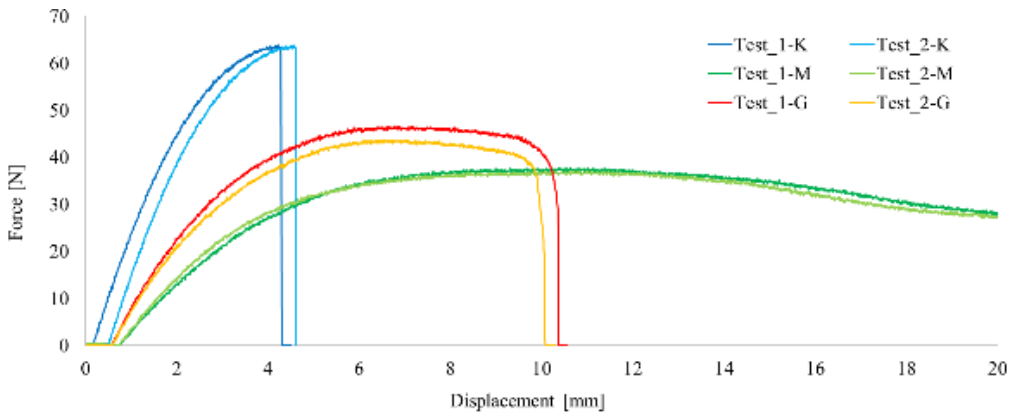

Fig. 10. *Force-displacement diagram for the 3-point flexural bending tests of the K, M and G polymeric materials*

THE ANNALS OF "DUNAREA DE JOS" UNIVERSITY OF GALATI
FASCICLE IX. METALLURGY AND MATERIALS SCIENCE
No. 4 - 2023, ISSN 2668-4748; e-ISSN 2668-4756
Article DOI: https://doi.org/10.35219/mms.2023.4.03

Among all the materials tested, the samples from the polymeric material K were the ones that deformed the least, recording in terms of displacement below 5 mm. In the case of the samples from the polymeric material M, we can observe that samples had the lowest resistance value from the point of view of the applied force, below the value of 40 N, but from the point of view of displacement, they have the highest and most constant strength, without obtaining cracks or breaks on the surface of the samples. After removing the applied force, the polymeric material M samples tended to return to their original shape but stopped before completely do so. Also, no cracks or breakage of these specimens were observed.

The last material tested was the polymeric material G, which, according to the data, is in the middle between the first two, both from the point of view of the displacement and the applied force. The samples of this material cracked on the outside, in a controlled manner, failing to break suddenly as in the case of the polymeric material K. The specimens of polymeric material G had a constant value of the bending strength up to about 45 N, for about 4 mm of displacement, then cracks occurred on the outer side of the specimens, ultimately registering a decrease in the applied force around 10 mm of displacement, without breaking suddenly like the samples from the polymeric material K.

The last material test analysis was compressive strength. For this type of analysis, the compressive strength was measured for two specimens for each material. Using the obtained results, a diagram was plotted with the comparative aim of observing the resistance of each material (Figure 11). The slight variation in height of samples is transposed in different starting points of data curves on the displacement axes.

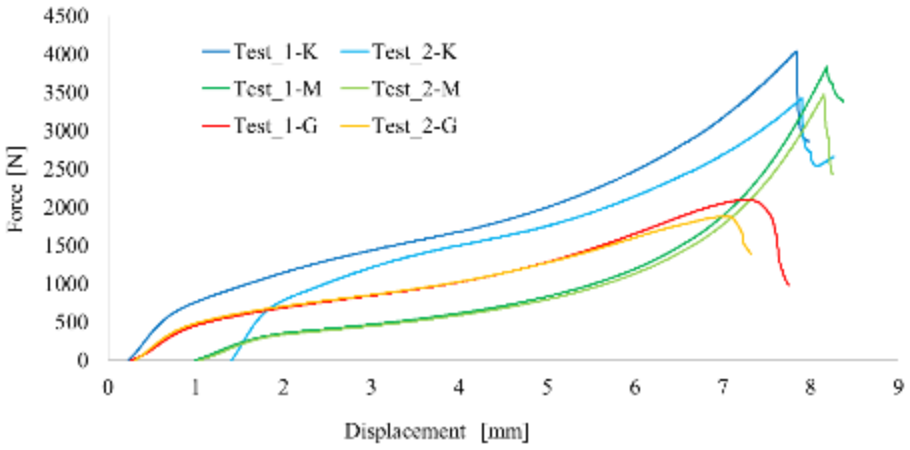

Fig. 11. *Force-displacement diagram for the compressive strength tests of the K, M and G polymeric materials*

The first test was carried out on samples of the polymeric material K. As can be seen from the graph, the samples of this material behaved with a small difference. The first specimen withstood a force of about 4000 N and deformed almost 8 mm. The second sample yielded at about 3000 N of force, and deformed almost 8 mm. Finally, the specimens registered cracks under the action of the upper platen, forming 3 vertical grooves along the specimens that connected each other (Figure 12).

The second material tested was the polymeric material M. In the case of these specimens, the curves of the graph in Figure 11 look similar. Also, the force and displacement values are similar to the ones registered for the previous material. At the end of the test, two long, vertical grooves running through their entire length were observed on each tested specimen (Figure 12).

The last material tested for compression was the polymeric material G. According to the graph, both samples had similar results. They deformed the fastest, under the action of the smallest force, approximately 2000 N, the displacement length a little more than 7 mm. At the end of the test, a short vertical groove was observed on each specimen (Figure 12).

Following the compression tests performed on the three types of materials, the polymeric materials K and M had similar results regarding the maximum withstanding force and displacement even though, the curves emphasize a greater elasticity of the polymeric material M, since it needs lower values of the applied force to obtain the same displacement. The results for the polymeric material G emphasize an elasticity between the other two materials and lower values for the withstanding force and displacement.

THE ANNALS OF "DUNAREA DE JOS" UNIVERSITY OF GALATI
FASCICLE IX. METALLURGY AND MATERIALS SCIENCE
No. 4 - 2023, ISSN 2668-4748; e-ISSN 2668-4756
Article DOI: https://doi.org/10.35219/mms.2023.4.03

Fig. 12. *Samples of polymeric materials K – left, M – middle and G – right, after compression strength testing*

Combining the results from the mechanical tests, it can be concluded that between the three polymeric materials, the K and M ones present the most promising results since the data from the compression tests are in their favour with similar values for the force and displacement. The choosing of one against the other can be based on the results from the 3-point flexural bending tests but also on the necessities of the patient, as is the case in the further presented case study.

3.5. Case study for a nail plate prosthesis

The prosthesis of a nail plate with onycholysis resulting from impact was put into practice, using one of the tested materials. Following a trauma, this nail suffered detachment of the nail plate from the nail bed, this problem being known as onycholysis, so that at the time of healing the external trauma, the nail kept this aspect which, with the growth of the nail, will return to normal (Fig. 13).

Fig. 13. *Onycholysis due to external trauma*

Fig. 14. *A healthy nail is presented against the one with onycholysis – left; onycholysis affected nail after prosthetics actions - right*

To provide an accurate picture of the normal condition of this type of nail bed, an image of a healthy nail is presented against the one with onycholysis for comparative purposes in Figure 14. The lack of a portion of the bed and nail plate would have created discomfort for the patient in carrying out physical activities. Figure 14 (right image) also presents the traumatised nail after prosthetics actions.

For the prosthesis of this nail plate the natural nail was brushed to favour the adhesion of the polymer material. After sweeping, it was dusted and degreased and a methacrylate acid solution was

THE ANNALS OF "DUNAREA DE JOS" UNIVERSITY OF GALATI
FASCICLE IX. METALLURGY AND MATERIALS SCIENCE
No. 4 - 2023, ISSN 2668-4748; e-ISSN 2668-4756
Article DOI: https://doi.org/10.35219/mms.2023.4.03

applied to maximize the adhesion between the material used and the nail plate [12, 19]. Since the desired appearance was a natural one, it was decided to use the polymeric material M, due to its transparency. A small amount of material was placed on the middle of the nail bed, to be shaped with the help of an applicator soaked in isopropyl alcohol. After placing the material, it was polymerized for 120 seconds in the 36 W ultraviolet light lamp. At the end of the polymerization, the material was degreased and finished to obtain a smooth surface and as similar as possible to the natural nail, both in terms of thickness and aesthetic point of view. As time passes and the natural nail grows, the nail bed will lengthen, allowing the nail to grow where the trauma occurred, and the polymer material can be removed by cutting or filing without affecting the natural nail in any way.

4. Conclusions

The importance of a healthy nail apparatus is supported both by the daily activities to which each person is subjected, whether it is constant protection against environmental factors, whether is about physical activities such as using the fingers, but also by the need for belonging and approval of society. The existence of medical or aesthetic problems leads to a decrease in the self-esteem of individuals, which makes nail prostheses a necessity for the mental health of patients but also for the performance of usual activities without feeling discomfort.

The materials tested in this study were structurally and mechanically compared, providing an overview of the microscopic image of each material, but also exact numerical values when tested for roughness and hardness. These tests are important for understanding the behaviour of the material from which the nail prostheses are made, but also to imitate as much as possible the natural appearance of the nail plates, thus providing a lasting resistance during their use but also a pleasant appearance.

The laboratory tests showed the differences in numerical values and in the case of mechanical analyses of the resistance of polymeric materials to bending and compression, thus providing an image of the physical properties of the K, M and G materials. All these materials can be used to make a nail prosthesis but used for different purposes. According to laboratory tests, the most recommended material from the point of view of bending and compression resistance, hardness and implicitly for all the physical activities that a nail prosthesis involves, is the K polymeric material, because it recorded the highest values to physical tests. On the other hand, due to the colouring pigments, the appearance that this material will provide is not natural or imperceptible.

From an aesthetic point of view, the most recommended material for making a prosthesis for a traumatized or diseased nail plate is the polymeric material M, due to its very natural appearance, but because it recorded the highest value of roughness, the use of this material in prosthesis of a nail plate necessitates grinding and finishing to be as close as possible to a natural nail. From the point of view of physical properties, the polymeric material M is in the middle of the ranking, obtaining numerical values in the bending and compression strength tests in correlation with the force to which they were subjected, lower than the polymeric material K.

The polymeric material G recorded low roughness values, offering the smoothest surface, but due to the silicon dioxide in the chemical composition, it acquires a false aesthetic appearance, inconsistent with the appearance of a natural nail. Also, the values from the mechanical tests ranked it last among all three materials tested, meaning low performances in daily activities.

Thus, it is very important that when constructing a prosthesis for a nail plate, to achieve a balance between the patient's needs and the purpose of the prosthesis, namely: treating the nail plate from an aesthetic point of view as well as its resistance depending on the loads to which it is to be subjected.

References

[1]. Dykyj D., *Anatomy of the nail*, Clin Podiatr Med Surg, 6, p. 215-28, 1989.
[2]. Tosti A., Cameli N., Piraccini B. M., Fanti P. A., Ortonne J. P., *Characterization of nail matrix melanocytes with anti-PEP1, anti-PEP8, TMH-1, and HMB-45 antibodies*, J Am Acad Dermatol, 31, p. 193-196, 1994.
[3]. Ito T., Ito N., Saathoff M., *et al.*, *Immunology of the human nail apparatus: the nail matrix is a site of relative immune privilege*, J Invest Dermatol, 125, p. 1139-48, 2005.
[4]. Walters K. A., Flynn G. L., Marvel J. R., *Physicochemical characterization of the human nail: permeation pattern for water and the homologous alcohols and differences with respect to the stratum corneum*, J Pharm Pharmacol, 35, p. 28-33, 1983.
[5]. de Berker D., *Nail anatomy*, Clin Dermatol, 31, p. 509-515, 2013.
[6]. Fleckman P., *Anatomy and physiology of the nail*, Dermatol Clin, 3, p. 373-381, 1985.
[7]. Rodriguez-Takeuchi S. Y., Villota V., Renjifo M., *Anatomy and pathology of the nail and subungual space: Imaging evaluation of benign lesions*, Clin Imaging, 52, p. 356-364, 2018.
[8]. Adams R. M., *Effects of mechanical trauma on nails*, Am J Ind Med, 8, p. 273-280, 1985.
[9]. Belyayeva E., Gregoriou S., Chalikias J., *et al.*, *The impact of nail disorders on quality of life*, Eur J Dermatol, 23, p. 366-371, 2013.
[10]. Lee D. K., *Optimal diagnosis and management of common nail disorders*, 54, p. 694-712, 2022.
[11]. Iorizzo M., Piraccini B. M., Tosti A., *Nail cosmetics in nail disorders*, J Cosmet Dermatol, 6, p. 53-58, 2007.
[12]. Kanerva L., Lauerma A., Jolanki R., Estlander T., *Methyl acrylate: a new sensitizer in nail lacquer*, Contact Dermatitis, 33, p. 203-204, 1995.

THE ANNALS OF "DUNAREA DE JOS" UNIVERSITY OF GALATI
FASCICLE IX. METALLURGY AND MATERIALS SCIENCE
No. 4 - 2023, ISSN 2668-4748; e-ISSN 2668-4756
Article DOI: https://doi.org/10.35219/mms.2023.4.03

[13]. ***, https://pubchem.ncbi.nlm.nih.gov/compound/4093#section=Structures.
[14]. Kinney S. M., Ortaleza K., Vlahos A. E., Sefton M. V., *Degradable methacrylic acid-based synthetic hydrogel for subcutaneous islet transplantation*, Biomaterials, 281, 2022.
[15]. ***, https://astromagazin.ro/microscoape-metalurgice/15202-microscop-metalurgic-inversat-kern-olm-171.html.
[16]. ***, Insize ISR-C002, http://www.insize.com/page-169-267.html.
[17]. Tretyakova T., Wildemann V., Tretyakov M., *Investigation of the Portevin-Le Chatelier effect in metals under additional vibration impact by using the DIC-technique and the IR-analysis*, Procedia Structural Integrity, 18, p. 837-842, 2019.
[18]. ***, *Instron 8850*. https://www.directindustry.com/prod/instron/product-18463-1663085.html.
[19]. Kerai L. V., Hilton S., Maugueret M., *et al.*, *UV-curable gels as topical nail medicines: In vivo residence, anti-fungal efficacy and influence of gel components on their properties*, Int J Pharm, 514, p. 244-254, 2016.

THE ANNALS OF "DUNAREA DE JOS" UNIVERSITY OF GALATI
FASCICLE IX. METALLURGY AND MATERIALS SCIENCE
No. 4 - 2023, ISSN 2668-4748; e-ISSN 2668-4756
Article DOI: https://doi.org/10.35219/mms.2023.4.04

ANALYSIS OF THE MATERIALS USED IN SOME RAPID PROTOTYPING TECHNOLOGIES, FROM THE POINT OF VIEW OF MICROHARDNESS AND SURFACE QUALITY

Beatrice TUDOR, Claudiu GRIGORAS
"Dunarea de Jos" University of Galati, Romania
e-mail: beatrice.tudor@ugal.ro

ABSTRACT

The paper presents a comparative study, from the point of view of microhardness and surface quality, of samples made from materials used in rapid prototyping technologies, namely photopolymer resin and PLA. Microhardness determinations were made for both materials, with Micro-Vickers HDT-VS1D INSIZE digital automatic hardness tester, and the surface of the samples was analysed, from a qualitative point of view, with the optical microscope, OLYMPUS BX51M.

KEYWORDS: microhardness, surface, photopolymer resin, PLA, hydrogels

1. Introduction

Rapid prototyping, along with computerization and automation technologies, have favoured mass production of customized models for the medical field. These designs have a low cost, it is made in a relatively short time and reduce the risk of errors.

Synthetic polymers are also known as artificial polymers, being structured into three large classes: thermoplastics, elastomers and synthetic fibres. These synthetic polymers have applications in biomedicine, diagnostics and tissue engineering. They form an important category of materials also used for 3D printing, not only for biomedical applications. They have very good mechanical properties and a low price. The most imported synthetic polymers that are 3D printed are: Poly (lactic acid - PLA), Poly (caprolactone- PCL), Poly (D, L-lactic-co-glycolic acid - PLGA), (PEEK) etc. [1, 3].

The most used materials for 3D printing are non-toxic hydrogels. The use of FDM extrusion printing and SLA rapid prototyping technology are essential in the 3D printing of hydrogels.

Other materials used in 3D printing, in addition to the mentioned materials, can be: silk, fibrin, decellularized ECM, matrigel of natural origin, elastin, etc. [2].

2. Experimental determinations

In the study, the microhardness of the samples made from photopolymer resin and PLA was determined.

To compare the strength of these two materials, used in dental bridges, we used the Micro-Vickers HDT-VS1D INSIZE digital automatic hardness tester.

Were made three different determinations, for each material, for make an average of the determinations.

The determinations were made on samples from PLA material, and

photopolymer resin.

Both samples were analyzed with the same specification of the, respectively:

- load (kg) - 0.5;
- replacement time (s)-10;
- the objective at 40x;
- brightness of 4 lx.

The stages through which the hardness on the device determinations were made are:

For both samples of PLA material and photopolymer resin, we performed the following steps:

- placing the sample on the support of the microhardness measuring device (Fig. 1);
- fixing the specifications of the device (Fig. 2);
- focusing on the area, by marking the length and width (Fig. 3);
- generating data by turning on the device.

THE ANNALS OF "DUNAREA DE JOS" UNIVERSITY OF GALATI
FASCICLE IX. METALLURGY AND MATERIALS SCIENCE
No. 4 - 2023, ISSN 2668-4748; e-ISSN 2668-4756
Article DOI: https://doi.org/10.35219/mms.2023.4.04

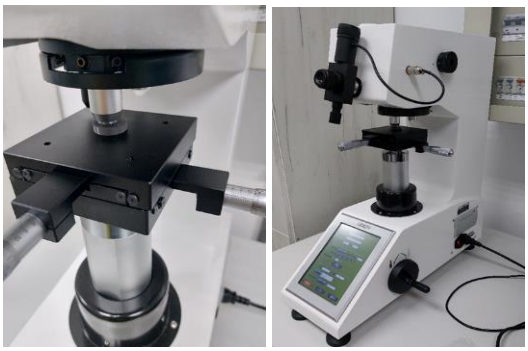

Fig. 1. *Placing the sample on the holder of the hardness measuring device*

Fig. 2. *Fixing the specifications of the device*

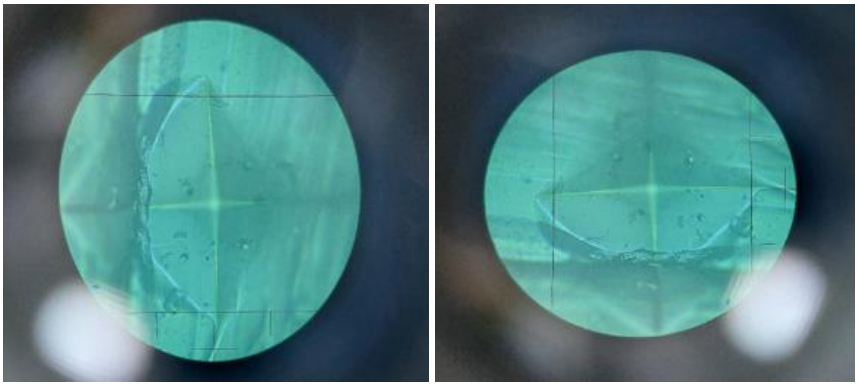

Fig. 3. *Marking the length and width of the sample from PLA material*

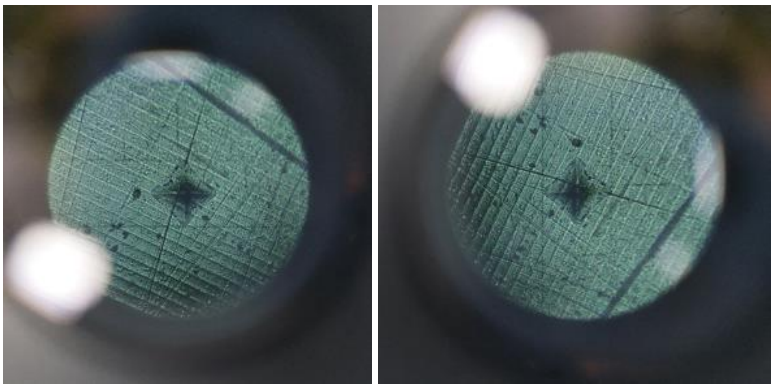

Fig. 4. *Marking the length and width of the sample from photopolymer resin*

THE ANNALS OF "DUNAREA DE JOS" UNIVERSITY OF GALATI
FASCICLE IX. METALLURGY AND MATERIALS SCIENCE
No. 4 - 2023, ISSN 2668-4748; e-ISSN 2668-4756
Article DOI: https://doi.org/10.35219/mms.2023.4.04

Table 1. *Results from hardness results*

Material	No. of determinations	D1 (Distance 1)	D2 (Distance 2)	HV Hardness
PLA	1	169.89	194.57	27.9
	2	160.15	203.05	28.1
	3	201.30	158.87	28.5
Average value		**177.11**	**185.49**	**28.2**
Photopolymer resin	1	101.37	108.53	84.1
	2	119.57	143.06	53.7
	3	114.55	99.35	81
Average value		**111.83**	**116.98**	**72.9**

Following the determinations, we notice that the photopolymer resin sample has a higher hardness than the PLA material sample. This is also due to the action of UV light, which increased the resistance of the sample. This determination of hardness recommends the use of photopolymer resin in the creation of models for maxillo-facial surgery [4, 7].

Following the results obtained after determining the microhardness, we notice that the photopolymer resin sample has a higher hardness than the PLA material sample. This is also due to the action of UV light, which increased the resistance of the sample. This results recommend the use of photopolymer resin in making models for maxillofacial surgery [4, 7].

The samples were analysed with the optical microscope OLYMPUS BX51M, from the metallography laboratory, in order to visualize the appearance of the surfaces as precisely as possible (Fig. 5).

The optical images obtained for the surfaces of PLA samples and photopolymer resin are presented in Fig. 6.

Fig. 5. *OLYMPUS BX51M optical microscope*

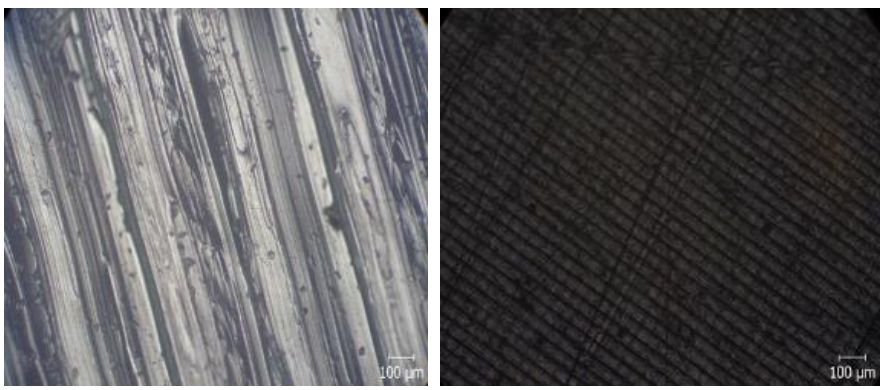

PLA material Photopolymer resin

Fig. 6. *Optical images for sample surfaces (100 µm)*

Nº. 4 - 2023, ISSN 2668-4748; e-ISSN 2668-4756
Article DOI: https://doi.org/10.35219/mms.2023.4.04

After visualizing the quality of the sample surfaces, it is observed that the sample made of photopolymer resin has a much lower roughness than the sample from PLA.

This study may be useful in choosing the optimal material in various simulations and medical applications.

3. Conclusions

The photopolymer resin sample has a higher hardness than the PLA material sample.

In terms of surface quality, the photopolymer resin sample has a much lower roughness than the PLA sample.

The higher hardness of the photopolymer resin and the quality of the surface, recommend the use of this type of material, in making models for maxillo-facial surgery.

References

[1]. Cernica D., Márton E., Mester A., Chițu M., Benedek I., *Tehnica imprimării 3D în imagistică și aplicațiile medicale*, 2021.
[2]. Tayebi L., Masaeli R., Zandsalimi K., *3D Printing in Oral & Maxillofacial Surgery*.
[3]. Tsoulfas G., Bangeas P. I., Suri J. S., *3D printing: applications in medicine and surgery*, Volume 1.
[4]. Tappa K., Jammalamadaka U., *Novel biomaterials used in medical 3D printing techniques*, J. Funct. Biomater., vol. 9, no. 1, doi: 10.3390/jfb9010017, 2018.
[5]. Meneghello R., Savio G., Raffaeli R., Cerardi A., Turchetto M., Planchenstainer L., *An integrated methodology for the functional design of dental prosthesis,* Int. J. Interact. Des. Manuf., vol. 7, no. 2, p. 103-114, doi: 10.1007/s12008-012-0169-5, 2013.
[6]. Budak I., Kosec B., Sokovic M., *Application of contemporary engineering techniques and technologies in the field of dental prosthetics Analysis and modelling*, J. Achiev. Mater. Manuf. Eng., vol. 54, no. 2, p. 233-241, 2012.
[7]. Strub J. R., Rekow E. D., Witkowski S., Strub J. R., Rekow E. D., Witkowski S., *Computer aided design and fabrication of dental restorations: current systems and future possibilities*, J Am Dent Assoc,137:1289-96., vol. 137, 2006.
[8]. Tian Y. *et al.*, *A Review of 3D Printing in Dentistry: Technologies, Affecting Factors, and Applications*, Scanning, vol. 2021, doi: 10.1155/2021/9950131, 2021.

THE ANNALS OF "DUNAREA DE JOS" UNIVERSITY OF GALATI
FASCICLE IX. METALLURGY AND MATERIALS SCIENCE
No. 4 - 2023, ISSN 2668-4748; e-ISSN 2668-4756
Article DOI: https://doi.org/10.35219/mms.2023.4.05

OPTIMIZATION OF THERMAL TREATMENT PARAMETERS FOR THE ALLOY AlZn4.5Mg1

Marian-Iulian NEACȘU
"Dunarea de Jos" Univeristy of Galati, Romania
e-mail: marian.neacsu@ugal.ro

ABSTRACT

The paper presents the method of finding the optimal variant of thermal processing through artificial aging that is applied to a non-ferrous aluminum-based alloy.

The criterion based on which the optimum for the thermal process of artificial aging is obtained is that of the minimum consumption of energy consumed with the heat treatment furnace.

With the help of MATLAB, we created a graphic interface for the calculation simulation of the energy consumed by the treatment furnace depending on the process parameters and the identification of the optimal variant.

KEYWORDS: optimization, aluminum alloy, thermal treatment, mathematical modeling, prediction of property values, graphic interface

1. Introduction

Optimization is understood as the process of studying a problem that leads to the best and most suitable result compared to other possible results at the time, on which technical and/or economic decisions are made.

Considering the characteristics of the metallurgical industry, which are:

- high consumption of raw materials, fuels and energy;
- very complex technological processes;
- the large production capacities of the machines (furnaces, steel mills, rolling mills), the need to introduce management methods, both of technological processes and of metallurgical enterprises, which lead to considerable savings of raw materials, fuels and energy [1, 2] is evident.

"Like any technical system, metallurgical processes have certain technical and economic performances, performances that depend on the parameters, conditions and mode of exploitation of the system. That is, among the possibilities of choosing these parameters and existing conditions at a given moment, those that will ensure the best technical-economic performances of the process (choice of optimal parameters) must be selected" [2].

The optimization of any technological process is based on a mathematical model that must describe that process as faithfully as possible, the mathematical model being the main element in managing the process. Hence the immense importance of obtaining a mathematical model that very faithfully describes the respective process, which means that between the model and the described process there must be as high a concordance as possible [3].

The achievement of the optimal solution is done by highlighting some values of the independent variables, so that the best value for the objective function (the function to be optimized) results. The phrase optimal value of the objective function means, depending on the case, its maximum or minimum value.

The choice of the objective function is the most important step in solving an optimization problem. The efficiency of the process is given by several indicators, not just by one; that is why it is necessary to choose the most representative or complete indicator and finally check how the optimal solution corresponds with the other indicators.

The performance function (objective, optimization criterion) expresses the dependence between the main independent variables and the main desired performance in the management of the process [3].

The performance function is expressed by the relation [2]: $Y = Y(X_1, X_2, ... X_n)$.

The performance function is the unique and objective criterion for process optimization and

THE ANNALS OF "DUNAREA DE JOS" UNIVERSITY OF GALATI
FASCICLE IX. METALLURGY AND MATERIALS SCIENCE
No. 4 - 2023, ISSN 2668-4748; e-ISSN 2668-4756
Article DOI: https://doi.org/10.35219/mms.2023.4.05

management [3]. Typically, the performance function represents an explicit economic criterion (for example: the manufacturing price of a product, maximum profit, etc.), but it can also be a non-economic criterion, but which is economically involved (as used in metallurgy extractive, where the obtained product undergoes subsequent changes) such as: productivity of aggregates (t/h; t/V of the aggregate, etc.), specific consumptions (raw materials/unit of product; electricity/unit of product, etc.), yields metallurgical (metal extraction, alloying element inclusion yields, impurity removal yields), etc. [4].

Optimization methods are generally reduction methods, which highlight the minimum of a "U" function of "n" real variables, which is called a goal function or objective function. Hence their name of methods for minimizing functions of several variables. Of course, the problem of finding the maximum returns to the minimization of the function with changed sign. Decreasing paths have global convergence, which means they allow finding the solution even if the starting point is far from the solution. Optimization methods belong to a very wide field of applicability. In other words, most natural or economic phenomena are compromises between contradictory causes and as such a lot of the problems of engineering, economics, statistics, mathematics, medicine, but more precisely decision-making processes can be mentioned as optimization problems. In other words, most numerical methods can be renamed as optimization problems [4].

2. Experimental conditions

Materials intended for experimentation are aluminum alloy from the Al, Zn, Mg, Cu system, with the chemical composition noted in Table 1.

The mechanical properties of the alloy according to EN 485-2-2007 are noted in Table 2.

Table 1. *Materials intended for experiments according to EN 485-2-2007*

AlZn4.5Mg1	Zn	Mg	Cu	Si	Fe	Cr	Mn	Al
%	4.5	1.4	0.2	0.35	0.4	0.35	0.5	rest

Table 2. *Mechanical properties of the alloy according to EN 485-2-2007*

Proprieties / Alloy	Rm [MPa]	$Rp_{0.2}$ [MPa]	A_5 [%]	HB
AlZn4.5Mg1	350	250	10	104

The experimental research variant aimed to study the fluctuation of the mechanical properties of the alloys after the thermal treatment of artificial aging at different values of the time and temperature parameters [5].

Artificial aging was carried out at the following temperatures: 140 °C, 160 °C, 180 °C, 200 °C and 220 °C, and the following times for maintaining the alloy: 4 hours, 8 hours, 12 hours, 16 hours and 20 hours for each aging temperature.

The objective function in the variant of optimizing the thermal processing parameters of the studied alloy is represented by the energy consumption "$Q = f(t, \tau)$" taking into account certain impositions considering the values of the investigated mechanical properties.

In order to find out which variant of thermal treatment from several variants resulting from the calculation with the help of the mathematical model created, represents the optimal variant economically and from the point of view of the property values, we proceed to calculate the thermal energy consumption Q, [kWh] for each among them.

The calculation of energy consumption in the form of heat (thermal energy) represents the calculation of the total energy consumed in the heat treatment furnace where artificial aging is carried out according to the relationship below:

$$Q_{total} = Q_{total\ oven} \quad (1)$$

Q_{total} - the amount of energy consumed for the thermal treatment; $Q_{total\ oven}$ - the amount of energy required to reach and maintain the treatment temperature during the entire period of performing the heat treatment.

The oven in which the heat treatment was carried out is an electric heating oven with silite bars, made of refractory fireclay brick, lined with mineral wool and with steel sheeting on the outside.

The energy consumed for the final thermal treatment will be determined after the thermal balance of the treatment furnace.

The energy consumption will be calculated by the amount of heat to be provided to reach and maintain the treatment temperature throughout the

THE ANNALS OF "DUNAREA DE JOS" UNIVERSITY OF GALATI
FASCICLE IX. METALLURGY AND MATERIALS SCIENCE
No. 4 - 2023, ISSN 2668-4748; e-ISSN 2668-4756
Article DOI: https://doi.org/10.35219/mms.2023.4.05

thermal treatment, according to relation (2) according to [6]:

$$Q_{total\ oven} = Q_A + Q_B, \quad (2)$$

Q_A – the amount of heat (energy) consumed during the furnace heating period; Q_B - the amount of heat (energy) consumed during the maintenance of the temperature under heat treatment conditions.

The heat needed to increase the temperature inside the furnace from the ambient temperature to the treatment temperature is, [6]:

$$Q_A = Q_{ac\ piece\ A} + Q_{ac\ masonry\ A} + Q_{perd\ masonry\ A} \quad (3)$$

$Q_{ac\ piece\ A}$ - the heat accumulated in the pieces (samples) during the heating period of the oven is given by relation (4) [7]:

$$Q_{ac\ piece\ A} = m_{piece} \cdot c_{piece} \cdot \Delta t1, [kJ] \quad (4)$$

m_{piece} - mass of samples, [kg]; $\Delta t_1 = tt - ta$, [°C]; Δt_1 - the temperature gradient between the treatment temperature tt and the ambient temperature ta; c_{piece} - the specific heat of the samples; $Q_{ac\ masonry\ A}$ - the heat accumulated in the furnace walls during the heating period is calculated with relation (5) [6, 7]:

$$Q_{ac\ wall\ A} = (m_{cs} \cdot c_{cs} + m_{vm} \cdot c_{vm} + m_t \cdot c_t) \cdot \Delta t_1, [kJ] \quad (5)$$

c_{cs} - specific heat of fireclay brick; c_{vm} - specific heat of mineral wool; c_t - specific heat of the plate; m_{cs} - the mass of the refractory fireclay brick of the furnace; m_{vm} - mineral wool mass used to insulate the oven; m_t - the mass of the steel sheet used to line the furnace; $Q_{perd\ masonry\ A}$ - the heat lost through the furnace walls during the heating period and is calculated using the thermal flow, ΦA [6, 7]:

$$Q_{perd\ masonry\ A} = \Phi_A \cdot \tau_A, [Wh] \quad (6)$$

τ_A - heating time of the oven interior, [h]; Φ_A - heat flow during the heating period, period A, is [7]:

$$\Phi_A = \Phi_{horizA} + \Phi_{vert\ A}, [W] \quad (7)$$

Φ_{orizA} - thermal flow through the horizontal walls of the furnace during the heating period; Φ_{vertA} - thermal flow through the vertical walls of the furnace during the heating period.

The heat required Q_B to maintain the samples, inside the furnace, at the treatment temperature is equal to the heat lost through the walls of the furnace during this entire period.

$$Q_B = Q_{loss\ of\ masonry\ B}, [kJ], [7] \quad (8)$$

This is also reproduced with the help of the thermal flow Φ_B [7]:

$$\Phi_B = \Phi_{horizB} + \Phi_{vertB}, [W] \quad (9)$$

Φ_{orizB} - thermal flow through the horizontal walls of the furnace during the period of maintaining the samples at the heat treatment temperature; Φ_{vertB} - thermal flow through the vertical walls of the furnace during the period of maintaining the samples at the heat treatment temperature.

$$Q_{loss\ of\ masonry\ B} = \Phi_B \cdot \tau_B, [kWh], [6] \quad (10)$$

τ_B - the time the samples are kept at the heat treatment temperature, [h].

By comparing each mechanical property, studied after applying the heat treatment, with a function of two variables Y = f(t, τ), it is possible to obtain a set of values for the studied mechanical properties if multiple interpolation is performed according to the variables t, τ, starting from to the values obtained through experimental research.

The MATLAB software package facilitates the interpolation of functions of two variables by using specific functions, such as *interp2* or *griddata2* [8, 9].

By interpolating the values for each studied mechanical property taking into account the two parameters of the final thermic treatment (t - artificial aging temperature, τ - artificial aging time), a volume of interpolated data of 289 values corresponding to each property was obtained.

Because aluminum alloys are "sensitive" to small changes in the treatment temperatures, a variation of the treatment temperature from five to five degrees was adopted, thus obtaining a number of 17 temperatures, between 140 °C and 220 °C.

The time for the artificial aging process was discretized from 4 hours to 20 hours with one-hour intervals, resulting in 17 interpolation values.

Under the given conditions, the goal of optimization is expressed by identifying among these data, only those that comply at the same time with the impositions of EN_485-2-2007 in terms of property values and are accompanied by the lowest energy consumption Q, [kWh].

3. Results and conclusions

After performing the calculations, a number of 164 variants (combinations of technological heat treatment parameters) resulted for each property out of the 289 possible ones, which simultaneously meet the conditions imposed for the four mechanical properties:

- mechanical resistance, Rm ≥ 290 MPa;
- yield strength, $Rp_{0.2}$ ≥ 240 MPa;

THE ANNALS OF "DUNAREA DE JOS" UNIVERSITY OF GALATI
FASCICLE IX. METALLURGY AND MATERIALS SCIENCE
No. 4 - 2023, ISSN 2668-4748; e-ISSN 2668-4756
Article DOI: https://doi.org/10.35219/mms.2023.4.05

• elongation at break, $A_5 \geq 11\%$;
• Brinell hardness, HB ≥ 78 MPa.

For each of these 164 combinations, the energy consumption required for thermal processing was calculated.

The program developed in MATLAB shows that whatever value we impose, within the limits of 164, to any of the four studied properties, we will obtain a number of variants for which the optimum in terms of total energy consumption can be determined by calculation.

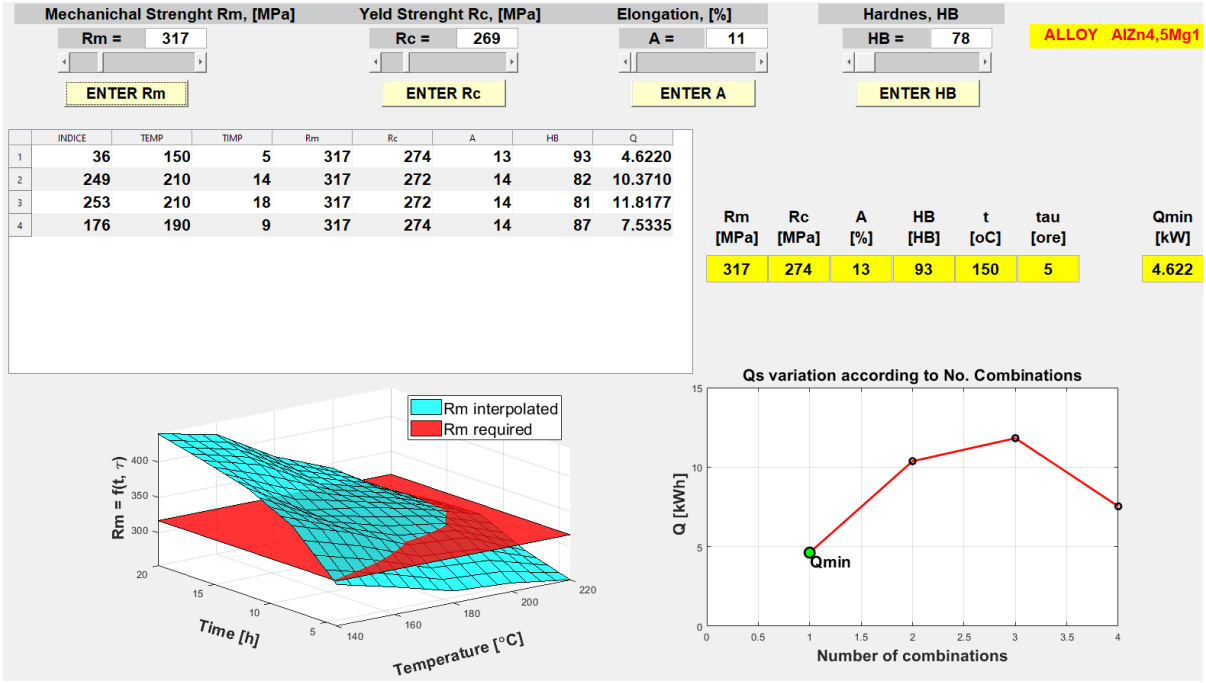

Fig. 1. *The values of the thermomechanical treatment parameters to obtain Rm = 317MPa*

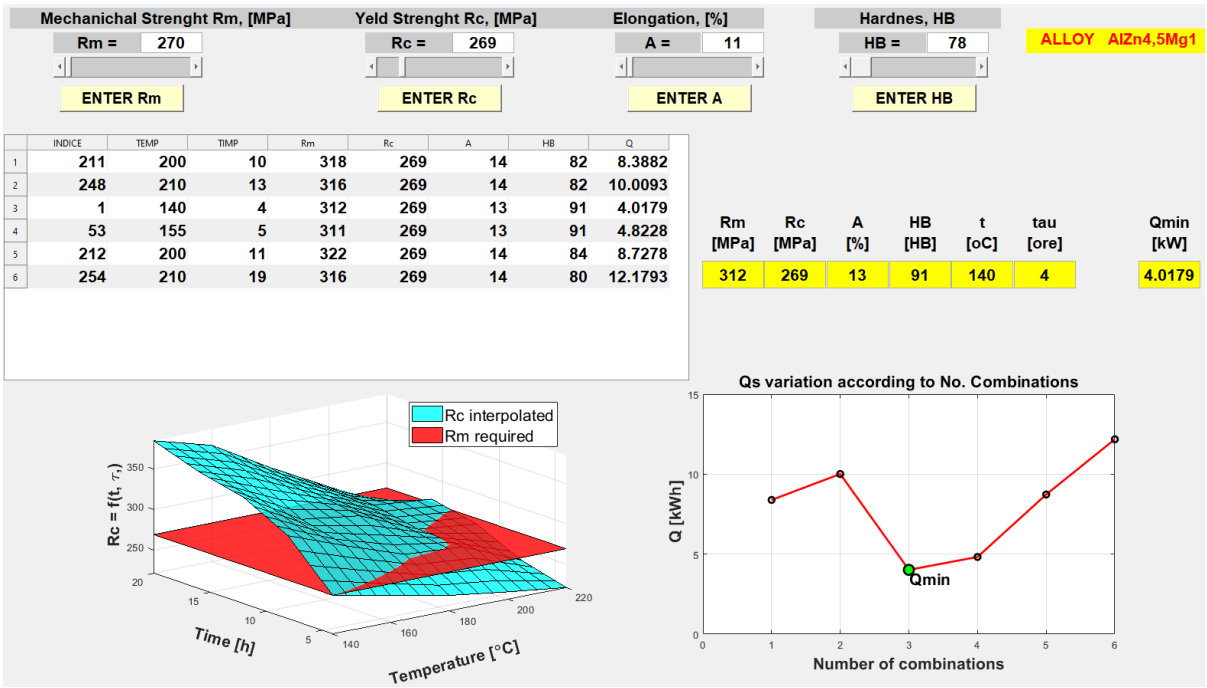

Fig. 2. *The values of the thermomechanical treatment parameters to obtain $Rp_{0.2}$ = 269 MPa*

THE ANNALS OF "DUNAREA DE JOS" UNIVERSITY OF GALATI
FASCICLE IX. METALLURGY AND MATERIALS SCIENCE
No. 4 - 2023, ISSN 2668-4748; e-ISSN 2668-4756
Article DOI: https://doi.org/10.35219/mms.2023.4.05

The graphical interface made with the help of this program allows viewing those possible situations and choosing a fairly large number of values for any of the four properties, as shown in Figures 1-4.

Figure 1 shows the situation when, for an imposed mechanical resistance of 317 MPa, the optimal option among the 5 possible, from the point of view of energy consumption, is the option in which the technological parameters of the heat treatment are: t = 150 °C, τ = 5 hours with an energy consumption of 4.622 kW.

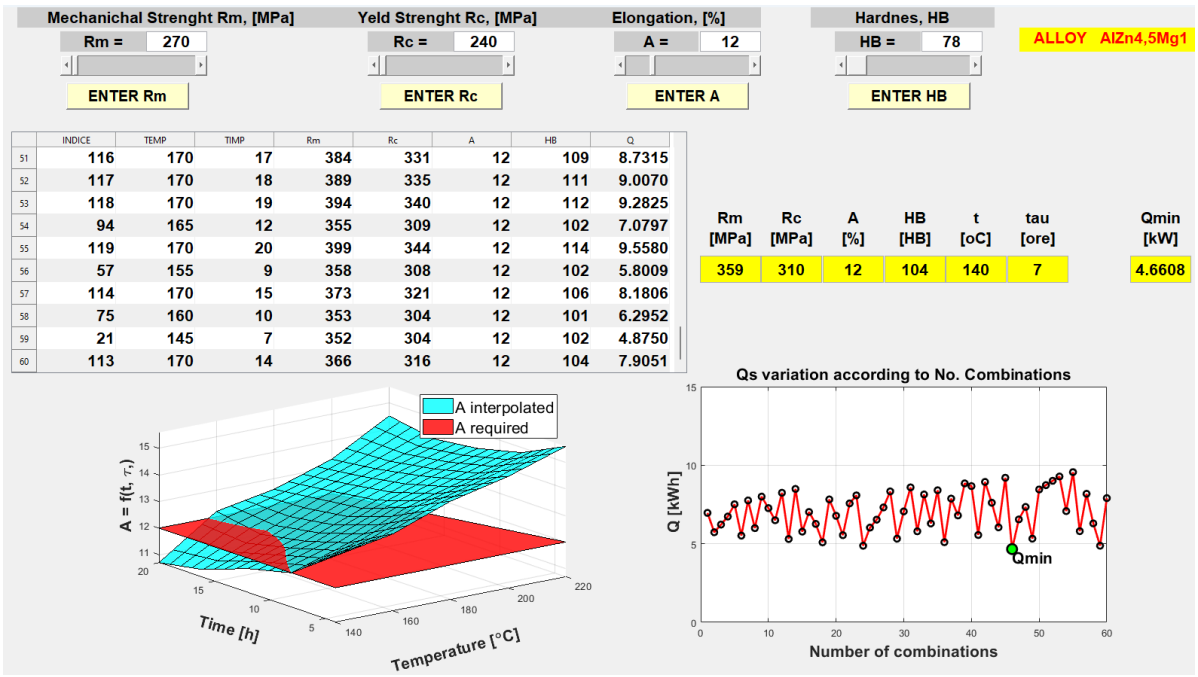

Fig. 3. *Values of heat treatment parameters to obtain A5 = 12 %*

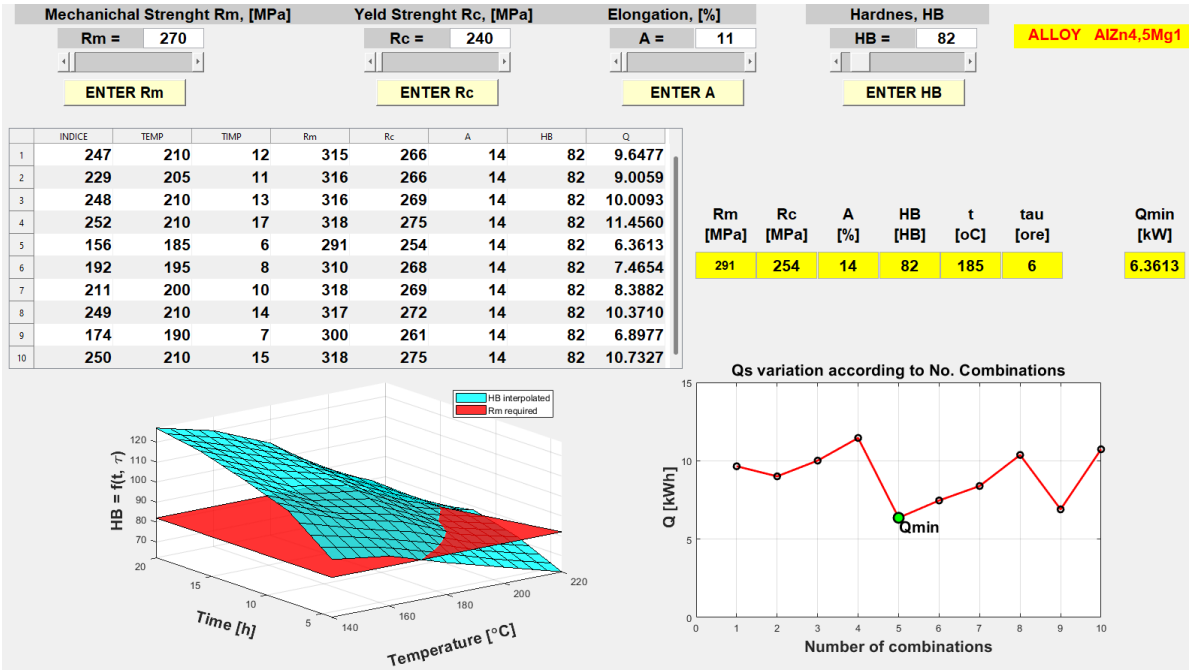

Fig. 4. *The values of the heat treatment parameters to obtain HB = 82 MPa*

THE ANNALS OF "DUNAREA DE JOS" UNIVERSITY OF GALATI
FASCICLE IX. METALLURGY AND MATERIALS SCIENCE
No. 4 - 2023, ISSN 2668-4748; e-ISSN 2668-4756
Article DOI: https://doi.org/10.35219/mms.2023.4.05

Figure 2 illustrates the situation in which, for a yield strength of 269 MPa, 6 possible cases appear, but among them the most economical is the one that has the following treatment parameters: t = 140 °C; τ = 4 hours; which give an energy consumption of Q_{tot} = 4.0179 kW.

Elongation at break of 12% is obtained from 60 possible variants, of which the optimal variant is the one with an energy consumption Q_{tot} = 4.66 kW for the optimal parameters shown in Figure 3, having the values: t = 140 °C, τ = 7 hours.

The HB hardness of 82 HB is obtained for t = 185 °C, τ = 6 hours, as shown in Figure 4, and the minimum value of Q_{tot} = 6.36 kW.

Also, with the help of this graphic interface, the values of thermal processing parameters can be highlighted, in tabular form, for those situations in which it is desired to obtain a certain value of one or more of the studied properties.

Simultaneously with the calculation of these values of the technological parameters of thermal treatment, the energy required to realize these variants is also calculated. Among these, the option with the lowest energy consumption is chosen and highlighted, i.e. the optimal option.

References

[1]. Ciucă I., Dumitriu S., *Modelarea şi Optimizarea Proceselor Metalurgice de Deformare Plastică şi Tratamente Termice*, Editura Didactică şi Pedagogică, Bucureşti, 1998.

[2]. Taloi D., *Optimizarea proceselor tehnologice – aplicaţii în metalurgie*, Editura Academiei, Bucureşti, 1987.

[3]. Şerban R., Dumitrescu T., *Metode de optimizare*, Editura Matrix Rom, Bucureşti, 1998.

[4]. Popescu D., Ionescu F., Dobrescu R., Ştefanoiu D., *Modelare în ingineria proceselor industriale*, Editura AGIR, Bucuresti, 2011.

[5]. Agus Sasmito, Mochammad Noer Ilman, Priyo Tri Iswanto, *Effects of rotational speed on the mechanical properties and performance of AA6061-T6 aluminium alloy in similar rotary friction welding*, Welding International, vol. 37, issue 9, 2023.

[6]. Ştefănescu D., Leca A., *et al.*, *Transfer de căldură şi masă. Teorie şi aplicaţii*, Editura didactică şi Pedagogică, Bucureşti, 1983.

[7]. Popa B., Man E., Popa M., *Termotehnică, agregate şi instalaţii termice*, Editura tehnică, Bucureşti, 1979.

[8]. Ghinea M., Fireţeanu V., *MATLAB - calcul numeric - grafică - aplicaţii*, Editura Teora, ISBN 973-601-275-1, Bucureşti, 1998.

[9]. Ghinea M., Fireţeanu V., *MATLAB. Calcul numeric. Grafică. Aplicaţii*, Ed. Teora, 2004.

THE ANNALS OF "DUNAREA DE JOS" UNIVERSITY OF GALATI
FASCICLE IX. METALLURGY AND MATERIALS SCIENCE
No. 4 - 2023, ISSN 2668-4748; e-ISSN 2668-4756
Article DOI: https://doi.org/10.35219/mms.2023.4.06

EVALUATION OF CORROSION BEHAVIOUR BY GRAVIMETRIC METHOD

Gina Genoveva ISTRATE[1,2], Ionica NEGRU[1], Daniela-Felicia BABENCU[1]

[1]Faculty of Engineering, [2]Interdisciplinary Research Centre in the Field of Eco-Nano Technology and Advance Materials CC-ITI, Faculty of Engineering, "Dunarea de Jos" University of Galati, Romania
47 Domneasca Street, RO-800008, Galati, Romania
e-mail: gina.istrate@ugal.ro

ABSTRACT

The study aims to evaluate the corrosion behaviour of two steels: BL245 and S235JR, produced at Liberty Steel Galati. BL245 is an alloy used in the oil and gas industry to manufacture pipes for pipeline transportation systems. S235JR is used to make hot finished hollow sections for construction. Gasoline, diesel and a 3.5% sodium chloride solution were chosen as corrosion environments for this study, considering the field of use of the two alloys (oil and construction). Corrosion assessment was analysed using the gravimetric method, which is based on weighing the samples before and after they were immersed for 7, 14, and 35 days in the above-mentioned corrosion environments. Based on the initial weighing and those recorded after the immersion periods, the mass variation of the samples was determined, and the corrosion rate and penetration index were calculated.

KEYWORDS: corrosion, gravimetric method, corrosion rate, penetration index, steel

1. Introduction

The concept of corrosion includes all chemical, electrochemical and biochemical processes resulting in spontaneous and continuous degradation of metal and alloy surfaces [1]. Chemical corrosion is triggered in dry gases, at high temperatures and in non-electrolyte solutions (corrosion is not accompanied by the appearance of an electric current) [2]. Electrochemical corrosion follows the laws of electrochemical kinetics and is accompanied by the appearance of an electric current (corrosion in electrolyte solutions or wet gases) [3]. Microbiological corrosion is a form of corrosion produced by living micro-organisms (bacteria, algae or fungi) often associated with the presence of organic substances and often accompanies electrochemical corrosion [4].

Corrosion is one of the most serious problems of modern society and an important scientific research topic. Corrosion of metals and materials is also an important problem both industrially and economically [5], with losses of billions of dollars every year [1]. A study published in 2016 on the cost of corrosion worldwide shows that the highest costs due to corrosion are found in Europe (28%), followed by the USA and China, as shown in Figure 1 [6].

Corrosion, as a chemical, electrochemical and biochemical process, has been studied over the years by several scientists, who have analysed in their experiments different alloys used in several branches of industry, using various methods and materials.

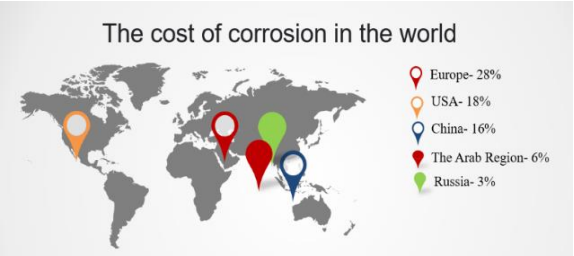

Fig. 1. *The cost of corrosion in the world in 2016* [6]

Some authors have analysed the corrosion behaviour of two types of carbon steel (OLC-45 and OL-37), used in the shipyards of Galati and Constanta. Two natural seawater salts collected from the Black Sea (Constanta area) and the Aegean Sea

THE ANNALS OF "DUNAREA DE JOS" UNIVERSITY OF GALATI
FASCICLE IX. METALLURGY AND MATERIALS SCIENCE
No. 4 - 2023, ISSN 2668-4748; e-ISSN 2668-4756
Article DOI: https://doi.org/10.35219/mms.2023.4.06

(Athen's area) were used as corrosion environments. By gravimetric method, following the calculations, it was found that the corrosion rate increases linearly with time and then remains constant, indicating that the corrosion product film formed on the surface of these two materials is more compact and provides better corrosion protection [1]. The results obtained throughout the study also revealed that the Aegean Sea, where both chloride and sulphate concentrations are almost double that of the Black Sea (indicating higher salinity) is a more corrosive environment compared to the Black Sea [7].

Some researchers have studied the behaviour of equipment in refineries and petrochemical plants in working environments. Samples of the steels from which refinery equipment is made were immersed in diesel fuel with sulphur compounds in a nitrogen atmosphere. The tests showed lower corrosion rates than measured and observed in the presence of air, which demonstrated the contribution of oxygen in the process fluid to the corrosion intensification, due to increased acidity caused by the oxidation reactions [8].

Another study on the corrosion of steels used in the manufacture of drill pipes and water-carrying pipes accompanying natural gas fields in contact with reservoir waters shows the salts dissolved in these waters greatly favour corrosion [9]. The retention time of the samples in the immersion environments was between 24-336 h. The results obtained indicate that the corrosion rate decreases with time and that the reservoir waters, due to the chlorides in their composition, show a high corrosion effect on the steel [10].

2. Materials and methods

The materials under investigation in this experiment are two types of steel manufactured at Liberty Steel Galati for industrial use: BL245 used in the oil industry to manufacture pipes for transportation systems and S235JR used in construction. According to the analysis bulletins issued by Total Materia, the chemical composition is shown in Table 1.

Table 1. *The chemical composition of steels BL245 and S235JR (%)* [11]

Proba	C	Cu	Mn	N	P	S	Si	V	Ti
BL245	0.22	-	1.20	0.05	0.025	0.015	0.45	0.05	0.04
S235JR	0.17	0.55	1.5	0.01	0.05	0.05	0.03	-	-

The corrosion environments gasoline, diesel and 3.5% NaCl solution were chosen for this study because of the areas in which the two types of steels are used, thus evaluating their corrosion resistance.

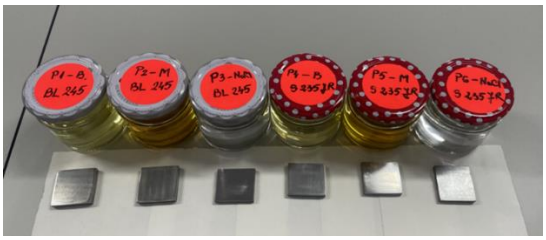

Fig. 2. *Samples prepared for immersion*

The first part of this experiment includes sample preparation. The six samples of the investigated materials have a parallelepiped shape and approximately equal dimensions (335 x 330 x 60 mm). Sanding was performed manually on three metallographic papers, starting with 800 grit, following 1000 grit and ending with 1200 grit. The purpose of sanding was to obtain perfectly flat, scratch-free, high-gloss surfaces. At the end of the sanding operation, the samples were washed under a water jet to remove traces of abrasive or metal dust, and then dried by wiping. The final stage of sample preparation included degreasing with acetone and blot drying with filter paper. Figure 2, below, illustrates the samples prepared for immersion.

The method chosen to assess corrosion compaction was gravimetric analysis. This method involves weighing the samples used in the experiment on an analytical balance before and after immersion in the corrosion environment [12]. Thus, the samples were weighed before and after each immersion period: 7, 14 and 35 days. Using the obtained data, after each weighing, the corrosion rate and penetration index were calculated using the formulas:

- corrosion rate:

$$V_{cor} = \frac{\Delta_m}{S \cdot t} \text{ [g/m}^2\text{h] [13]} \quad (1)$$

where:

Δ_m - change in mass [g];
S - area of sample [m^2];
t - immersion period [h].

- penetration index with the formula:

$$P = \frac{24 \cdot 365 \cdot V_{cor}}{1000 \cdot \rho} \text{[mm/an] [13]} \quad (2)$$

THE ANNALS OF "DUNAREA DE JOS" UNIVERSITY OF GALATI
FASCICLE IX. METALLURGY AND MATERIALS SCIENCE
No. 4 - 2023, ISSN 2668-4748; e-ISSN 2668-4756
Article DOI: https://doi.org/10.35219/mms.2023.4.06

V_{cor} - corrosion rate; ρ - density of steel, in our case, having the value of 7.4 g/cm³ for BL245 steel and 7.8 g/cm³ for S235JR.

3. Results and discussions

After calculations using the formulas for corrosion rate and penetration index, the results are shown in the graphs below.

From Figure 3, the BL245 alloy shows the corrosion rate with the highest value in 3.5% NaCl solution, regardless of the immersion period. It is also observed that in 3.5% NaCl solution, the corrosion rate is accelerated in the first immersion period of 7 days and then starts to decrease. In the case of gasoline, experimental data show an increase in the corrosion rate value with increasing immersion time. In diesel, a sharp increase in the corrosion values is observed in the second immersion period and then a decrease.

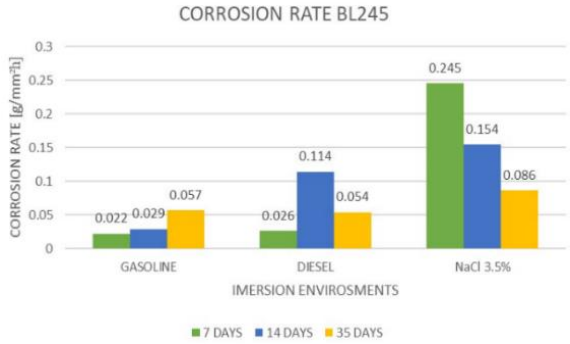

Fig. 3. *Corrosion rate values obtained for BL245*

Figure 4 shows the corrosion rate values obtained for the S235JR alloy. It can be seen that the corrosion rate is higher in the 3.5% NaCl solution that the other two environments in all immersion periods. In diesel, there was an increase in the first two immersion periods (7 and 14 days), followed by a sharp decrease in the third period (after 35 days). In gasoline, the corrosion rate is approximately equal, not exceeding a value of 0.027 [g/mm²*h].

Comparing the results obtained for the corrosion rate for the two materials, it is observed that the BL245 alloy shows a higher corrosion rate in all three environments, regardless of the immersion duration.

Figures 5 and 6 show the penetration index values for the two types of analysed steel in this study. Both graphs show that the highest values of the penetration index are recorded in the 3.5% NaCl solution in all immersion periods.

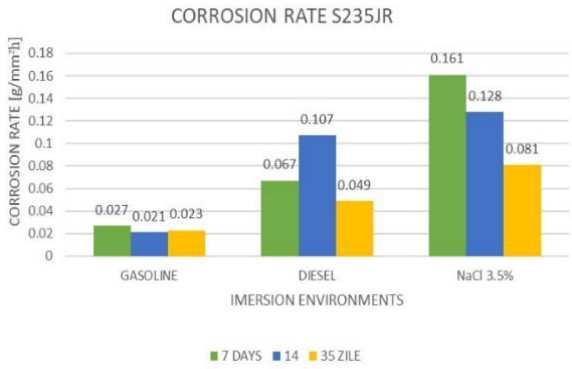

Fig. 4. *Corrosion rate values obtained for S235JR*

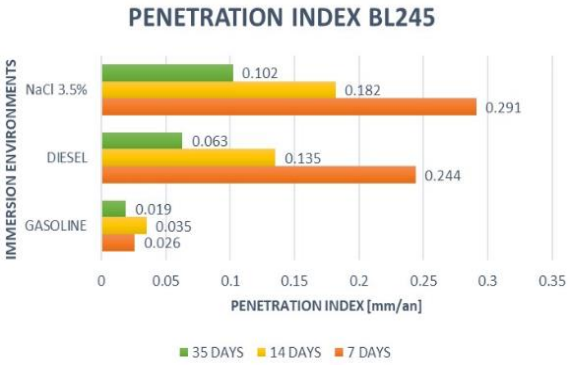

Fig. 5. *Penetration index values obtained for BL245*

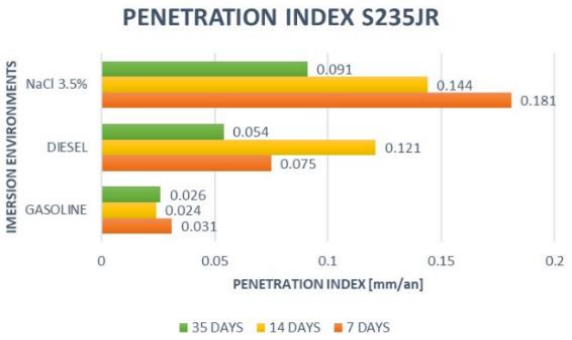

Fig. 6. *Penetration index values obtained for S235JR*

In comparison, it can be seen that the BL245 alloy shows the highest values, which increase with the immersion time. In diesel, the BL245 steel shows increasing values over time, while for the S235JR steel, the penetration index increases in value in the first two periods (7 and 14 days), sharply decreasing in the third period of the experiment. This may indicate the formation of continuous and adherent corrosion products on the surface of the material that provides better corrosion protection as concluded by

THE ANNALS OF "DUNAREA DE JOS" UNIVERSITY OF GALATI
FASCICLE IX. METALLURGY AND MATERIALS SCIENCE
No. 4 - 2023, ISSN 2668-4748; e-ISSN 2668-4756
Article DOI: https://doi.org/10.35219/mms.2023.4.06

other authors [1]. The same is observed for the BL245 steel in gasoline.

In order to determine whether the investigated materials are corrosion resistant, the conventional corrosion resistance scale for metals was consulted. Its values are: 0.001 mm/year for perfectly stable metals, 0.01-0.1 mm/year for stable metals, 0.1-1 mm/year for relatively stable metals and 10 mm/year for unstable metals [14]. The resulting values from graphs 5 and 6 indicate the following: both samples are stable in diesel, gasoline and relatively stable in 3.5% NaCl solution, as shown in Figure 7.

The corrosion products resulting from immersion in 3.5% NaCl solution are solid and adherent to the surface (which is also evident from the corrosion rate value which is higher in the first immersion period) shallow pitting type [13].

Also, for the samples immersed in NaCl 3.5%, the ferroxalic indicator was used to perform the drop test (Ewans), where the presence of Fe^{2+} ions and OH^- ions were detected. It was observed the variable and inhomogeneous appearance of pink and blue spots, indicating the following: the pink portion corresponds to the cathodic portion (presence of Fe^{2+} ions) and the blue portion to the anodic portion (presence of OH^- ions) [13], as shown in Figures 10 and 11.

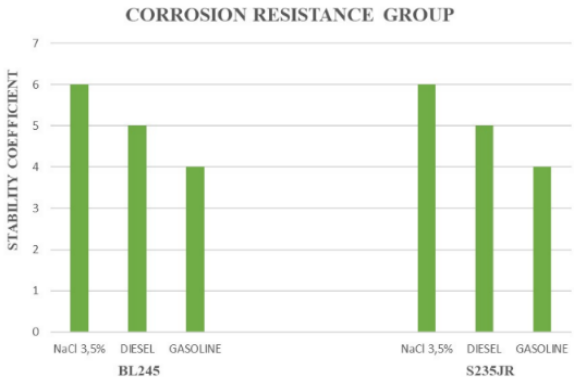

Fig. 7. *Corrosion resistace group for BL245 and S235JR*

Using the Kern optical microscope in the laboratory, optical scanning micrographs (X50) were taken of both samples undergoing the experiment, before and after 35 days of immersion in 3.5% NaCl solution, to better highlight the corrosion products, as shown in Figure 8 and 9.

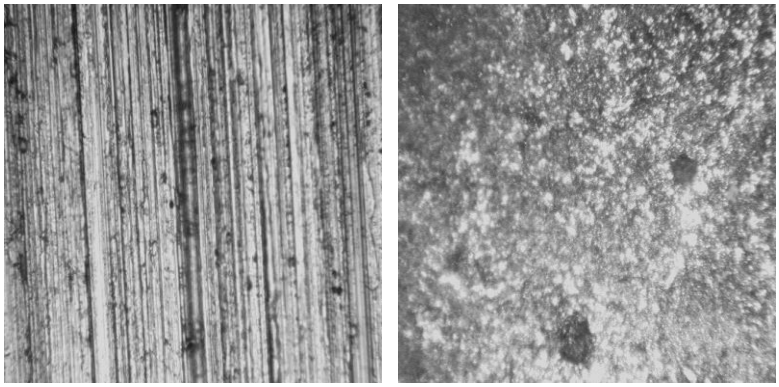

a) b)

Fig. 8. *Optical scanning micrographs(X50) for BL245: a) initial; b) after 35 days in 3.5% NaCl*

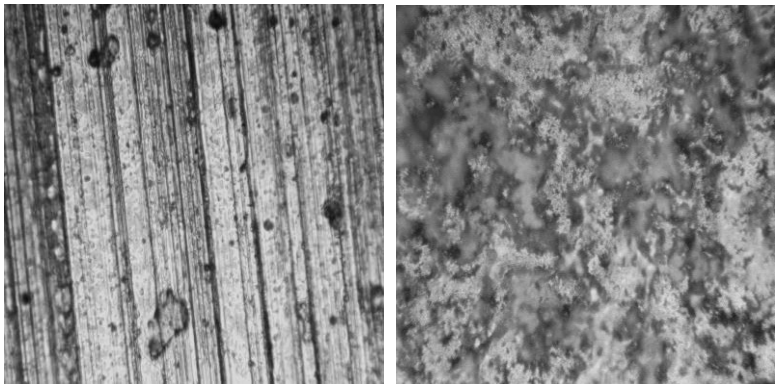

a) b)

Fig. 9. *Optical scanning micrographs(X50) for S235JR: a) initial; b) after 35 days in 3.5 % NaCl*

THE ANNALS OF "DUNAREA DE JOS" UNIVERSITY OF GALATI
FASCICLE IX. METALLURGY AND MATERIALS SCIENCE
No. 4 - 2023, ISSN 2668-4748; e-ISSN 2668-4756
Article DOI: https://doi.org/10.35219/mms.2023.4.06

Fig. 10. *The presence of ions of Fe^{2+} and OH^- for BL245*

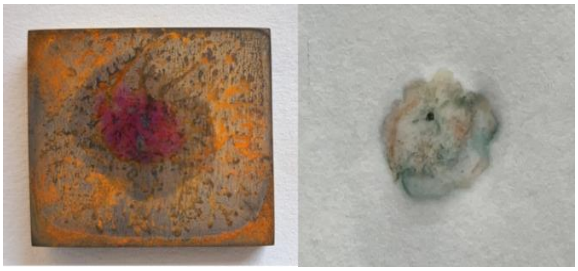

Fig. 11. *The presence of ions of Fe^{2+} and OH^- for S235JR*

4. Conclusions

In this experiment, the corrosion behaviour of the two steels BL245 and S235 JR, used in the oil industry and construction was studied. Gasoline, diesel and 3.5% NaCl solution were chosen as corrosion environments. Three immersion periods were established: 7, 14 and 35 days.

The gravimetric method was used for the study, calculating the corrosion rate and penetration index. After processing the obtained data, the following was discovered:

- the highest corrosion rate value is recorded after 7 days of immersion in 3.5% NaCl for the BL245 sample;
- the lowest corrosion rate value is recorded for the S235JR sample immersed in gasoline for 14 days;
- also, both alloys have a higher corrosion rate in 3.5% NaCl, regardless of the immersion period, indicating that the presence of chlorine in the immersion solution accelerates the corrosion rate;
- the highest penetration index values are observed for the BL245 alloy, regardless of the immersion time;
- the penetration index is higher in the 3.5% NaCl solution than in the other two immersion environments for all three periods of exposure to the corrosive environment;
- fitting the obtained data in the experiment in the conventional material strength scale, it is observed that both investigated steel alloys are stable in diesel and gasoline and relatively stable in 3.5% NaCl solution.

References

[1]. Lungu (Costea) M., *Corrosion of metals in the natural marine environment - summary of the doctoral thesis (Coroziunea metalelor in mediu marin natural - rezumatul tezei de doctorat)*, Technical University "Gheorghe Asachi" Iași, http://www.didactic.icpm.tuiasi.ro/studii/td/2012/TD_LunguM2012.pdf, 2012.

[2]. Pică E. M., Horovitz O., Niac G., Vermeșan E., Marta L., *Chemistry for engineers Vol 2 (Chimie pentru ingineri)*, U. T. Press Cluj-Napoca, ISBN 978-973-662-296-0, 2007.

[3]. Benea L., *General chemistry (Chimie general)*, Galați, Publishing House Academica, ISBN 978-973-8937-45, 2009.

[4]. ***, *API, Damage Mechanisms Affecting Fixed Equipment in the Refining Industry*, Recommended Practice 571 First Edition, American Petroleum Institute Standards department, 2003.

[5]. Bobină M., *Use of natural products as corrosion inhibitors for metals and alloys – doctoral thesis (Utilizarea produșilor naturali ca inhibitori de coroziune pentru metale și aliaje)*, Doctoral thesis of UPT, series 4, no. 76, Polytechnic Publishing House, 2014.

[6]. Koch G., Varney J., Thompson N., Moghissi O., Gould M., and Payer J., *International Measures of Prevention, Application, and Economics of Corrosion Technologies Study*, NACE Int., p. 1-3, 2016.

[7]. Aelenei N., Lungu M., Mareci D., Cimpoeșu N., *HSLA steel and cast iron corrosion in natural seawater*, Environ Eng Manag J., 10 (no. 12), p. 1951-1958, 2011.

[8]. Petrescu M. G., *Contributions to the improvement of the technical performance of the machines in the field of processing, transportation and storage of petroleum products – Summary of the habilitation thesis (Contribuții la îmbunătățirea performanțelor tehnice ale utilajelor din domeniul prelucrării, transportului și depozitării produselor petroliere) – Rezumat teză de abilitare)*, Petrol-Gaze University of Ploiești, 2020.

[9]. Oniciu L., Constantinescu E., *Electrochemistry and corrosion (Electrochimie și coroziune)*, Didactic and Pedagogical Publishing House, București, 1982.

[10]. Dumitrescu V., Moraru M., Cameniță I., Brânzoi I. V., Chiopescu A., *Corrosion kinetics of steels in sediment waters, (Cinetica coroziunii oțelurilor în ape de zăcământ)*, Rev. Chim. (București), 59, no. 4, 2008.

[11]. *******, https://www.totalmateria.com/page.aspx?ID=Home&LN=RO.

[12]. Skoog D., West D. M., Holler F. J., *Gravimetric Analysis. Fundamentals of Analytical Chemistry*, ed. 7th, Fort Worth: Saunders College Publishing Harcourt Brace, p. 71-96, 1996.

[13]. Mureșan A. C., Istrate G. G., *Elements of electrochemistry and corrosion. Course notes (Elemente de electrochimie si coroziune. Note de curs)*, Galati University Press, 2021.

[14]. Badea T., Popa M. V., Nicola M., *Corrosion science and engineering (Știința și ingineria coroziunii)*, Romanian Academy Publishing House, București, ISBN: 973-27-0856-5, 2002.

THE ANNALS OF "DUNAREA DE JOS" UNIVERSITY OF GALATI
FASCICLE IX. METALLURGY AND MATERIALS SCIENCE
No. 4 - 2023, ISSN 2668-4748; e-ISSN 2668-4756
Article DOI: https://doi.org/10.35219/mms.2023.4.07

FLOW SIMULATION OF FLUID UNDER PRESSURE, THROUGH PIPES FOR OIL AND GAS TRANSPORT

Beatrice TUDOR, Mirela NOUR
"Dunarea de Jos" University of Galati, Romania
e-mail: beatrice.bodor@ugal.ro

ABSTRACT

The work presents a simulation of the flow of liquids under pressure, through pipelines intended for the transport of oil and natural gas. The simulation was done using the SOLIDWORKS program. Computational Fluid Dynamics (CFD) simulation facilitates the analysis of complex fluid flow problems involving liquid-gas, fluid-solid, or fluid-fluid interactions. CFD allows us to design products and systems that meet fluid flow and heat transfer requirements.

KEYWORDS: pipes, simulation, fluid flow

1. Introduction

Romania has a gas exploitation industry developed on the basis of its own resources, ranking among the top 12 gas industries in the world. But due to a long period of exploitation (over 90 years), the natural flow and pressure decline is felt, as in any extractive industry.

The natural gas industry, both extraction and transport, presents a series of risks for the workers in these activities (work accidents), for the population of neighbouring towns (major accidents) and for the environment [1, 3].

The process of gas transportation through pipelines and their distribution to consumers is subject to specific regulations in all the member countries of the European Union.

The legislation in force aims to create distribution networks, dimensioned according to the source-consumption balance, which will ensure the prospects for the development of consumption and supply over time.

From the point of view of the technological elements within the production, transport, distribution and use of natural gas, pipelines fall into the following pressure ranges:

- high pressure > 6 bar (collector, transport pipes and technological installations related to oil sites);
- medium pressure, between 2 and 6 bar (gas supply systems);
- low pressure, between 0.05 and 2 bar (gas supply systems);
- low pressure < 0.05 bar (gas supply systems) [2].

2. Flow simulation of liquids under pressure through pipes

The flow simulation was carried out using the SOLIDWORKS program.

Computational Fluid Dynamics or CFD, is a technique that deals with the analysis and study of fluid flow fields through numerical analysis. SOLIDWORKS is a CFD software designed to provide dynamic feedback on fluid flow. It has parametric optimization capability, and can automate the design and analysis process to discover the best design in SOLIDWORKS CAD.

Computational Fluid Dynamics (CFD) is an analysis tool for multiphysics systems that simulates the behavior of fluids taking into account their thermodynamic properties, using numerical models [4].

CFD simulation facilitates the analysis of various complex fluid flow problems involving liquid-gas, fluid-solid or fluid-fluid interactions. The program uses advanced solutions to transform physical laws from differential equations into algebraic equations, and to solve them as efficiently as possible. Engineers and analysts use computers to simulate the free-flowing fluid and its interaction with surfaces.

CFD simulations are widely used in many fields to analyse fluid flow and heat transfer of design components, to inform design decisions and ultimately to bring products to market in a timely

THE ANNALS OF "DUNAREA DE JOS" UNIVERSITY OF GALATI
FASCICLE IX. METALLURGY AND MATERIALS SCIENCE
No. 4 - 2023, ISSN 2668-4748; e-ISSN 2668-4756
Article DOI: https://doi.org/10.35219/mms.2023.4.07

manner. shorter. CFD software provides various tools for optimizing system design by simulating fluid flow and its free movement over surfaces.

System-level design requires optimization of fluid behavior and material strength. SOLIDWORKS is a 3D CAD (Computer Aided Design) design software for modeling 3D, 2D plans and assemblies. The software offers a wide range of solutions for designing, simulating, manufacturing, publishing and managing design process data [6].

This program allows the simulation of different liquids, gases and oil, for different engineering scenarios. Some common applications involve flow through manifolds, heat exchangers, electronic cooling. Fluid-structure interactions (FSI) refers to the interaction between a fluid flow and a solid structure.

When a fluid flows around or through a solid object, it can exert forces on the object, which can cause it to deform or vibrate. This involves deformation or vibration of the object and can affect the flow of the fluid, leading to changes in the behavior of the fluid.

For certain applications, the fluid in a project may contain solid or liquid particles. The behavior of these particles, and the fluid that interacts with them, is essential to the operation and effectiveness of the system. With the help of the SOLIDWORKS program, we can analyse the behavior of the particles and we can see results, regarding the erosion and accumulation of the particles in the system. Based on the material properties, high flow and other physical characteristics of the system design, this can be analysed.

A combination of fluid dynamics and mechanics is used to analyse FSI. Computational fluid dynamics (CFD) can be used to model the fluid flow, while finite element analysis (FEA) can be used to model the solid structure. The coupling of these two simulations allows studying the effects of FSI [5].

FSI analysis is important for the design and optimization of structures and systems that interact with fluids. By modeling and analysing FSI, engineers can optimize the design of structures to reduce the effects of fluid-induced vibration or deformation, and improve the performance and safety of these structures.

Computational fluid dynamics is the simulation and analysis performed in computer-aided design (CAD) software to calculate the flow of liquids or gases in or around a product.

It is a multiphysics solution because it involves the interaction of several phenomena, including fluid dynamics, thermodynamics, and conservation of momentum. Like finite element analysis (FEA), the fluid volume is divided into smaller elements that are composed into a matrix. CFD has many uses beyond product development and aerodynamics, such as weather forecasting and visual effects.

CFD allows us to design products and systems that meet fluid flow and heat transfer requirements.

Using CFD software, we can calculate:

- the speed and direction of particles inside or outside the model;
- the temperature;
- the pressure;
- vortices, which give an indication of the rotational movement of the fluid at different points.

These results can be calculated and displayed in a model. When displayed in fluid, the results can be represented as contours of different colours, particles, a direction field, or fluid lines. To facilitate the understanding of the behavior and to speed up the calculations, the results can be displayed at a specific cutting plane [6].

The CFD can be executed by following these steps:

1. It starts with a model. Before entering the CFD simulation environment, the 3D CAD part or assembly to be analysed is created. The geometry can be native to the CAD software or imported.

2. The fluid domain is defined, the liquid or gas in the simulation can be either internal, such as water flowing through a piping system, or external, such as air flowing over the exterior surfaces of a vehicle. The volume region is defined and the material properties of the fluid are applied, including density, viscosity, coefficient of thermal expansion, specific heat capacity, and thermal conductivity.

3. Boundary conditions are established. They represent fluid movement at the inlet and outlet of the analysis model. Fluid motion can be defined by flow velocity, inlet and outlet pressure, and mass flow rate. For internal flow, additional boundary conditions include eddy inlet (velocity with both normal and radial components), rotating wall to simulate moving components, and gravity.

4. Thermal conditions are included. Thermal loads in the system can be defined as heat flux, heat flux, convection, and convection radiation.

5. The analysis is carried out.

6. The system is optimized, providing instant feedback to improve the model.

Unsteady and complicated flow can cause pipe and circuit damage due to the velocity of liquid flow.

Pipeline flow is applied in various industries such as chemical industry and petroleum industry, pipeline manufacturing engineering, power plants, biomedical engineering.

In the chemical industry, these problems can occur when transporting oil and gas.

THE ANNALS OF "DUNAREA DE JOS" UNIVERSITY OF GALATI
FASCICLE IX. METALLURGY AND MATERIALS SCIENCE
No. 4 - 2023, ISSN 2668-4748; e-ISSN 2668-4756
Article DOI: https://doi.org/10.35219/mms.2023.4.07

Phase distribution is an important component in the design of engineering structures, due to its impact on flow rates and pressure rise.

The simulation was carried out in several stages:

The first stage of the simulation was the realization of the objective to be tested and analysed (Fig. 1).

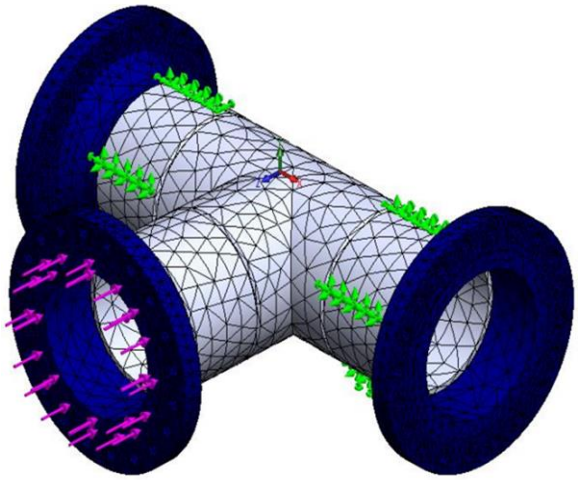

Fig. 1. *Making the model, for analysis and testing*

At this stage, the way it deforms and how the stresses appear, for a T-shaped pipe, was simulated. At the inlet we have a pressure of 10 bar, and the gas is distributed to the other pipes.

I have considered that there are bolts on each flange and the restrictions are as follows:

- each flange is fastened with screws and between the two pipes we have a welding connection.

The second stage of the simulation is presented in (Fig. 2).

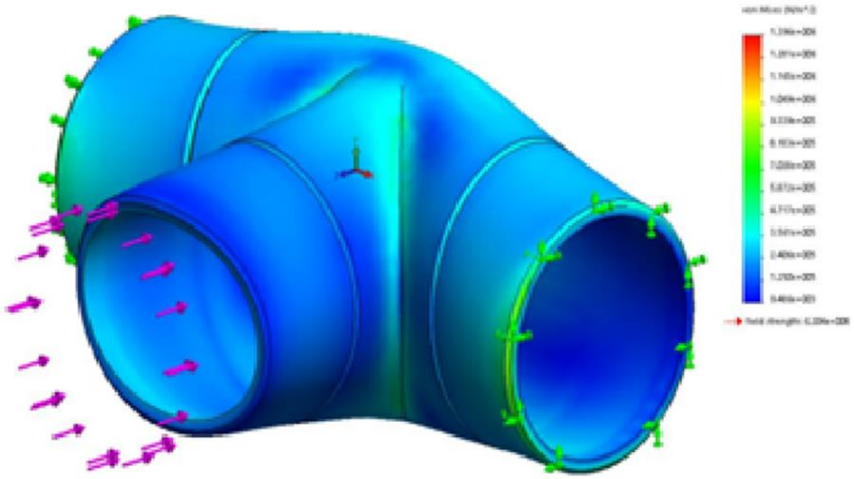

Fig. 2. *Distribution of stresses in pipes*

At this stage we realized the distribution of von Mises stresses in the pipes. I should point out that the model is enlarged several times, to intuitively show the user where deformations occur.

In the third stage of the simulation (Fig. 3) we presented the maximum displacements and their distribution.

THE ANNALS OF "DUNAREA DE JOS" UNIVERSITY OF GALATI
FASCICLE IX. METALLURGY AND MATERIALS SCIENCE
No. 4 - 2023, ISSN 2668-4748; e-ISSN 2668-4756
Article DOI: https://doi.org/10.35219/mms.2023.4.07

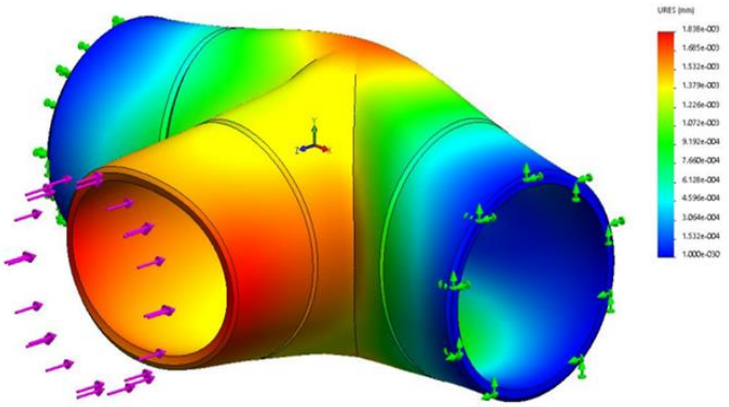

***Fig. 3.** Distribution of displacements*

For the maximum displacements and their distribution, it is observed that somewhere at the virtual intersection of the weld lines, a maximum displacement and the displacement is approximately $1.8*10^{-3}$ mm, which is acceptable for the high pressure used in pipeline testing.

The fourth part of the simulation is done on a model of the shape of the part (Fig. 4).

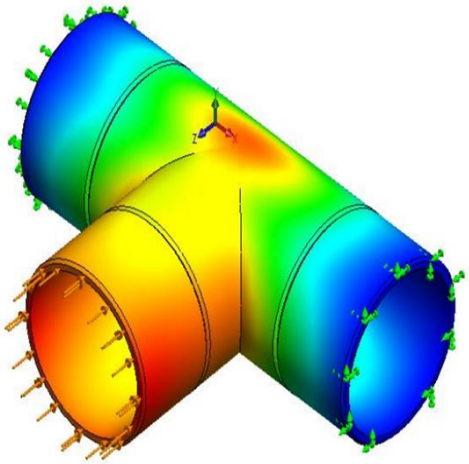

***Fig. 4.** Movements without changing the shape of the piece*

3. Conclusions

CFD simulation is important for the design and optimization of structures and systems that interact with fluids.

Using fluid-structure interaction (FSI) modeling and analysis, engineers can optimize the design of structures to reduce the effects of fluid-induced vibration or deformation and improve the performance and safety of these structures.

SOLIDWORKS, allows the simulation of various liquids, gases and oil for various engineering scenarios. Fluid - structure interactions (FSI) refer to the interaction between a fluid flow and a solid structure.

CFD simulation facilitates the analysis of complex fluid flow problems involving liquid-gas, fluid-solid, or fluid-fluid interactions.

An unstable and complicated flow can cause damage to the pipes and the circuit due to the speed of the liquid flow.

The flow of liquids and gases through pipes is applied in various industrial fields, such as the chemical industry and the petroleum industry, pipeline engineering, power plants, biomedical engineering.

References

[1]. Oroveanu T., Stan A., Talle V., *Transportul Petrolului*, Editura Tehnică Bucureşti, 1985.
[2]. Trifan C., *et al.*, *Activitatea Gazieră din România*, Editura Universităţii "Petrol-Gaze" din Ploieşti, 2008.

[3]. Tudorache V. P., *et al.*, *Maintenance of the Romanian National Transportation System of Crude Oil and Natural Gas*, DAAAM, 2013.

[4]. Tudorache V. P., *Research on optimization of the National System of Pipeline Crude Oil Transportation in Romania*, Teza de Doctorat, 2014.

[5]. Ungureanu O., Drug, V., *Transportul Gazelor Naturale*, Editura Tehnică Bucureşti, 1971.

[6]. Prakash R., Akhtar M. J., Behera R. K., Parida S. K., *Design of a Three Phase Squirrel Cage Induction Motor for Electric Propulsion System*, Third International Conference on Advances in Control and Optimization of Dynamical Systems, Kanpur, India, March 13-15, 2014.

THE ANNALS OF "DUNAREA DE JOS" UNIVERSITY OF GALATI
FASCICLE IX. METALLURGY AND MATERIALS SCIENCE
No. 4 - 2023, ISSN 2668-4748; e-ISSN 2668-4756
Article DOI: https://doi.org/10.35219/mms.2023.4.08

PROPERTIES OF DENTAL ZIRCONIUM OXIDE AND METAL-CERAMIC: A COMPARATIVE STUDY

Camelia-Nicoleta NEGUŢ[1], Marius BODOR[2], Viorica GHISMAN[2], Alina Crina MUREŞAN[2,*]

[1]Faculty of Engineering, [2]Interdisciplinary Research Centre in the Field of Eco-Nano Technology and Advance Materials CC-ITI, Faculty of Engineering, "Dunarea de Jos" University of Galati, 47 Domneasca Street, RO-800008, Galati, Romania
e-mail: alina.muresan@ugal.ro

ABSTRACT

Zirconium oxide which is intended to be a material that is quite attractive due to its key characteristics, i.e. aesthetic appearance and mechanical resistance, compared to dental metal-ceramics, which to date it has proven to be a satisfactory solution for many of the requirements in the dental market. Understanding the characteristics and properties of these materials provides a starting point for new trends in the development or improvement of solutions for various medical conditions. The research topic of this work aims to understand the characteristics and properties of two categories of materials that are so competitive in the field of dental restoration. For this purpose, the behaviour of some dental crowns made of zirconium oxide and metal ceramic was evaluated in order to obtain experimental data regarding microhardness, corrosion and roughness, before and at different time intervals of immersion in a solution of corrosion, respectively saline solution (3.5% NaCl).

KEYWORDS: zirconium oxide, metal-ceramic, morphology, roughness, hardness, corrosion behaviour

1. Introduction

Although bioceramics are among the oldest materials used by humans in medical applications, their widespread use occurred only after 1960. A possible cause could have been the impossibility of obtaining a pure bioceramic until that date that would respect entirely the vital biocompatibility conditions, and the second cause could be related to the mechanical properties of ceramics, so controversial at the time [1]. Only after 1960, by the discovery of new properties, such as for example a high resistance to wear, a coefficient reduced friction or even the property of being inert in biological environments, allowed the use of these materials to be much more extensive in the medical field. Medical ceramics or bioceramics is a biomaterial used in various constructions of medical nature starting from the construction of prostheses, bone substitutes, stimulators and up to tooth reconstruction. The medical industry with all its cutting-edge techniques would be unthinkable without it the use of bioceramic materials, due to their valuable properties and biocompatibility [1].

Zirconium oxide (ZrO_2) (Zircona or Zirconia) is a very studied and exploited ceramic material due to its excellent mechanical properties such as tear resistance, high hardness, high density, chemical inertness [2, 3]. Pure zirconia is an oxide that presents three symmetry polymorphisms: monoclinic, temperature unstable tetragonal and cubic. So that this oxide can be used for the manufacture of various components, it is necessary to be stabilized with oxides such as yttrium oxide (Y_2O_3) [4-6]. Fabrication of pure zirconia components is not possible due to spontaneous failure. The addition of stabilizing oxides is important because it allows the tetragonal shape to be maintained at room temperature. Different oxides such as yttrium oxide (Y_2O_3), calcium oxide or magnesium oxide, may be added for stabilization, allowing the tetragonal shape zirconia to exist at room temperature after sintering.

The advantages of using dental crown made of zirconium are: it does not taste like metal and does not cause inflammation of the gums like lyserium;

THE ANNALS OF "DUNAREA DE JOS" UNIVERSITY OF GALATI
FASCICLE IX. METALLURGY AND MATERIALS SCIENCE
No. 4 - 2023, ISSN 2668-4748; e-ISSN 2668-4756
Article DOI: https://doi.org/10.35219/mms.2023.4.08

they are primarily aesthetic due to a physical principle, namely that zirconium is penetrated by light from all angles, a fact that gives the dental work a special aesthetic aspect. Zirconium dental crown have some disadvantages, such as: very expensive, not being an affordable option for many patients. Not only the material itself, but also the sophisticated equipment required to process the material leads to a high final cost. Another disadvantage is related to the fact that zirconium has an affinity for dental plaque, and poor hygiene is one of the causes of implant failure [7-11].

The present research study intends to understand the characteristics and properties of two categories of materials that are so competitive in the field of dental restoration. For this scope it was evaluate the behaviour of dental crowns made of zirconium oxide and metal ceramic in order to obtain experimental data regarding microhardness, corrosion and roughness, before and at different time intervals of immersion in a solution of corrosion, respectively saline solution (3.5% NaCl).

2. Materials and methods

The biomaterials of the case study were zirconium oxide and dental metal ceramics (SuperPorcelain EX-3 ceramic and Cr-Ni alloys), two commonly used materials for dental prostheses (Fig. 1).

Fig. 1. *Samples of zirconium oxide ceramics and metal ceramics (MC) (A3.5B-NoritakeEX-3-Cr-Ni alloy)*

Zirconium is a powder under the trade name Katana Zirconia-Noritake, type II/class 4 with coefficient of thermal expansion of 9.8 x 10^{-6}/K (25-500 °C).

Metal ceramic is a Noritake Super Porcelain EX-3, a ceramic that is superior to others dental ceramics because its coefficient of thermal expansion (CTE) remains stable over time of repeated baking. It is compatible with precious, semi-precious, non-precious silver-free alloys for metal-ceramic prostheses. Its fluorescence is ideal, and it is very resistant to greening induced by silver. This combination of characteristics makes this type of dental ceramic an ideal choice for ceramic restorations [12]. Some characteristics of Noritake Super Porcelain EX-3 ceramics are: very good tear resistance; the coefficient of expansion is 12.14 x 10^{-8}/K (50-500 °C) (the range of thermal expansion coefficients of compatible alloys with EX-3 ceramic is 13.44 x 10^{-6}/K. As a result, the alloys that fall into these ranges are compatible with EX-3 ceramic); prevention of silver-induced greening. Greening of EX-3 porcelain is minimal, even in furnaces contaminated with silver; ideal fluorescence-successfully imitates the fluorescence of natural teeth [13].

2.1. Surface morphology

The morphology of the surfaces for studied materials was evaluated with an optical microscope type Kern Optics-OLM 171, as well as with a scanning electron microscope type TESCAN VEGA coupled with energy dispersive X-Ray analysis.

2.2. Microhardness and roughness

The tests for the evaluation of microhardness were carried out with an INSIZE equipment–Digital Micro Vickers Hardness Tester and the roughness of the tested surfaces were carried out with an INSIZE-ISR C002 equipment.

2.3. Corrosion tests

The corrosion resistance (corrosion rate and penetration index) was evaluated using the gravimetric method. The determinations were made with the KERN type analytical balance (accuracy of 0.0001 g). Zirconium oxide and dental metal ceramics was tested in 3.5% NaCl solution after different times of immersion (at immersion time, after five days and 12 days).

3. Results and Discussion

3.1. Surface morphology

The morphology of the tested samples before immersion and after different times of immersion in 3.5% NaCl solution is presented in Figures 2-7. Microscopic observations from the initial stage revealed surfaces with a porous appearance, as well as some smoother surfaces, depending on the material processing technique in the laboratory. The blurriness of the images in certain samples is due to the irregularity of the samples.

THE ANNALS OF "DUNAREA DE JOS" UNIVERSITY OF GALATI
FASCICLE IX. METALLURGY AND MATERIALS SCIENCE
No. 4 - 2023, ISSN 2668-4748; e-ISSN 2668-4756
Article DOI: https://doi.org/10.35219/mms.2023.4.08

The results of microscopic observations revealed similar aspects regarding surface porosity. No representative surface changes were found.

To determine the spectrum of the chemical composition of the studied materials, observations were made using the scanning electron microscope coupled with energy dispersive X-ray spectroscopy.

SEM microscopy was used to complete information about morphology of the surfaces after corrosive tests (Figures 8-9).

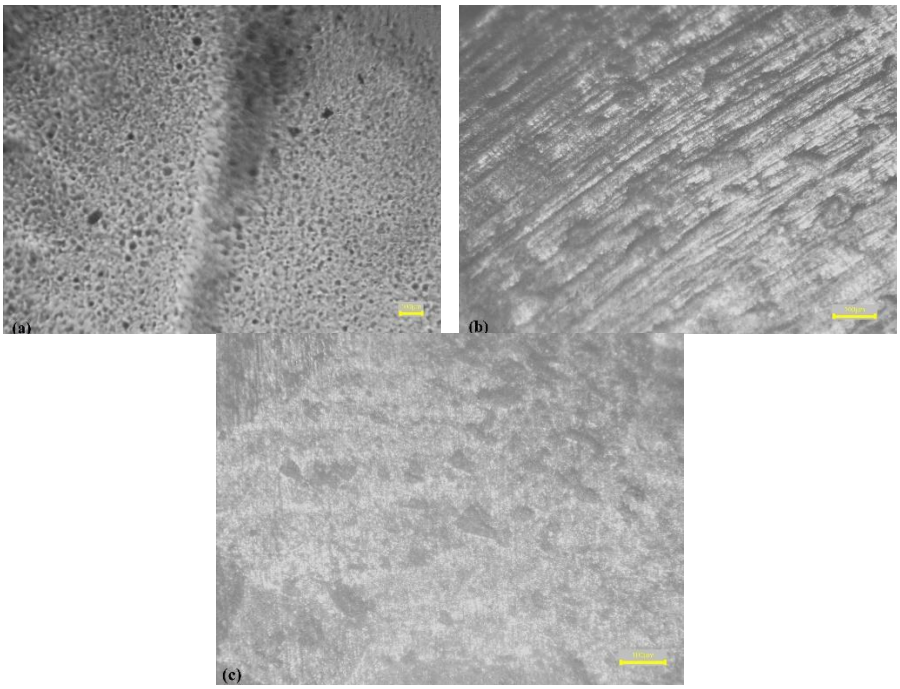

Fig. 2. *Optical microscopy of ZrO_2 samples before immersion in corrosive solution: (a) - sample 1; (b) - sample 2 and (c) - sample 3*

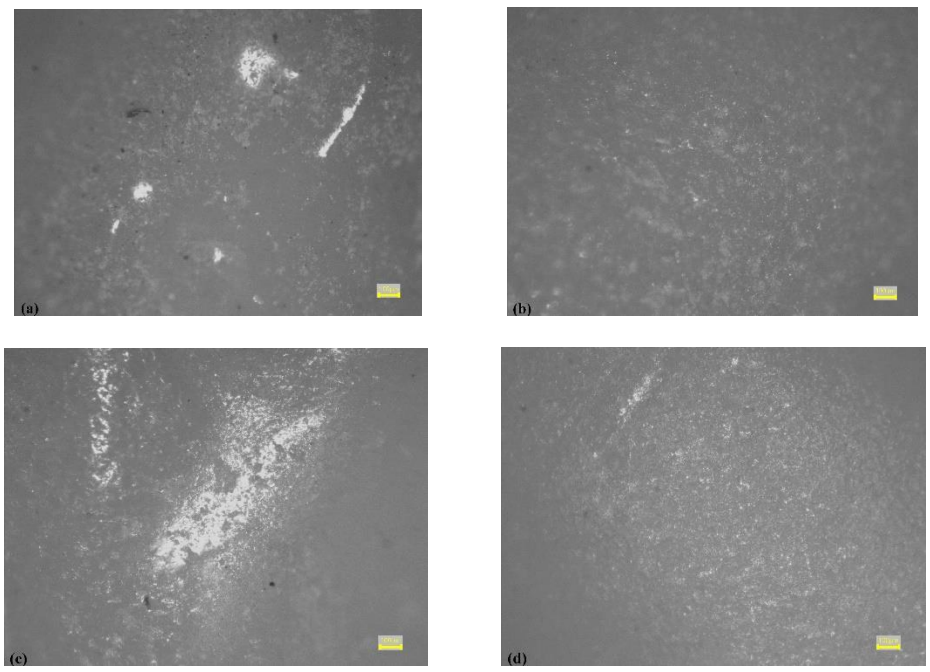

Fig. 3. *Optical microscopy of MC samples before immersion in corrosive solution: (a) - sample 1; (b) - sample 2; (c) - sample; (d) - sample 4*

THE ANNALS OF "DUNAREA DE JOS" UNIVERSITY OF GALATI
FASCICLE IX. METALLURGY AND MATERIALS SCIENCE
No. 4 - 2023, ISSN 2668-4748; e-ISSN 2668-4756
Article DOI: https://doi.org/10.35219/mms.2023.4.08

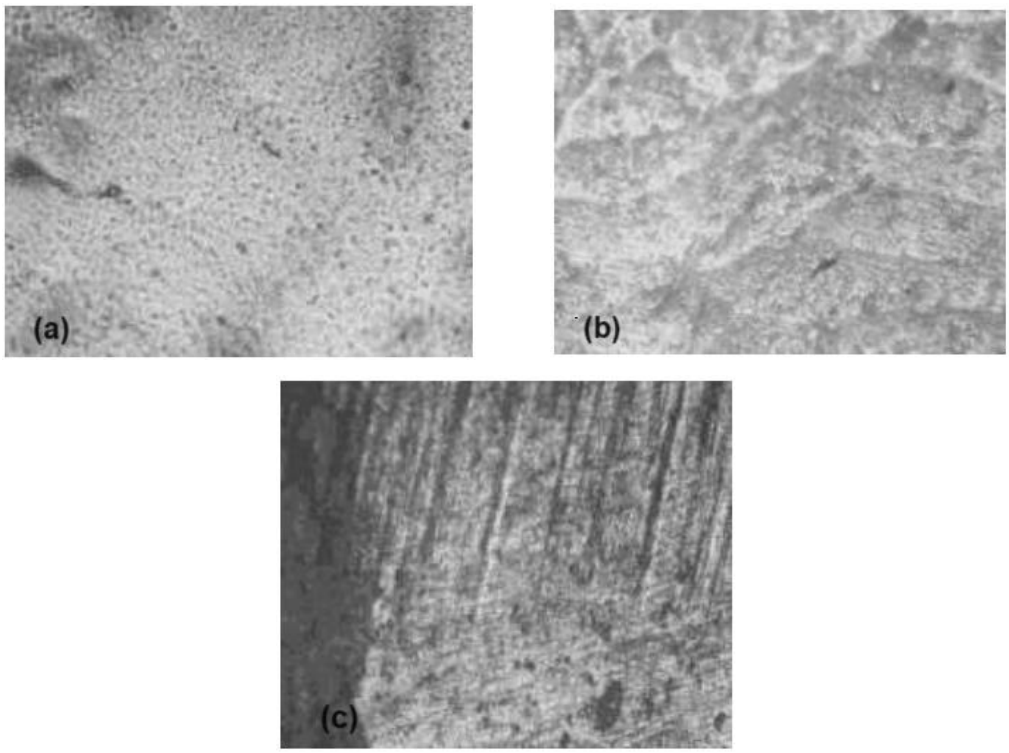

Fig. 4. *Optical microscopy of ZrO_2 samples after five days of immersion in 3.5 % NaCl solution: (a) - sample 1; (b) - sample 2 and (c) - sample 3*

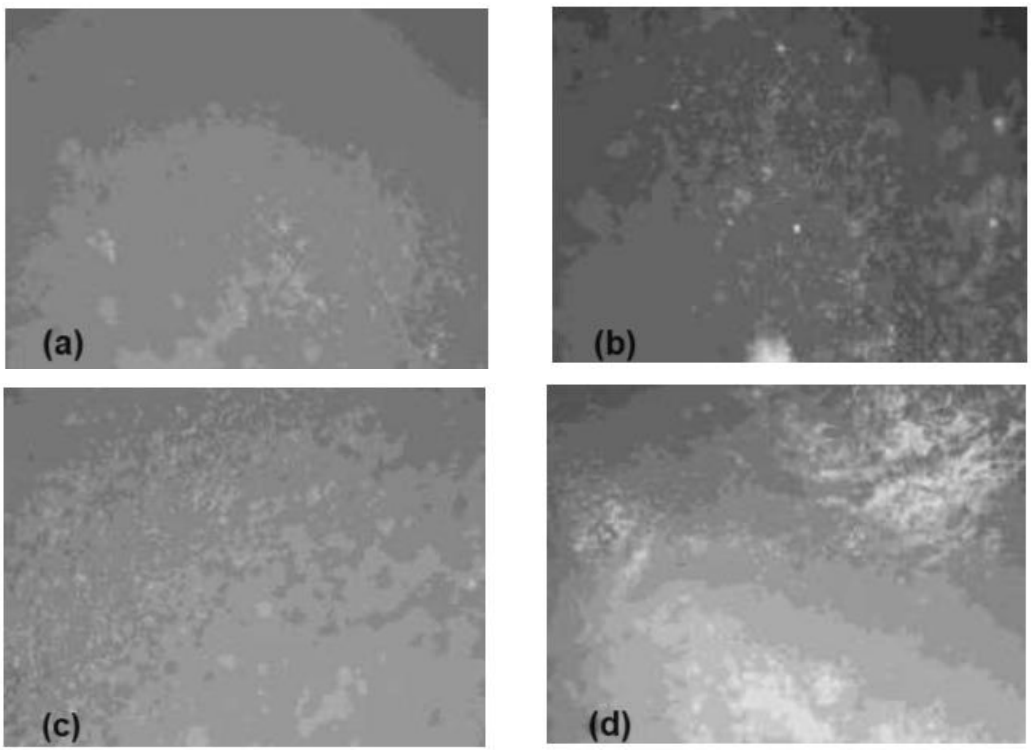

Fig. 5. *Optical microscopy of MC samples after five days of immersion in 3.5 % NaCl solution: (a) - sample 1; (b) - sample 2; (c) - sample; (d) - sample 4*

THE ANNALS OF "DUNAREA DE JOS" UNIVERSITY OF GALATI
FASCICLE IX. METALLURGY AND MATERIALS SCIENCE
No. 4 - 2023, ISSN 2668-4748; e-ISSN 2668-4756
Article DOI: https://doi.org/10.35219/mms.2023.4.08

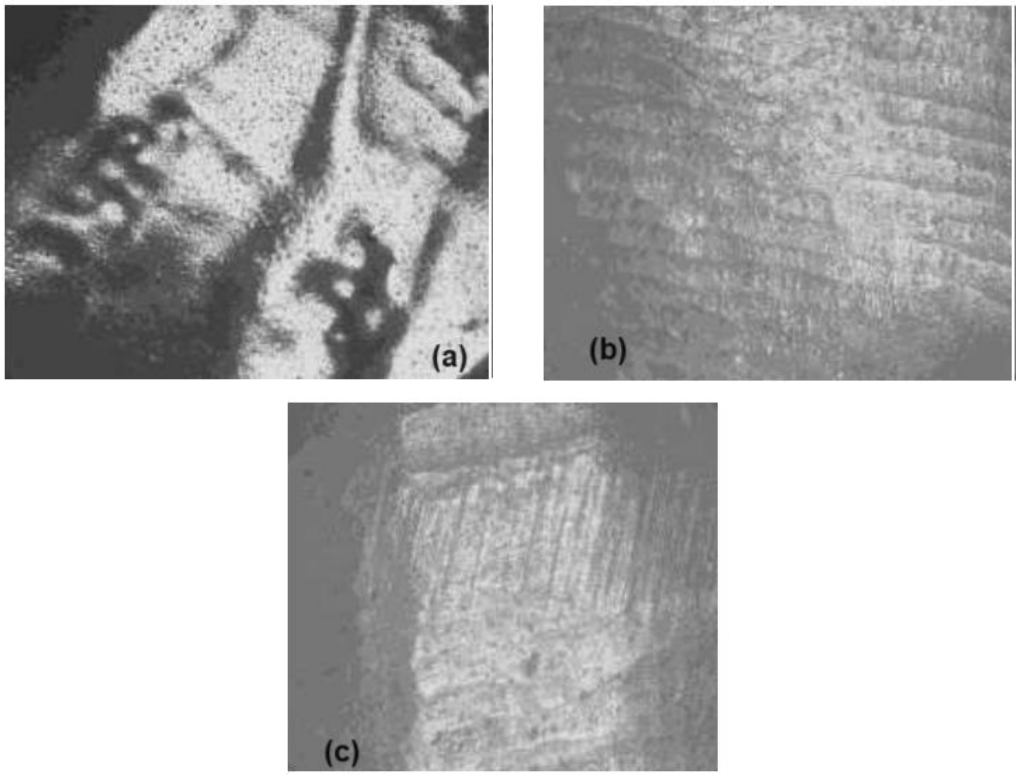

Fig. 6. *Optical microscopy of ZrO_2 samples after 12 days of immersion in 3.5 % NaCl solution: (a) - sample 1; (b) - sample 2 and (c) - sample 3*

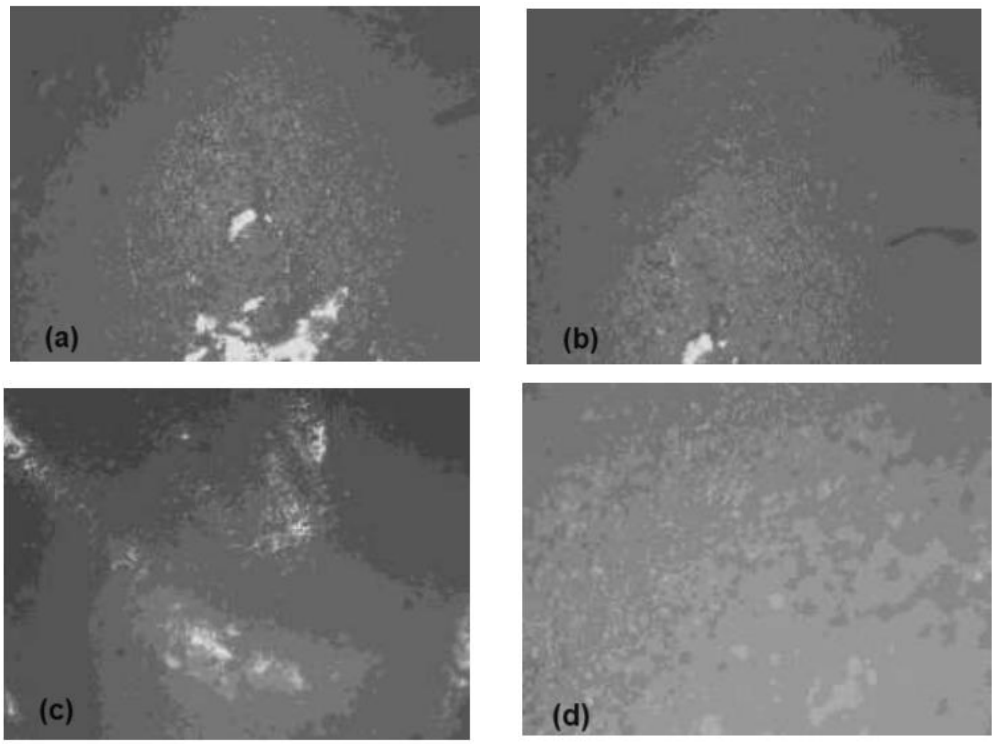

Fig. 7. *Optical microscopy of MC samples after 12 days of immersion in 3.5 % NaCl solution: (a) - sample 1; (b) - sample 2; (c) - sample; (d) - sample 4*

THE ANNALS OF "DUNAREA DE JOS" UNIVERSITY OF GALATI
FASCICLE IX. METALLURGY AND MATERIALS SCIENCE
No. 4 - 2023, ISSN 2668-4748; e-ISSN 2668-4756
Article DOI: https://doi.org/10.35219/mms.2023.4.08

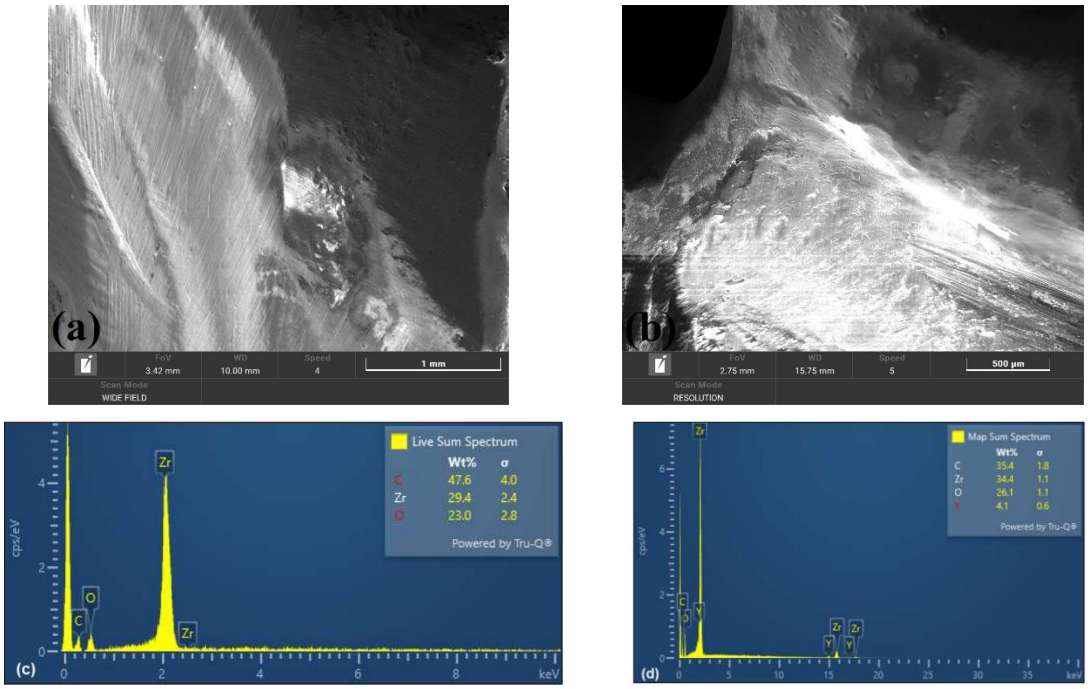

Fig. 8. *SEM -EDX of ZrO_2 samples after 5 days of immersion in 3.5 % NaCl solution: (a, c) - sample 2; (b, d) - sample 3*

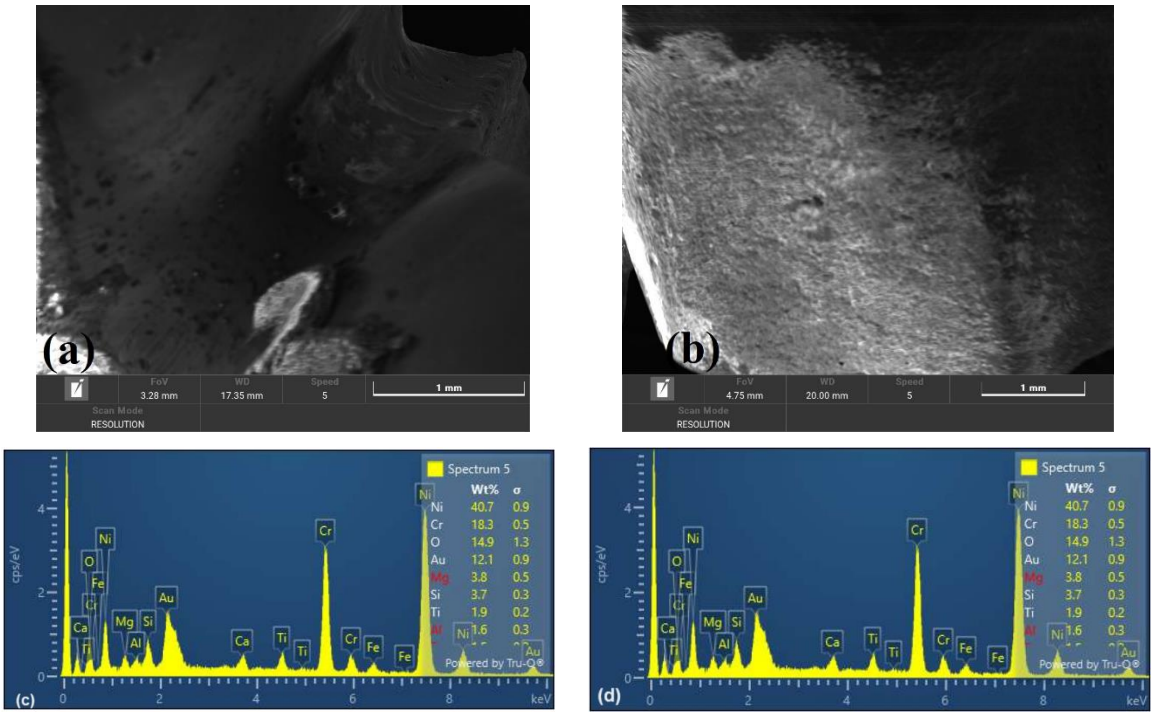

Fig. 9. *SEM -EDX of MC samples after 5 days of immersion in 3.5 % NaCl solution: (a, c) - sample 1; (b, d) - sample 2*

From the analysis of the samples, variations can be observed in the composition of the ZrO_2 ceramic that could be determined by an incorrect preparation of the product in the laboratory.

Regarding the spectral analysis for metal-ceramics, the composition of the alloy is similar for all tested samples.

THE ANNALS OF "DUNAREA DE JOS" UNIVERSITY OF GALATI
FASCICLE IX. METALLURGY AND MATERIALS SCIENCE
No. 4 - 2023, ISSN 2668-4748; e-ISSN 2668-4756
Article DOI: https://doi.org/10.35219/mms.2023.4.08

3.2. Microhardness and roughness

Microhardness testing was performed on two types of materials, zirconium oxide and metal-ceramic. During the testing it was used a load of 0.5 kgf, at an exposure time of 10 seconds. The results obtained for the evaluation of microhardness are presented in Table 1.

The results vary both depending on the quality of the tested material and depending on the technological conditions of manufacturing the respective sample.

Table 1. *Microhardness values for the tested materials*

Tested material	Microhardness, HV
ZrO_2 – sample 1	153.2
ZrO_2 – sample 2	121.8
ZrO_2 – sample 3	118.4
MC – sample 1	215.2
MC – sample 2	7.3
MC – sample 3	853.1

The roughness value can be calculated either on a profile (line) or on a surface (area, zone). The parameter for the profile roughness, Ra, is the most frequent [13]. The values of the tested samples before corrosion tests are presented in Table 2.

Table 2. *Roughness values for the tested materials*

Tested material	Roughness values, µm
ZrO_2 – sample 1	0.510
ZrO_2 – sample 3	0.780
MC – sample 1	0.250
MC – sample 2	1.961

After corrosion tests the microhardness and roughness of the samples was not evaluated because the samples surfaces were not uniform.

3.3. Corrosion tests

Corrosion testing was performed using the gravimetric method in 3.5% NaCl corrosive solution.

The gravimetric methods for corrosion evaluation have applications in the study of general corrosion (uniform and generalized) of metals, applying to solutions of electrolytes or substances non-polar organics as a corrosive environment. Using this method, the mass variation (gravimetric index), corrosion rate and average penetration depth (penetration index) of corrosion in the mass of the metal/alloy can be determined [15].

The gravimetric index (Kg) is expressed in $g/m^2 \cdot h$ or in $mg/dm^2 \cdot day$ and represents the weight variation of a metal/material sample (Δm) corroded, per unit area (S) in unit time (t), according to relation (1). The gravimetric index can express the weight loss of the material, but it can also express the increase in weight of the material if products appear on its surface adheres to the surface or forms corrosion-resistant oxide films.

$$K_g = \frac{\Delta m}{S \cdot t} \quad (1)$$

The corrosion rate can also be calculated with the relationship (2):

$$v_{corr} = \frac{K \cdot W}{A \cdot t \cdot d} \quad (2)$$

where: v_{corr} represents the corrosion rate; K is a constant depending on the unit of measurement of the corrosion rate; W is mass loss; A is the surface of the corroded material; t is the exposure time of the material to corrosion and d represents the density of the corroding material.

The penetration index (P) expresses the average depth of penetration of the corrosive medium into the metal mass or the average decrease in the thickness of the exposed sample (d) in the unit of time (t) and is expressed in mm/year (relation 3):

$$P = \frac{d}{t} \quad (3)$$

Relation (4) represent the relationship between the gravimetric index and the penetration index:

$$P = \frac{K_g}{d} \cdot 8.760 \quad (4)$$

where: d - metal/material density (g/cm^3); K_g - gravimetric index ($g/m^2 \cdot h$); 8.760 - the number of hours in a year [16].

To test the corrosion behavior, the samples were immersed for 12 days in 3.5% NaCl corrosive solution. Table 3 shows the physico-chemical parameters of the corrosion solution. After 5 days of immersion in 3.5% NaCl solution, the samples were weighed again, and the results indicate a slight weight loss of the tested samples. The same tendency was observed after 12 days of immersion. Since no significant mass loss was observed during this interval, the tests will be continued for a period of three and six months for further observations.

THE ANNALS OF "DUNAREA DE JOS" UNIVERSITY OF GALATI
FASCICLE IX. METALLURGY AND MATERIALS SCIENCE
No. 4 - 2023, ISSN 2668-4748; e-ISSN 2668-4756
Article DOI: https://doi.org/10.35219/mms.2023.4.08

Tabel 4. *Physico-chemical parameters of corrosive solution*

pH	5.77
Potential, V	+73.82
Conductivity, mS	57
Salinity, g/L	41.4
Total dissolved solids, ppt	38.1

The values of corrosion rate and penetration index are presented in Table 5 (density of ZrO_2 was 6.05 g/cm^3 and density of metal-ceramic tested samples was 0.9 g/cm^3 - according to technical data give from producers).

The penetration index is correlated with a conventional scale of resistance of metals to corrosion (Table 6), which provides indicative information on the corrosion tendency of a material in a corrosive environment [17].

Tabel 5. *Corrosion rate and penetration index for tested samples*

Sample tested	Corrosion rate after five days of immersion, mm/an	Penetration index after five days of immersion	Corrosion rate after 12 days of immersion, mm/an	Penetration index after 12 days of immersion
ZrO_2 - sample 1	0.1508	0.218	0.213	0.308
ZrO_2- sample 2	0.0402	0.058	0.040	0.057
ZrO_2-sample 3	0.0006	0.0008	0.185	0.267
MC - sample 1	0.506	4.925	5.388	52.326
MC 2 - sample 2	1.216	11.835	33.835	329.32
MC 3 - sample 3	0.234	2.277	10.557	102.75
MC 4 - sample 4	2.676	26.052	91.65	892.06

Table 6. *Conventional scale of corrosion resistance of materials*

Corrosion resistance	Mass losses, g/m^2·h	Penetration index P, mm/year	The stability coefficient
Perfectly stable	< 0.007	< 0.001	1
Very stable	0.007 – 0.035	0.001 – 0.005	2
	0.035 – 0.07	0.005 – 0.01	3
Stable	0.07 – 0.35	0.01 – 0.05	4
	0.35 – 0.7	0.05 –0.1	5
Relatively stable	0.7 – 3.5	0.1 –0.5	6
	3.5 – 7.0	0.5 –1.0	7
Little stabile	7.0 - 35	1.0 – 5.0	8
	35 - 70	5.0 – 10.0	9
	> 70	>10	10

In correlation with Table 6 the zirconium samples vary from the Perfectly stable category < 0.007 with a stability coefficient of 1 in the first five days of immersion in corrosive solution and respectively the Very stable category 0.007 – 0.035/0.035 – 0.07, with a stability coefficient of 2 and 3. For MC samples, they range from the Very stable category 0.007 – 0.035/0.035 – 0.07. with a stability coefficient of 2 and Stable 0.07 – 0.35 with a stability coefficient of 3.

4. Conclusions

From practical observations the greatest advantage of zirconium crowns is their resistance. The hardness of the material makes this type of dental crown an optimal choice for both teeth and molars, being able to withstand very high forces. On the other hand, it has been found that they can last as long as metal-ceramic works.

The hardness of ceramics made of zirconium oxide ZrO_2 (zirconia) is very high, if one takes into account the correct technological process of preparing ceramics from ZrO_2, namely baking in sintering furnaces at the right temperature and the necessary time. Thus, the hardness of the material can be affected in the sense that it can vary in places, as was observed in the case of samples from this study.

Metal-ceramic crowns are very durable and are widely used in molar areas, where the mastication process is more concentrated. The hardness of metal-ceramic dental works is also increased, due to the metal support, but failure to comply with the indications for wearing, maintenance of dental works

can cause major defects such as cracking of the ceramic or even its detachment from the metal support.

The spectral analysis of the composition of the zirconium oxide ceramic identified a slight difference in composition between the studied samples, a fact that could also be related to the technological process, in the sense of faulty homogenization.

The porosity of the surfaces observed in the microscopic analysis, both optical and SEM, indicates a medium sintering biscuit firing, in the case of samples of zirconium oxide. In the case of samples with a smooth surface, the ceramic indicates a high sintering The roughness of the surfaces in the case of ceramic masses indicates that there was no proper vibration and condensation of the ceramic mass layers.

From the first investigations, a reduced mass loss was found. The samples have been shown to be resistant to corrosion and should be left for a longer interval of at least three-six months to observe a significant change.

From the results obtained in the corrosion tests, it was observed that the ZrO_2 samples had a lower mass loss. The same was found to be the corrosion rate in the five- and 12-days interval respectively, implying a lower penetration index.

References

[1]. Shi D., *Introduction to Biomaterials*, Beijing: Tsinghua University Press, 2005.

[2]. Geuzens E., Vanhoyland G., Hayen J. D., *Synthesis of Tetragonal Zirconia*, Nanoparticles via Angoeus Solitions Gel Method, Key Engineering Materials, vol. 264-268, p. 343-346, 2004.

[3]. Winnubst A. J. A., Keizer K., Burggraaf A. J., *Mechanical properties and fracture behaviour of ZrO_2-Y_2O_3 ceramics*, Twente University of Technology, 1982.

[4]. Janyavula S., Lawson N., Cakir D., Beck P., Ramp L. C., Burgess J. O., *The wear of polished and glazed zirconia against enamel*, The Journal of Prosthetic Dentistry, vol. 109, p. 22-29, 2013.

[5]. Preis V., Weiser F., Handel G., Rosentritt M., *Wear performance of monolithic dental ceramics with different surface treatments*, Quintessence International, vol. 44, p. 393-405, 2013.

[6]. Sripetchdanond J., Leevailoj C., *Wear of human enamel opposing monolithic zirconia, glass ceramic, and composite resin: an in vitro study*, The Journal of Prosthetic Dentistry, vol. 112, p. 41-50, 2014.

[7]. Yoon S., Jung H. J., Knowles J. C., Lee H. H., *Digital image correlation in dental materials and related research: A review*, Dental Materials, vol. 37, issue 5, p. 758-771, 2021.

[8]. Dewan H., *Clinical Effectiveness of 3D-Milled and 3D-Printed Zirconia Prosthesis - A Systematic Review and Meta-Analysis*, Biomimetics, vol. 8, issue 5, article nr. 394, 2023.

[9]. Schweiger J., Bomze D., Schwentenwein M., *3D Printing of Zirconia–What is the Future?*, Current Oral Health Reports, vol. 6, p. 339-343, 2019.

[10]. Khanlar L. N., Salazar Rios A., Tahmaseb A., Zandinejad A., *Additive Manufacturing of Zirconia Ceramic and Its Application in Clinical Dentistry: A Review*, Dental Journal, vol. 9, 104, 2021.

[11]. Pjetursson B. E., Valente N. A., Strasding T., Zwahlen M., Liu S., Sailer I., *A systematic review of the survival and complication rates of zirconia-ceramic and metal-ceramic single crowns*, Clinical Oral Implants Research, vol. 29, p. 199-214, 2018.

[12]. ***, https://www.kuraraynoritake.eu/ro/super-porcelain-ex-3.

[13]. ***, *Revista Asociației Naționale a tehnicienilor dentari*, an VI, no. 1(24), ISSN1583-2937, p. 8., 2007.

[14]. ***, https://ro.wikipedia.org/wiki/Rugozitate.

[15]. Sherif El-Sayed M., *Electrochemical and Gravimetric Study on the Corrosion and Corrosion Inhibition of Pure Copper in Sodium Chloride Solutions by Two Azole Derivatives*, International Journal of Electrochemistry Science, vol. 7, p. 1482-1495, 2012.

[16]. Mureşan A. C., Istrate G. G., *Elemente de electrochimie şi coroziune. Note de curs*, Editura Galati University Press, ISBN: 978-606-696-219-3, 2021.

[17]. Badea T., *eta al.*, *Ştiinţa şi ingineria coroziunii*, Editura Academiei Române, Bucureşti, 2004.

THE ANNALS OF "DUNAREA DE JOS" UNIVERSITY OF GALATI
FASCICLE IX. METALLURGY AND MATERIALS SCIENCE
No. 4 - 2023, ISSN 2668-4748; e-ISSN 2668-4756
Article DOI: https://doi.org/10.35219/mms.2023.4.09

CHOLESTEROL IN HUMAN BODY: IMPORTANCE AND DOSAGE

Florentina GÎRBOIU[1], Alina Crina MUREŞAN[2,*]
[1]Faculty of Engineering, [2]Interdisciplinary Research Centre in the Field of Eco-Nano Technology and Advance Materials CC-ITI, Faculty of Engineering, "Dunarea de Jos" University of Galati,
47th Domneasca Street, RO-800008, Galati, Romania
e-mail: alina.muresan@ugal.ro

ABSTRACT

For a healthy life, specialists recommend us to take care of what food we eat and to what extent we do it and how we approach a satisfying lifestyle. Cholesterol is not a bad thing, but often, in large quantities it becomes dangerous for human body. The medical world is faced with frequent changes in the concept of "normal values" of cholesterol, but also with a continuously developing pharmaceutical industry in this field, and the tendency is in this sense, towards an individualized treatment. This aspect in presented in our paper, which aims to describe the role of cholesterol in the functioning of human body; preventing the occurrence of heart diseases due increasing the level of cholesterol in the body and creating a healthy lifestyle that can reduce cholesterol levels. The paper presents some case studies on laboratory investigations of values cholesterol that includes determinations, studying and the research of medical equipment (Cobas Integra 400 Plus analyser), but also the results obtained during practice in the medical analysis laboratory.

KEYWORDS: cholesterol, low-density lipoproteins (LDL), high-density lipoproteins (HDL), Cobas Integra 400 Plus

1. Introduction

Cholesterol is a lipid with the chemical formula $C_{27}H_{46}O$. Is based on sterol with molar mass 386.65 g/mol, melting point 146-147 °C and boiling point 200 °C (Figure 1). Cholesterol is identified in the cell membrane and in the tissues, it is transported in blood and concentrates at the level of the spinal cord of the liver, the brain, and at the level of the plate of atheroma forms cholesterol stones leading to atherosclerosis. It is not absorbed through food having an important role in the body. It is the precursor to various processes produced in body [1-3]. In excess, cholesterol (cholesterolemia) leads to vascular diseases: cerebrovascular, cardiac, ocular, very life-threatening accidents.

Two fractions of cholesterol are known: LDL cholesterol represented by low-density lipoproteins, in popular terms "bad" cholesterol and HDL cholesterol, or the "good" cholesterol represented by high-density lipoproteins.

Cholesterol is the factor responsible for several biochemical processes produced in our body when its values are within normal limits. When the values cholesterol is modified beyond normal limits, problems appear, being perceived as "the enemy of health". Of the two forms of HDL cholesterol and LDL cholesterol, we note the fact that LDL (bad cholesterol) deposits on the walls of the arteries and can cause heart diseases in case which doctors will recommend a more complex analysis called a lipidogram [4].

Researchers from the Heart Research Institute in Newtown Australia found that there is a close connection between high cholesterol and the risk of developing a mental illnesses dementia. Statistical data from over 1 million patients worldwide were analysed, with ages below 65 years, in 17 international studies and confirmed a worsening of the incidence cognitive decline for high cholesterol. Mild cognitive impairment can evolve into severe forms in correlation with high cholesterol. The normal cholesterol level is 5.17 mmol/L, and every increase of one mmol/L causes dementia to worsen by 8%. 75% of cholesterol is manufactured in the liver, in dietary fats and 25% comes directly from food. According to statistics, as patients grow and age, it is expected that in 30 years of from now on the numbers will double, reaching an average of 850 thousand sufferers of dementia [5].

THE ANNALS OF "DUNAREA DE JOS" UNIVERSITY OF GALATI
FASCICLE IX. METALLURGY AND MATERIALS SCIENCE
No. 4 - 2023, ISSN 2668-4748; e-ISSN 2668-4756
Article DOI: https://doi.org/10.35219/mms.2023.4.09

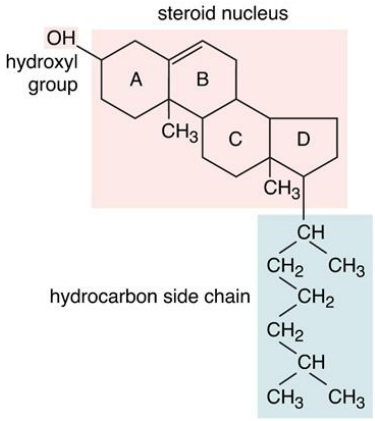

Fig. 1. *Chemical structure of cholesterol Source: https://www.britannica.com/science/cholesterol*

Teenagers and young people up to the age of 30 with a level increased cholesterol, risks the appearance of heart diseases: heart attack; of vascular accidents cerebral or other cardiovascular diseases in middle age. People who have managed to lower cholesterol levels to normal values, before reaching 40 years. Increased cholesterol inherited from families with pathologies such as heart attacks or accidents vascular, is more dangerous than cholesterol caused by unbalanced diet, because evolves rapidly. The risk of inheriting cholesterol is higher when both parents have it suffer from conditions related to blood lipids ≈ 75% [6].

The role of cholesterol in the body are maintaining cellular integrity; regulation of blood viscosity; bile synthesis; in the metabolism of hyposoluble vitamins A, K, E and vitamin D; decisive is also the precursor role of steroid hormone synthesis reactions, (cortisol and aldosterone in the adrenal glands) and sex hormones (progesterone, testosterone, estrogen); intervenes at the level of nerve synapses and in the immune system, including against cancer [7-9].

Cholesterol consumed in excess (fats) leads to adverse effects and most importantly among these is the atherogenic effect causing the vascular abnormality also called atherosclerosis. This is caused by the thickening of the lumen of the arteries by the deposition of lipids on the wall's vessels, leading to increased cardiovascular risk.

Because of this, it would be ideal for the cholesterol value not to exceed 200 mg/dL and HDL cholesterol to be above 40 mg/dL in men and above 50 mg/dL in women [10].

2. Materials and methods

When the patient presents himself to the laboratory and requests the performance of medical analyses it is good to be informed about the conditions that must be met to obtain results precise about his health condition. That is why he will maintain an unchanged diet for a long time of three weeks before harvest as well as a stable weight. Must not consume food 12-16 hours before investigations and no alcohol 72 hours before collection. It's good to find out, if possible, if the patient has a pathological history or if he has signs and symptoms that led him to perform these laboratory investigations to be informed if other additional analyses are needed to help him discover possible causes and conditions [11].

Blood samples are collected in red or yellow vacutainer systems for biochemistry, without additives, volume 6 mL, with or without separating gel. Collected blood samples are identified with barcodes, with names the patient, sit on the stands and get ready to work. It should be noted that tourniquet pressure prolonged over 2 minutes increases the value of cholesterolemia by 2-5%. Variations in cholesterol values are also associated with the season (higher values in winter by up to 8%), with medications, age and sex [12].

Cobas Integra 400 Plus (Figure 2) is a biochemistry device designed for a strengthen testing and increase the efficiency of investigational biological fluid testing. It has a patented design and sophisticated software programs to simplify the difficulty of working in laboratory.

Fig. 2. *Cobas Integra 400 Plus*

Reagents are incorporated into Cobas packs and STATs are automatically given up to 800 determinations/sample by automatic barcode reading. The on-board reagent has high stability from 8-12 weeks; thus, a reduced number of calibrations will be performed and will produce small amounts of resulting waste.

Quality control charts are run daily at the beginning of the analysis investigation process. For variable data, the diagrams are taken in pairs where the control limits are highlighted over time by adding two horizontal lines: the upper one (LCS) and the lower one (LCI) (Figure 3). Device calibrations are presented in Figures 4-8.

THE ANNALS OF "DUNAREA DE JOS" UNIVERSITY OF GALATI
FASCICLE IX. METALLURGY AND MATERIALS SCIENCE
No. 4 - 2023, ISSN 2668-4748; e-ISSN 2668-4756
Article DOI: https://doi.org/10.35219/mms.2023.4.09

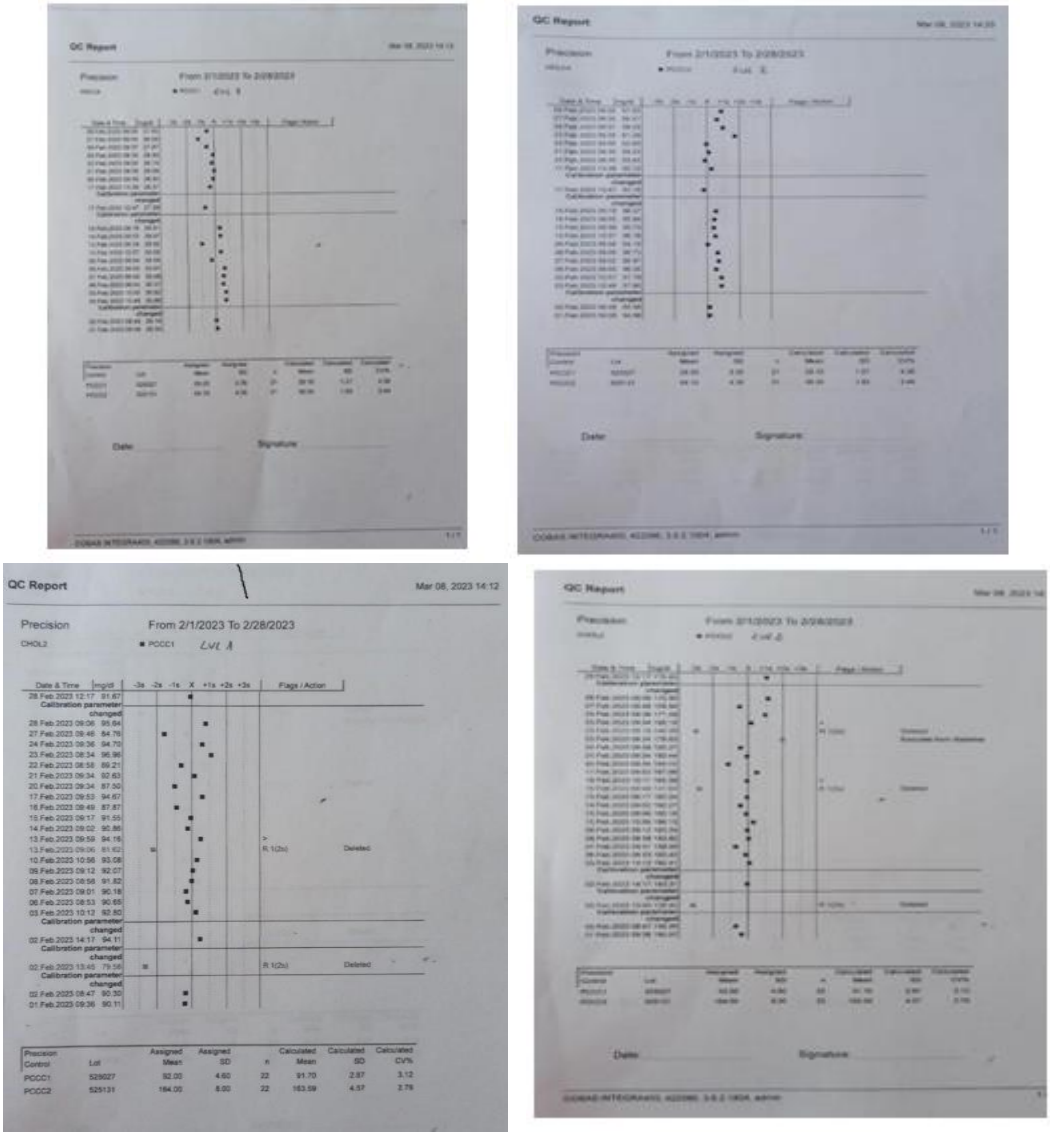

Fig. 3. *Quality control charts*

Fig. 4. *Control of the device before starting the activity. Liquid waste check*

Fig. 5. *Solid waste box*

THE ANNALS OF "DUNAREA DE JOS" UNIVERSITY OF GALATI
FASCICLE IX. METALLURGY AND MATERIALS SCIENCE
No. 4 - 2023, ISSN 2668-4748; e-ISSN 2668-4756
Article DOI: https://doi.org/10.35219/mms.2023.4.09

Fig. 6. *Calibration control*

Fig. 7. Test control and level of ionic solutions

Fig. 8. *Cholesterol and HDL cholesterol control reagent boxes*

3. Results and Discussion

Different outcomes were determined such as basic biochemical parameters (total cholesterol, HDL cholesterol, LDL cholesterol), were analysed in serum by standard biochemical procedures, using the automatic analyser Cobas Integra 400 Plus by the spectrophotometric method.

Table 1 show the normal and pathological values of the lipid profile, the risk factors involved in the processes favouring cardiovascular and nutritional diseases. During life, these factors become modifiable and non-modifiable for various conditions [13, 14].

The normal values (Fig. 9) are made for a male patient with no history of chronic diseases, and it is observed that the values of total cholesterol and its two subdivisions HDL cholesterol and LDL cholesterol are within normal limits.

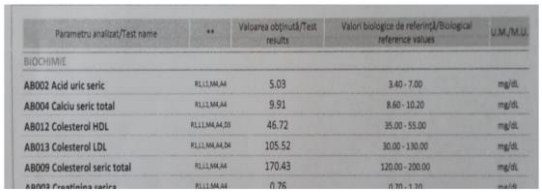

Fig. 9. *Normal values*

Figures 10-13 shows the results of the analyses (normal lipid profile) with parameters within normal limits, for different patients such as gender and age, but with present pathologies.

Table 1. *Representation of lipid profile values*

Lipid profile	Normal values, mg/dL	Limit values, mg/dL	Values above the normal limit, mg/dL	Risk values	Remarks
Total lipids	400 - 750				LT = 2,25 x total cholesterol + 90
Triglycerides	50 – 150	151 - 200	< 200	Over 500	
Fatty acids	200 – 450				Acid values > reference range = lipolytic answer
Lipoproteins	150 - 200				
Total cholesterol	< 200	200 - 339	< 240		
HDL cholesterol	> 40 (increased risk of atherosclerosis)	39	≤ 60 (decreased risk of atherosclerosis)		
LDL cholesterol	< 130	130 - 159	160 – 189	≤ 190	LDL = total cholesterol – HDL cholesterol
VLDL colesterol	2 - 38				VLDL = TG/5

THE ANNALS OF "DUNAREA DE JOS" UNIVERSITY OF GALATI
FASCICLE IX. METALLURGY AND MATERIALS SCIENCE
No. 4 - 2023, ISSN 2668-4748; e-ISSN 2668-4756
Article DOI: https://doi.org/10.35219/mms.2023.4.09

52-year-old man known to have type II diabetes, routine tests have the result total cholesterol and fractions of LDL and HDL cholesterol within normal limits (total cholesterol -167 mg/dL, HDL cholesterol -55.0 mg/dL, LDL cholesterol -94.9 mg/dL) (Figure 10).

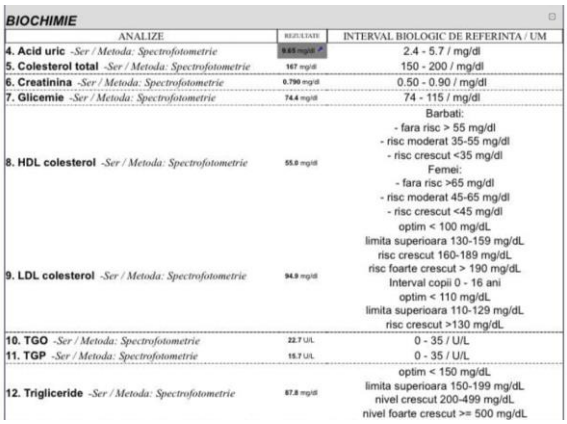

BIOCHIMIE		
ANALIZE	REZULTATE	INTERVAL BIOLOGIC DE REFERINTA / UM
4. Acid uric -Ser / Metoda: Spectrofotometrie	9.65 mg/dl	2.4 - 5.7 / mg/dl
5. Colesterol total -Ser / Metoda: Spectrofotometrie	167 mg/dl	150 - 200 / mg/dl
6. Creatinina -Ser / Metoda: Spectrofotometrie	0.790 mg/dl	0.50 - 0.90 / mg/dl
7. Glicemie -Ser / Metoda: Spectrofotometrie	74.4 mg/dl	74 - 115 / mg/dl
8. HDL colesterol -Ser / Metoda: Spectrofotometrie	55.0 mg/dl	Barbati: - fara risc > 55 mg/dl - risc moderat 35-55 mg/dl - risc crescut <35 mg/dl Femei: - fara risc >65 mg/dl - risc moderat 45-65 mg/dl - risc crescut <45 mg/dl
9. LDL colesterol -Ser / Metoda: Spectrofotometrie	94.9 mg/dl	optim < 100 mg/dL limita superioara 130-159 mg/dL risc crescut 160-189 mg/dL risc foarte crescut > 190 mg/dL Interval copii 0 - 16 ani optim < 110 mg/dL limita superioara 110-129 mg/dL risc crescut >130 mg/dL
10. TGO -Ser / Metoda: Spectrofotometrie	22.7 U/L	0 - 35 / U/L
11. TGP -Ser / Metoda: Spectrofotometrie	15.7 U/L	0 - 35 / U/L
12. Trigliceride -Ser / Metoda: Spectrofotometrie	87.8 mg/dl	optim < 150 mg/dL limita superioara 150-199 mg/dL nivel crescut 200-499 mg/dL nivel foarte crescut >= 500 mg/dL

Fig. 10. *Normal result for a patient with diabetes*

37-year-old woman, (total cholesterol -180 mg/dL, HDL cholesterol 64.8 mg/dL, LDL cholesterol -94.8 mg/dL) with conditions thyroid (Figure 11).

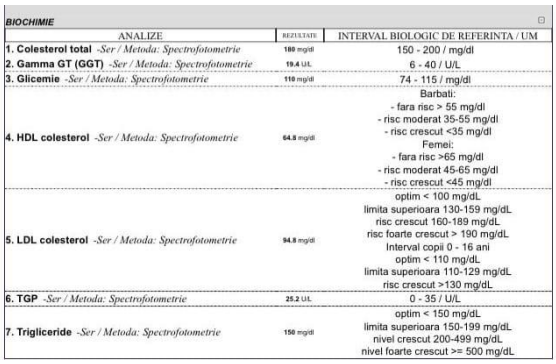

BIOCHIMIE		
ANALIZE	REZULTATE	INTERVAL BIOLOGIC DE REFERINTA / UM
1. Colesterol total -Ser / Metoda: Spectrofotometrie	180 mg/dl	150 - 200 / mg/dl
2. Gamma GT (GGT) -Ser / Metoda: Spectrofotometrie	19.4 U/L	6 - 40 / U/L
3. Glicemie -Ser / Metoda: Spectrofotometrie	110 mg/dl	74 - 115 / mg/dl
4. HDL colesterol -Ser / Metoda: Spectrofotometrie	64.8 mg/dl	Barbati: - fara risc > 55 mg/dl - risc moderat 35-55 mg/dl - risc crescut <35 mg/dl Femei: - fara risc >65 mg/dl - risc moderat 45-65 mg/dl - risc crescut <45 mg/dl
5. LDL colesterol -Ser / Metoda: Spectrofotometrie	94.8 mg/dl	optim < 100 mg/dL limita superioara 130-159 mg/dL risc crescut 160-189 mg/dL risc foarte crescut > 190 mg/dL Interval copii 0 - 16 ani optim < 110 mg/dL limita superioara 110-129 mg/dL risc crescut >130 mg/dL
6. TGP -Ser / Metoda: Spectrofotometrie	25.2 U/L	0 - 35 / U/L
7. Trigliceride -Ser / Metoda: Spectrofotometrie	150 mg/dl	optim < 150 mg/dL limita superioara 150-199 mg/dL nivel crescut 200-499 mg/dL nivel foarte crescut >= 500 mg/dL

Fig. 11. *Normal result for a patient with autoimmune thyroiditis*

49-year-old female known to have chronic liver disease, although transaminase results are modified, cholesterol and its fractions are within normal limits (total cholesterol -154 mg/dL, HDL cholesterol 43.6 mg/dL, LDL cholesterol -97.1 mg/dL), liver functions should be monitored further and administration treatment according to the specialist doctor's recommendations (Figure 12).

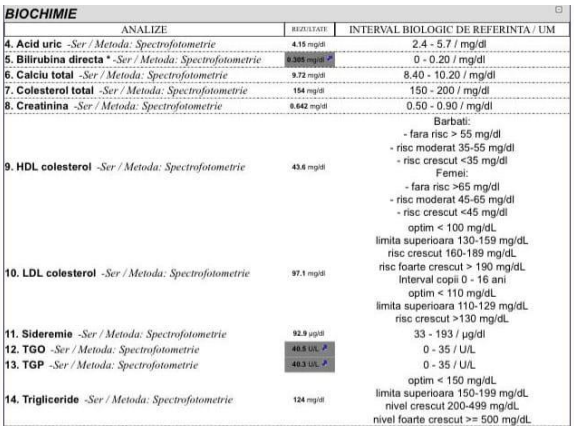

BIOCHIMIE		
ANALIZE	REZULTATE	INTERVAL BIOLOGIC DE REFERINTA / UM
4. Acid uric -Ser / Metoda: Spectrofotometrie	4.15 mg/dl	2.4 - 5.7 / mg/dl
5. Bilirubina directa * -Ser / Metoda: Spectrofotometrie	0.305 mg/dl	0 - 0.20 / mg/dl
6. Calciu total -Ser / Metoda: Spectrofotometrie	9.72 mg/dl	8.40 - 10.20 / mg/dl
7. Colesterol total -Ser / Metoda: Spectrofotometrie	154 mg/dl	150 - 200 / mg/dl
8. Creatinina -Ser / Metoda: Spectrofotometrie	0.642 mg/dl	0.50 - 0.90 / mg/dl
9. HDL colesterol -Ser / Metoda: Spectrofotometrie	43.6 mg/dl	Barbati: - fara risc > 55 mg/dl - risc moderat 35-55 mg/dl - risc crescut <35 mg/dl Femei: - fara risc >65 mg/dl - risc moderat 45-65 mg/dl - risc crescut <45 mg/dl
10. LDL colesterol -Ser / Metoda: Spectrofotometrie	97.1 mg/dl	optim < 100 mg/dL limita superioara 130-159 mg/dL risc crescut 160-189 mg/dL risc foarte crescut > 190 mg/dL Interval copii 0 - 16 ani optim < 110 mg/dL limita superioara 110-129 mg/dL risc crescut >130 mg/dL
11. Sideremie -Ser / Metoda: Spectrofotometrie	92.9 µg/dl	33 - 193 / µg/dl
12. TGO -Ser / Metoda: Spectrofotometrie	40.5 U/L	0 - 35 / U/L
13. TGP -Ser / Metoda: Spectrofotometrie	40.3 U/L	0 - 35 / U/L
14. Trigliceride -Ser / Metoda: Spectrofotometrie	124 mg/dl	optim < 150 mg/dL limita superioara 150-199 mg/dL nivel crescut 200-499 mg/dL nivel foarte crescut >= 500 mg/dL

Fig. 12. *Normal result for patient with chronic liver disease*

The results of the validated samples are continuously transmitted to the LIS (the system computer science from the laboratory) through the communication mode with host query.

Pathological results that indicate various conditions and are obtained from harvesting of patients with confirmed diagnoses of dyslipidemia are presented in Figure 13.

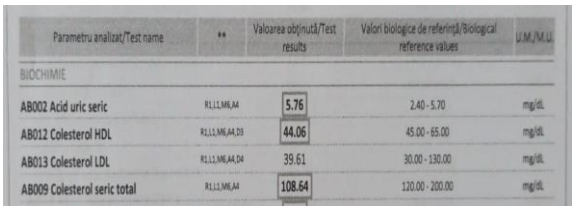

Parametru analizat/Test name	**	Valoarea obținută/Test results	Valori biologice de referință/Biological reference values	U.M./M.U.
BIOCHIMIE				
AB002 Acid uric seric	R1,L1,M6,A4	5.76	2.40 - 5.70	mg/dL
AB012 Colesterol HDL	R1,L1,M6,A4,D3	44.06	45.00 - 65.00	mg/dL
AB013 Colesterol LDL	R1,L1,M6,A4,D4	39.61	30.00 - 130.00	mg/dL
AB009 Colesterol seric total	R1,L1,M6,A4	108.64	120.00 - 200.00	mg/dL

Fig. 13. *Pathological result*

HDL cholesterol has the role of transporting other forms of lipids and cholesterol through the blood to the liver where they are synthesized and eliminated. The higher the number of its value, the better it is for the human body.

When the level of HDL cholesterol is low for various reasons, the transport of fats can no longer be carried out at the same standards and then their excess is deposited on the blood vessels, forming atheroma plaques. Also, the arteries narrow, and blood flow is limited, accelerating the risk of developing atherosclerosis.

72-year-old man with dyslipidemia, diabetes and renal impairment. The patient must medically monitored and re-evaluation of additional cardiological investigations, dietary regimen. (total cholesterol -206 mg/dL, HDL cholesterol -37 mg/dL, LDL cholesterol -126 mg/dL, triglycerides-231 md/dL).

It can be observed that the HDL cholesterol value is at the lower limit and the LDL cholesterol at

THE ANNALS OF "DUNAREA DE JOS" UNIVERSITY OF GALATI
FASCICLE IX. METALLURGY AND MATERIALS SCIENCE
No. 4 - 2023, ISSN 2668-4748; e-ISSN 2668-4756
Article DOI: https://doi.org/10.35219/mms.2023.4.09

the limit higher, which means that there is a possibility of developing cardiovascular diseases (Figure 14).

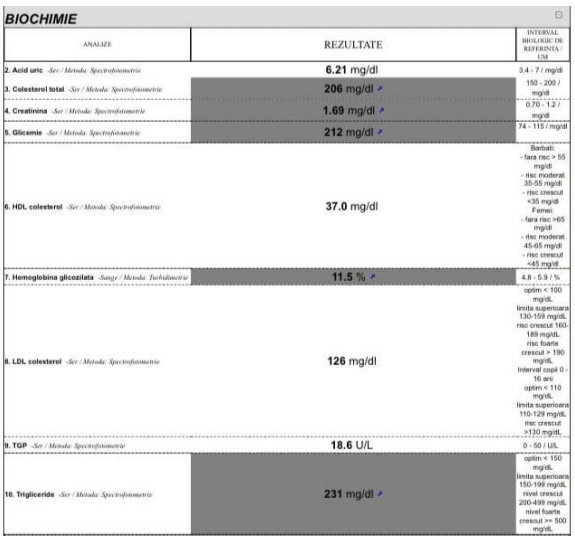

BIOCHIMIE		
ANALIZE	REZULTATE	INTERVAL BIOLOGIC DE REFERINTA / UM
2. Acid uric -Ser / Metoda: Spectrofotometrie	6.21 mg/dl	3.4 - 7 / mg/dl
3. Colesterol total -Ser / Metoda: Spectrofotometrie	206 mg/dl	150 - 200 / mg/dl
4. Creatinina -Ser / Metoda: Spectrofotometrie	1.69 mg/dl	0.70 - 1.2 / mg/dl
5. Glicemie -Ser / Metoda: Spectrofotometrie	212 mg/dl	74 - 115 / mg/dl
6. HDL colesterol -Ser / Metoda: Spectrofotometrie	37.0 mg/dl	Barbati: - fara risc > 55 mg/dl - risc moderat 35-55 mg/dl - risc crescut <35 mg/dl Femei: - fara risc >65 mg/dl - risc moderat 45-65 mg/dl - risc crescut <45 mg/dl
7. Hemoglobina glicozilata -Sange / Metoda: Turbidimetrie	11.5 %	4.8 - 5.9 / %
8. LDL colesterol -Ser / Metoda: Spectrofotometrie	126 mg/dl	optim < 100 mg/dL limita superioara 130-159 mg/dL risc crescut 160-189 mg/dL risc foarte crescut > 190 mg/dL Interval copii 0 - 16 ani optim < 110 mg/dL limita superioara 110-129 mg/dL risc crescut >130 mg/dL
9. TGP -Ser / Metoda: Spectrofotometrie	18.6 U/L	0 - 50 / U/L
10. Trigliceride -Ser / Metoda: Spectrofotometrie	231 mg/dl	optim < 150 mg/dL limita superioara 150-199 mg/dL nivel crescut 200-499 mg/dL nivel foarte crescut >= 500 mg/dL

***Fig. 14**. Pathological result*

Male patient, 49 years old, with insulin-dependent diabetes mellitus, obesity, dyslipidemia, high-risk hypertension, chronic ischemic heart disease-with increased values of total cholesterol-301 mg/dL, LDL cholesterol-221 mg/dL, HDL cholesterol at the lower limit 43.3 mg/dL. It is in the records of specialist doctors with established treatment, diet and regimen hyposodium, hypocaloric and periodic medical reassessment (electrocardiogram, coronary angiography, investigations biological, nuclear magnetic resonance) (Figure 15).

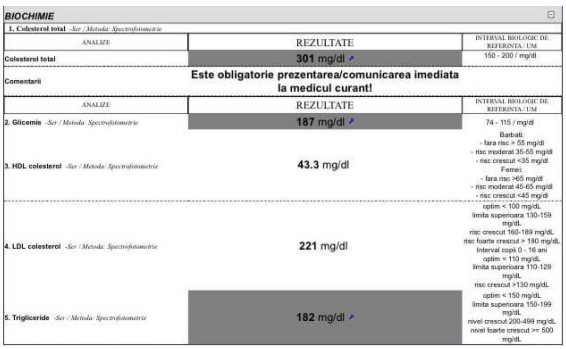

BIOCHIMIE		
1. Colesterol total -Ser / Metoda: Spectrofotometrie		
ANALIZE	REZULTATE	INTERVAL BIOLOGIC DE REFERINTA / UM
Colesterol total	301 mg/dl	150 - 200 / mg/dl
Comentarii	Este obligatorie prezentarea/comunicarea imediata la medicul curant!	
ANALIZE	REZULTATE	INTERVAL BIOLOGIC DE REFERINTA / UM
2. Glicemie -Ser / Metoda: Spectrofotometrie	187 mg/dl	74 - 115 / mg/dl
3. HDL colesterol -Ser / Metoda: Spectrofotometrie	43.3 mg/dl	Barbati: - fara risc > 55 mg/dl - risc moderat 35-55 mg/dl - risc crescut <35 mg/dl Femei: - fara risc >65 mg/dl - risc moderat 45-65 mg/dl - risc crescut <45 mg/dl
4. LDL colesterol -Ser / Metoda: Spectrofotometrie	221 mg/dl	optim < 100 mg/dL limita superioara 130-159 mg/dL risc crescut 160-189 mg/dL risc foarte crescut > 190 mg/dL Interval copii 0 - 16 ani optim < 110 mg/dL limita superioara 110-129 mg/dL risc crescut >130 mg/dL
5. Trigliceride -Ser / Metoda: Spectrofotometrie	182 mg/dl	optim < 150 mg/dL limita superioara 150-199 mg/dL nivel crescut 200-499 mg/dL nivel foarte crescut >= 500 mg/dL

***Fig. 15**. Pathological result*

In Figure 16 it was presented a result from a 14-year-old male patient with obesity, diabetes mellitus type I, insulin-dependent.

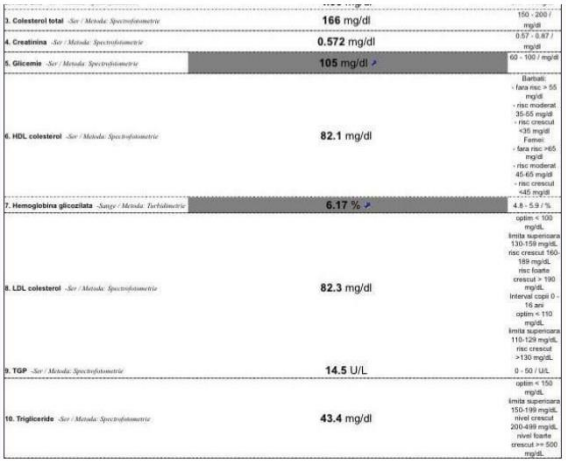

3. Colesterol total -Ser / Metoda: Spectrofotometrie	166 mg/dl	150 - 200 / mg/dl
4. Creatinina -Ser / Metoda: Spectrofotometrie	0.572 mg/dl	0.57 - 0.87 / mg/dl
5. Glicemie -Ser / Metoda: Spectrofotometrie	105 mg/dl	60 - 100 / mg/dl
6. HDL colesterol -Ser / Metoda: Spectrofotometrie	82.1 mg/dl	Barbati: - fara risc > 55 mg/dl - risc moderat 35-55 mg/dl - risc crescut <35 mg/dl Femei: - fara risc >65 mg/dl - risc moderat 45-65 mg/dl - risc crescut <45 mg/dl
7. Hemoglobina glicozilata -Sange / Metoda: Turbidimetrie	6.17 %	4.8 - 5.9 / %
8. LDL colesterol -Ser / Metoda: Spectrofotometrie	82.3 mg/dl	optim < 100 mg/dL limita superioara 130-159 mg/dL risc crescut 160-189 mg/dL risc foarte crescut > 190 mg/dL Interval copii 0 - 16 ani optim < 110 mg/dL limita superioara 110-129 mg/dL risc crescut >130 mg/dL
9. TGP -Ser / Metoda: Spectrofotometrie	14.5 U/L	0 - 50 / U/L
10. Trigliceride -Ser / Metoda: Spectrofotometrie	43.4 mg/dl	optim < 150 mg/dL limita superioara 150-199 mg/dL nivel crescut 200-499 mg/dL nivel foarte crescut >= 500 mg/dL

***Fig. 16.** Results for a child with obesity*

As it can be observed in the presented results, the patients of different ages suffer from associated diseases, due to the increase in the value of cholesterol and must be considered assessment of established or emerging cardiovascular disease risks and investigation the risk of atheromatosis, which favours stroke.

4. Conclusions

The study briefly outlines the links between cholesterol, obesity and genetic factors, describing dyslipidemia and risk factors.

The case study summarized the results of some patients with the following medical conditions: disorders lipid metabolism, diabetes, kidney disorder, thyroid disease, obesity, hypertension, chronic liver disorder, ischemic heart disease.

Total cholesterol values between 154-301 mg/dL are observed, which reveals that these patients are at risk of dyslipidemia diagnosis if they have not already received specialist confirmation.

In the case of HDL cholesterol, it was found that the determined limit values are from 37 mg/dL to 64.8 mg/dL, which shows a potential pathological risk factor. For LDL cholesterol, the obtained results reveal limits of 94.8 mg/dL, respectively 221 mg/dL - which determines increased cardiovascular risks.

HDL cholesterol has the role of transporting other forms of lipids and cholesterol through the blood to the liver where they are synthesized and eliminated. The higher the number of its value, the better it is for organism. When the level of HDL cholesterol is low for various reasons, the transport of fats can no longer be carried out at the same standards and then their excess is deposited on the blood vessels forming atheroma plaques. Also, the arteries narrow, and the blood flow is limited, accelerating the risk of developing atherosclerosis, which favours stroke.

THE ANNALS OF "DUNAREA DE JOS" UNIVERSITY OF GALATI
FASCICLE IX. METALLURGY AND MATERIALS SCIENCE
No. 4 - 2023, ISSN 2668-4748; e-ISSN 2668-4756
Article DOI: https://doi.org/10.35219/mms.2023.4.09

Patients will be monitored from a medical point of view and periodically reevaluated, recommending additional cardiological investigations, as well as a dietary regimen. The investigation of serum lipids provides information regarding the analysed limits specific to age, sex, and pathology.

The data obtained in the study will be used for preventive purposes. Regular checking of biological parameters, healthy diet and physical activities are the main ways to keep cholesterol levels under control.

References

[1]. Garban Z., Garban G., *Nutriţia umană*, vol. I, Probleme fundamentale, ed. 3-a, Editura Orizonturi Universitare, ISBN 973-638-091-2, Timişoara, 2003.
[2]. Billimoria J. D., Fahmy M. F., Jepson E. M., Maclagen N. F., *The use of the esterified fatty acid index in the classification and quantitation of hyperlipoproteinaemia*, Atherosclerosis, vol. 14, issue 3, p. 359-374, 1971.
[3]. ***. https://pubchem.ncbi.nlm.nih.gov/compound/5997, Biblioteca Națională de Medicină, Institutele Naționale de Sănătate din SUA, 2019.
[4]. Silbernagl S., *Fiziologia omului*, Editura Callisto, București, 2017.
[5]. Lustig R., *Metabolical*, Editura Hodder & Stoughton, New York, USA, 2021.
[6]. Havel R. J., Rappaport E., *Management of primary hyperlipidemia*, New England Journal of Medicine, vol. 332, p. 1491-1498, 1995.
[7]. ***, https://ro.khanacademy.org/science/biology/macromolecules/lipids/a/lipids.
[8]. Manu R., *Obesity and cardiovascular risk in children and adolescents*, Indian Journal of Endocrinology Metabolism, vol. 16 (1), p. 13-19, 2012.
[9]. Marchesseau P. V., *Colesterolul - Prieten Sau Duşman?*, Colecția sănătate și conștiință, Editura Sens, 2019.
[10]. ***, https://www.csid.ro/sanatate/sanatate-health/colesterol-bun-hdl-si-colesterol-rau-ldl- 10399596/.
[11]. Mach F., *et al.*, *Grupul de Lucru pentru diagnosticul şi tratamentul dislipidemiilor al Societăţii Europene de Cardiologie (ESC) şi al Societăţii Europene de Ateroscleroză (EAS), Ghidul Societăţii Europene de Cardiologie (ESC)/ Societăţii Europene de Ateroscleroză (EAS) pentru diagnosticul şi tratamentul dislipidemiilor 2019: modificările lipidice în vederea reducerii riscului cardiovascular*, Romanian Journal of Cardiology, vol. 30, no. 2, p. 263-357, 2020.
[12]. Kreisberg R. A., Oberman A., *Lipids and atherosclerosis:lesson learned from randomized controlled trial of lipid lowering and other relevant studies*, The Journal of Clinical Endocrinology and Metabolism, vol. 87 (2), p. 423-437, 2002.
[13]. Bezu G., *Modificările electrocardiografice în infarct miocardic acut şi angor pectoral*, https://medinsemiologie.usmf.md/sites/default/files/inline-files/Optional.ECG_.IMA_.Angor_.Ro_.a.V.Medicina.2021.pdf.
[14]. Ference B. A., *et al.*, *Effect of long-term exposure to lower low-density lipoprotein cholesterol beginningearly in life on the risk of coronary heart disease: a Mendelian randomization analysis*, Journal of the American College of Cardiology, vol. 60, article 2631-9, 2012.

THE ANNALS OF "DUNAREA DE JOS" UNIVERSITY OF GALATI
FASCICLE IX. METALLURGY AND MATERIALS SCIENCE
No. 4 - 2023, ISSN 2668-4748; e-ISSN 2668-4756
Article DOI: https://doi.org/10.35219/mms.2023.4.10

MATHEMATICAL MODELING TO PREDICT MECHANICAL PROPERTIES VALUES FOR HOT ROLLED S235 STEEL

Marian-Iulian NEACSU
"Dunarea de Jos" University of Galati, Romania
e-mail: marian.neacsu@ugal.ro

ABSTRACT

The present paper presents the creation of a mathematical model for predicting the values of the mechanical properties of hot-rolled strips. The paper presents the way of developing the mathematical model, based on a statistical development method, namely, the active experiment method.

The equations of the developed mathematical model successfully allow the prediction of the values of the studied mechanical properties, thus saving material, time and money.

KEYWORDS: steel, hot rolling, thermal treatment, mathematical modeling, prediction of property values

1. Introduction

Even today, steel remains the most used material in the car construction industry, the construction of oil and gas pipelines and many others. Many of the semi-finished products from which various benchmarks are obtained, are obtained through the metallurgical processing of hot plastic deformation.

Mathematical modeling of technological processes in general and of metallurgical ones in the present case, is a basic tool that is extremely useful both in the conception phase and in the one in which the operation of metallurgical installations is analysed [1].

Mathematical modeling together with the use of computers, allows obtaining the optimal regimes for metallurgical processes. By performing mathematical modeling through statistical methods, it is possible to approach the optimal decision problem as a problem of great technical and economic effectiveness [2].

Mathematical modeling operates with numerical quantities without conditioning the way of subjective interpretation, in a certain context of the results obtained. It requires the knowledge of all the elements that contribute to the description of the phenomenon, the possibility of quantitative expression and, as far as possible, without any subjective addition, the most thorough knowledge of the conditions in which the phenomenon takes place, the specification of the restrictions imposed on some quantities or functions, as well as the complete definition of the pursued goal [3].

Mircea Maliţa defines the model as "a mental or written, qualitative or mathematical representation of a part of a reality that constitutes a system (i.e. a whole with interconnected parts). The model selects the most representative components of the system and describes the relationships that select" [4].

Creating a model not only serves knowledge but also has practical purposes, constituting a basis for experimentation.

The large number of mathematical models made over time have shown that for the same model the formulated requirements form a contradictory set. From this it follows that any mathematical model satisfies, as a rule, only a part of the established requirements. Mathematical models can be classified according to several criteria. The most representative, in this sense, are: the information they contain and the mathematical tool used.

The main requirements imposed on a quality model are: coherence, correctness, consistency, efficiency and usability [5].

The use of monofactorial methods for the study of multifactorial processes, in addition to the fact that they require a long period of work, cannot guarantee the determination of the conditions for achieving the optimal values of the performance function. From this point of view, the introduction and development of statistical processing methods and especially those that concern modeling by using experiment programming methods is a useful and highly effective tool [6].

The mathematical models obtained by these methods can be used not only to reveal the extreme

THE ANNALS OF "DUNAREA DE JOS" UNIVERSITY OF GALATI
FASCICLE IX. METALLURGY AND MATERIALS SCIENCE
No. 4 - 2023, ISSN 2668-4748; e-ISSN 2668-4756
Article DOI: https://doi.org/10.35219/mms.2023.4.10

(optimal) conditions, but also as an important source of information, necessary for the optimal management of metallurgical processes [7].

In the analysis of a system when it is required to find out by calculation the performance indicators of the given system, this requires knowledge of the mathematical model of the system, that is, of the relations between the output quantities and the exogenous quantities [8].

2. Experimental conditions and obtained results

The paper presents the way to create a mathematical model for predicting the values of the mechanical properties of hot-rolled strips.

Experiments were carried out in a trial with hot-rolled S235 steel strip, having thicknesses of: 2 mm, 6 mm, 10 mm, and the carbon concentration being: 0.1101 %C; 0.1261 %C; 0.1421 %C, for steel grade S235.

Table 1 shows the chemical composition according to EN10111:2008(E) for the steel brand S235 studied.

For each tape thickness studied, having the three carbon concentrations, determinations were made in order to find out the values of the mechanical properties: R_m, $Rp_{0.2}$, A_5.

Following the laboratory tests on the samples taken from the rolls caught in the experimental program, the values of the studied mechanical properties were recorded, values which are reproduced in Table 2.

Table 1. *Chemical composition according to EN10111:2008(E) for steel grade S235*

Chemical Composition											
C%	**Mn%**	**Si%**	**P%**	**S%**	**Al%**	**Cu%**	**Cr%**	**Ni%**	**V%**	**Ti%**	**Mo%**
0.04-0.08	0.45-0.55	0.01-0.02	0.013-0.019	0.011-0.016	0.020-0.040	0.050-0.080	0.030-0.040	0.030-0.050	0.002-0.003	0.000-0.001	0.003-0.005

Table 2. *Values of the S235 steel properties*

Thickness [mm]	%C	R_m - measured [MPa]	$Rp_{0,2}$ - measured [MPa]	A_5 measured [%]
2	0.1101	419	344	29
	0.1261	434	371	30
	0.1421	478	397	30
6	0.1101	415	270	32
	0.1261	419	287	31
	0.1421	448	327	30
10	0.1101	378	270	32
	0.1261	416	284	31
	0.1421	427	298	30

We considered the following technological parameters as the main influencing factors (independent variables):

a) Tape thickness - G, [mm];

b) Carbon concentration - C, [%].

The set of mechanical properties is considered as a parameter to be optimized: R_m, $Rp_{0.2}$, A_5.

We established the following experimental conditions:

- for the tape thickness, G, the values for the upper level, the base level, the lower level and the range of value variations were set:

base level: $x_1(0) = 6$ mm;
variation range: $\Delta x_1 = 4$ mm;
upper level: $x_1(+1) = 10$ mm;
lower level: $x_1(-1) = 2$ mm.

For carbon concentration:
base level: $x_2(0) = 0.1261$ %;
variation range: $\Delta x_2 = 0.016$ %;
upper level: $x_2(+1) = 0.1421$ %;
lower level: $x_2(-1) = 0.1101$ %.

For the coded representation of the experiment, the following notations and symbols were used:

Independent variables:
x_1 - tape thickness, G [mm];
x_2 - carbon concentration, C [%].
Dependent variables (parameters to optimize)
Y1 - breaking strength, R_m [MPa];
Y2 - yield strength, Rp_{02} [MPa];
Y3 - specific elongation at break, A_5 [%];
Yi values are expressed in natural units.

THE ANNALS OF "DUNAREA DE JOS" UNIVERSITY OF GALATI
FASCICLE IX. METALLURGY AND MATERIALS SCIENCE
No. 4 - 2023, ISSN 2668-4748; e-ISSN 2668-4756
Article DOI: https://doi.org/10.35219/mms.2023.4.10

Since the influence of two factors on the performance of the process (Y) is being studied, we carried out a complete factorial experiment of type 22 [2].

The calculated values for the coefficients: for the three equations of the mathematical model of S235 steel are shown in table 4.

Table 3. *Matrix of full 22 factorial experiment for S235 steel*

Nr. exp.	X_0	X_1	X_2	$X_1 \cdot X_2$	Y_1	Y_2	Y_3
1	1	1	1	1	427	298	30
2	1	-1	1	-1	478	397	30
3	1	1	-1	-1	378	270	32
4	1	-1	-1	1	419	344	29

Table 4. *Values of coefficients C_0, C_1, C_2, C_{12} for S235 steel*

Y_i \ The coefficients	C_0	C_1	C_2	C_{12}
Y_1	425.5	-23	27	-2.5
Y_2	327.25	-43.25	-20.25	-6.25
Y_3	30.25	0.75	-0.25	-0.75

After calculating the coefficients, the equations of the mathematical model in the form of equation 1, in coded quantities, respectively equations 2, 3 and 4 [2] resulted:

$$Y_n = C_0 + C_1X_1 + C_2X_2 + C_{12}X_1X_2 \quad (1)$$

$$Y_1 = 425.5 - 23 \cdot X_1 + 27 \cdot X_2 - 2.5 \cdot X_1 \cdot X_2 \quad (2)$$

$$Y_2 = 327.25 - 43.25 \cdot X_1 + 20.25 \cdot X_2 - 6.25 \cdot X_1 \cdot X_2 \quad (3)$$

$$Y_3 = 30.25 + 0.75 \cdot X_1 - 0.25 \cdot X_2 - 0.75 \cdot X_1 \cdot X_2 \quad (4)$$

After replacing the coded sizes (X_1, X_2) with the natural sizes (G - band thickness, C - carbon percentage) the equations of the mathematical model expressed in natural sizes will be obtained.

$$Y_1 = 435.81 - 5.25 \cdot G + 192.15 \cdot C - 3.90 \cdot C \cdot G \quad (5)$$

Y_1 - equation of the mathematical model in natural sizes for Rm of S235 steel.

$$Y_2 = 368.82 - 9.58 \cdot G + 185.12 \cdot C - 9.76 \cdot C \cdot G \quad (6)$$

Y_2 - equation of the mathematical model in natural sizes for Rp0.2 of S235 steel.

$$Y_3 = 28.443 + 0.3345 \cdot G + 5.46 \cdot C - 1.17 \cdot C \cdot G \quad (7)$$

In the Figures from 1 to 9, the values of the mechanical properties studied, obtained experimentally, are shown in a comparative way with those obtained by calculation with the help of the developed mathematical model.

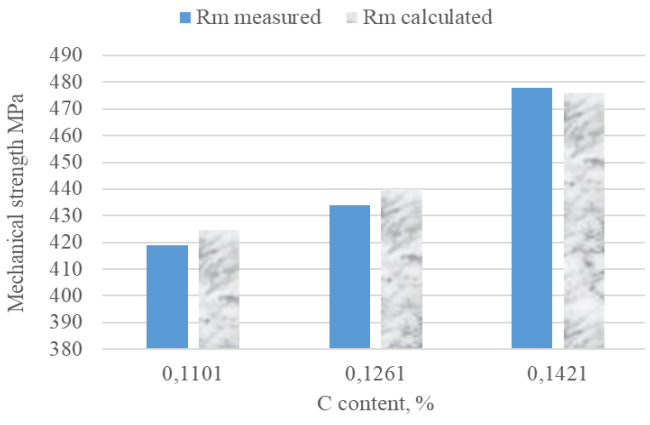

Fig. 1. *Variation of R_m as a function of %C for 2 mm tape thickness*

THE ANNALS OF "DUNAREA DE JOS" UNIVERSITY OF GALATI
FASCICLE IX. METALLURGY AND MATERIALS SCIENCE
No. 4 - 2023, ISSN 2668-4748; e-ISSN 2668-4756
Article DOI: https://doi.org/10.35219/mms.2023.4.10

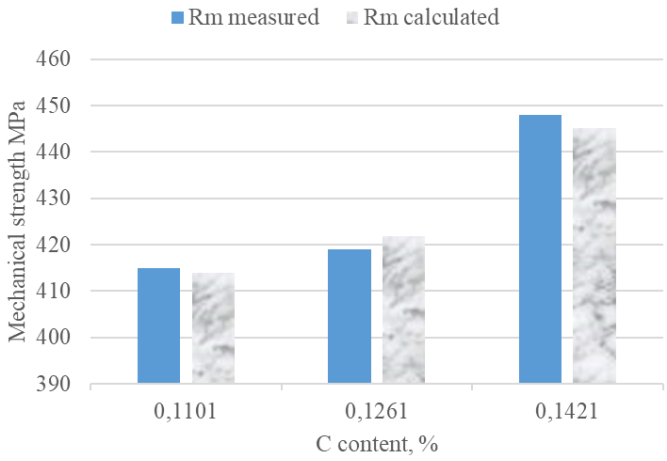

Fig. 2. *Variation of R_m as a function of %C for 6 mm tape thickness*

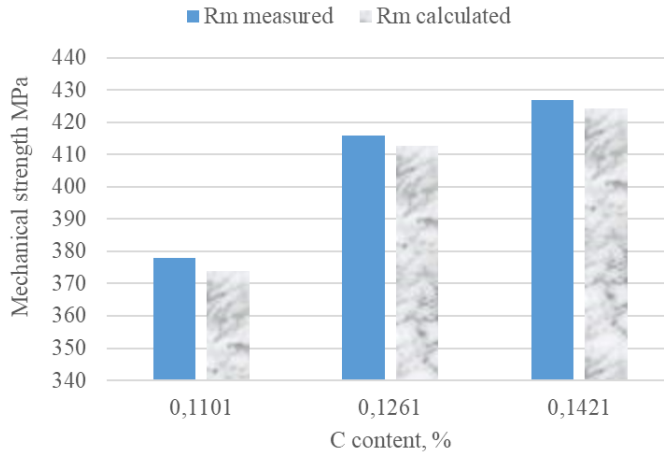

Fig. 3. *Variation of R_m as a function of %C for tape thickness of 10 mm*

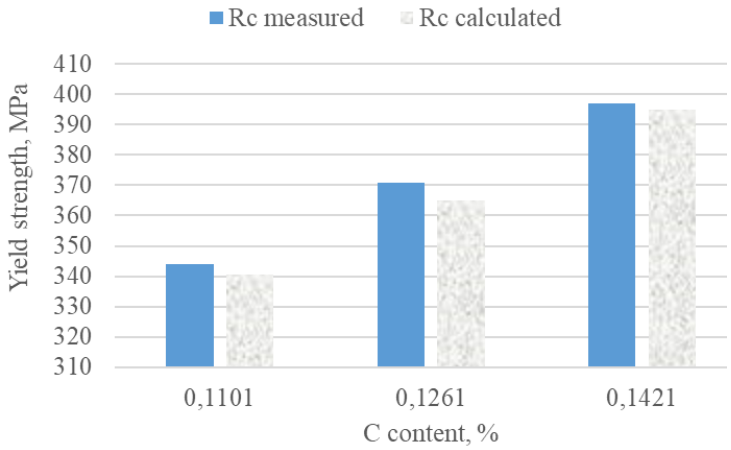

Fig. 4. *Variation of $Rp_{0.2}$ as a function of %C for tape thickness of 2 mm*

THE ANNALS OF "DUNAREA DE JOS" UNIVERSITY OF GALATI
FASCICLE IX. METALLURGY AND MATERIALS SCIENCE
No. 4 - 2023, ISSN 2668-4748; e-ISSN 2668-4756
Article DOI: https://doi.org/10.35219/mms.2023.4.10

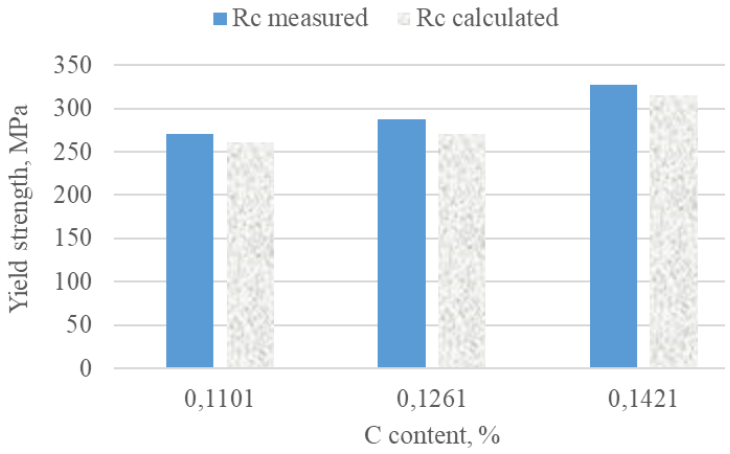

Fig. 5. *Variation of $Rp_{0.2}$ as a function of %C for tape thickness of 6 mm*

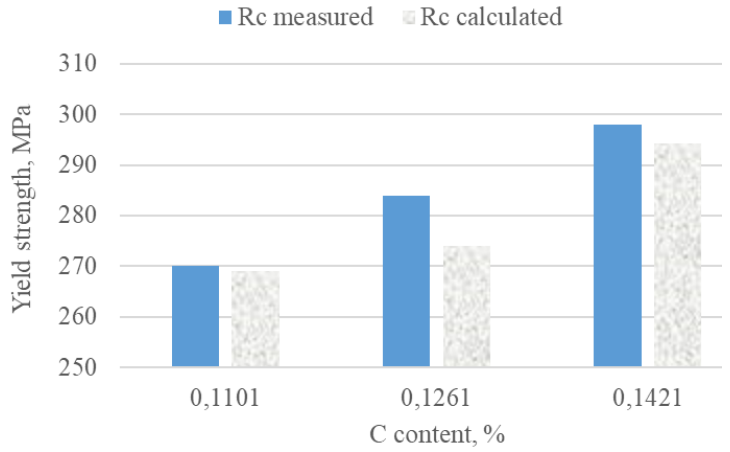

Fig. 6. *Variation of $Rp_{0.2}$ as a function of %C for 10 mm tape thickness*

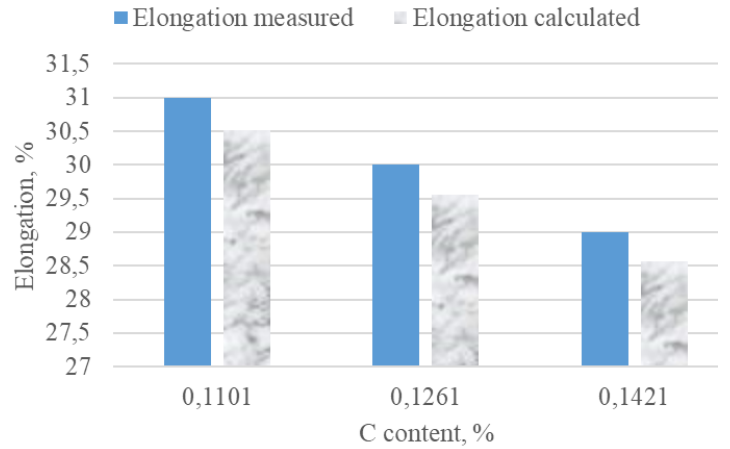

Fig. 7. *Variation of A_5 as a function of %C for 2 mm tape thickness*

THE ANNALS OF "DUNAREA DE JOS" UNIVERSITY OF GALATI
FASCICLE IX. METALLURGY AND MATERIALS SCIENCE
No. 4 - 2023, ISSN 2668-4748; e-ISSN 2668-4756
Article DOI: https://doi.org/10.35219/mms.2023.4.10

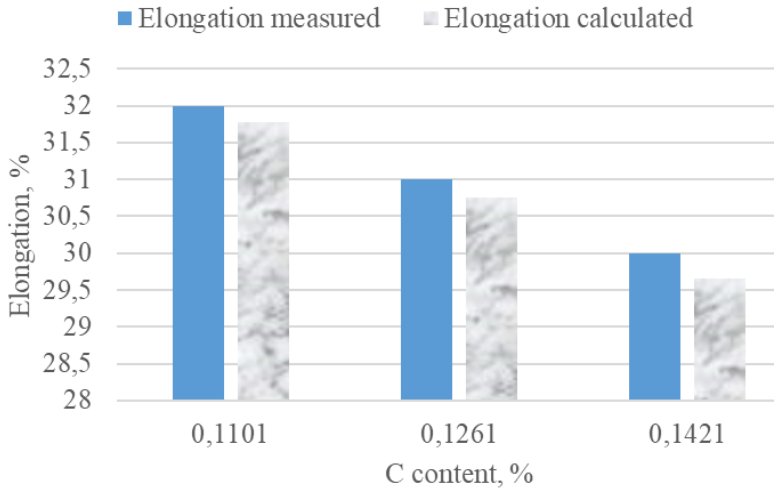

Fig. 8. *Variation of A_5 as a function of %C for 6 mm tape thickness*

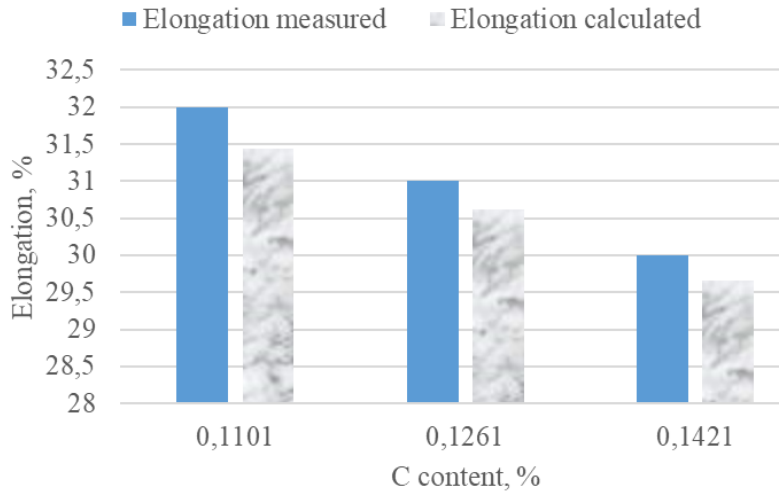

Fig. 9. *Variation of A_5 as a function of %C for 10 mm tape thickness*

By analysing the graphs above, it can be seen that between the values of the mechanical properties calculated, using the equations of the mathematical model, and the measured values, there are very small differences that can be neglected.

For this reason, it can be said that the obtained mathematical model can be successfully used to express the values of the mechanical properties without the need to measure them by specific methods.

3. Conclusion

Following the development of the mathematical model, three equations were obtained that express the dependence of each studied mechanical property on the two factors taken into account (independent variables = input variables), namely: strip thickness and carbon percentage.

From the analysis of the coefficients of the mathematical model equation for Rm it follows that as the carbon content increases there is also an increase in the value of R_m and as the strip thickness decreases there is also an increase in the value of R_m.

The mathematical model equation for $Rp_{0.2}$ shows that the value of $Rp_{0.2}$ increases with decreasing carbon content and strip thickness.

It is observed that the elongation decreases as the carbon content increases.

The calculation of the values of the studied mechanical properties, with the help of the equations of the mathematical model compared to the measured values, highlights small differences between the values of the measured and calculated properties.

Thus, it can be said that the developed mathematical model can be successfully used to predict the values of the mechanical properties without the need to measure them by specific

methods and in this way, there is an economy of materials, time and labour.

References

[1]. Ciucă I., Dumitriu S., *Modelarea şi Optimizarea Proceselor Metalurgice de Deformare Plastică şi Tratamente Termice*, Editura Didactică şi Pedagogică, Bucureşti, 1998.
[2]. Taloi D., *Optimizarea proceselor tehnologice – aplicaţii în metalurgie*, Editura Academiei, Bucureşti, 1987.
[3]. ***, https://www.academia.edu/39946148/.
[4]. Mircea Malița, *Zece mii de culturi o singură civilizație*, Editura Nemira, Bucureşti, 2002.
[5]. Cătălin Zisu, Alexandru Mihalcea, *Securitatea sistemelor informaţional-decizionale*, Editura Tritonic, Bucureşti, 2007.
[6]. Şerban R., Dumitrescu T., *Metode de optimizare*, Editura Matrix Rom, Bucureşti, 1998.
[7]. Popescu D., Ionescu F., Dobrescu R., Ştefanoiu D., *Modelare în ingineria proceselor industriale*, Editura AGIR, Bucuresti, 2011.
[8]. Mureşan S. Anton, *Modelare matematică*, Editura Mega – Cluj Napoca, România, ISBN 978-606-543-139-3, 2011.

THE ANNALS OF "DUNAREA DE JOS" UNIVERSITY OF GALATI
FASCICLE IX. METALLURGY AND MATERIALS SCIENCE
No. 4 - 2023, ISSN 2668-4748; e-ISSN 2668-4756
Article DOI: https://doi.org/10.35219/mms.2023.4.11

RESEARCH ON THE INFLUENCE OF CHEMICAL COMPOSITION AND TECHNOLOGICAL PARAMETERS ON THE MECHANICAL PROPERTIES OF X60M STEEL USED IN THE PRODUCTION OF OIL AND GAS PIPELINES

Beatrice TUDOR, Mirela NOUR
"Dunarea de Jos" University of Galati, Romania
e-mail: beatrice.tudor@ugal.ro

ABSTRACT

The work analyses and determines the mechanical properties of the X60M steel used to make welded pipes for oil and gas transportation. X60M type steels are among the materials most used in the construction of pipelines for the transport of natural gas and oil, due to an advantageous price/performance ratio. Determinations were made of resilience and resistance to breaking, yield strength, elongation and transverse contraction, determined by tensile tests, as well as an analysis of the microstructure.

KEYWORDS: mechanical properties, welded pipes, microstructure

1. Introduction

The steels for constructions and welded structures are carbon and low-alloy steels, intended for the production of metal structures through technological processes of high productivity, satisfying, as the case may be, resistance and tightness conditions.

The main usage characteristics of these steels are:

- Mechanical strength characteristics - yield strength and breaking strength - according to which the steel brands are defined and the allowable design stresses of welded constructions and structures are established.

- The weldability characteristics, considered both in terms of the technological aspect of the facility in execution, and that of safety against brittle breakage by grouping the products into quality classes [1, 3].

The mechanical characteristics are conditioned by the chemical composition and the metallographic structure. At least the following characteristics must be determined:

• breaking strength, yield strength, elongation and transverse contraction, determined by tensile tests;

• breaking energy when bending by shock, at different temperatures;

• the static bending angle without the appearance of cracks.

2. Experimental research

The structural analysis was carried out on X60M steel samples used to make welded pipes for the transportation of oil and gas. 3 7.5 mm V-groove specimens were used to determine resilience and an intermediate sample to determine tensile tests.[4]

General characteristics of X60 M steel, according to API 5L/95 standard, are presented in Table 1 and 2.

Table 1. *Chemical composition (%)*

C%	Mn%	Si%	P%	S%	Al%	Nb%	V%
0.09-0.12	1.30-1.50	0.20-0.40	max. 0.01	max. 0.01	0.02-0.05	0.02-0.04	0.02-0.04

Table 2. *Mechanical properties*

R_m [MPa]	$Rp_{0,2}$ [MPa]	A [%]	KV [J]
525-700	425-550	min. 30	min. 45

THE ANNALS OF "DUNAREA DE JOS" UNIVERSITY OF GALATI
FASCICLE IX. METALLURGY AND MATERIALS SCIENCE
No. 4 - 2023, ISSN 2668-4748; e-ISSN 2668-4756
Article DOI: https://doi.org/10.35219/mms.2023.4.11

The special requirements of the beneficiary are presented in Table 3.

The steel charge with the number 928400 taken in the study, from which the tests were carried out, is according to the requirements of the beneficiary and was developed in the LD converter having the following chemical composition for the liquid, presented in Table 4.

Table 3. *Beneficiary requirements*

Steel	C%	Mn%	Si%	P%	S%	Cu%	Ni%	Cr%	V%	Ti%	Mb%	Nb%	Al%	N%	B%
X60M	max 0.19	max 1.60	max 0.45	max 0.025	max 0.015	max 0.25	max 0.30	max 0.30	max 0.10	max 0.040	max 0.10	max 0.05	0.020-0.060	max 0.012	max 0.001

Table 4. *Chemical composition of batch number 928400*

X60M Batch 928400	C	Mn	SI	P	S	Ti	V	Cu	Al	Ni	Cr	Mo	Nb
[%]	0.13	1.47	0.38	0.010	0.004	0.015	0.062	0.04	0.034	0.02	0.03	0.003	0.022

The treatment applied to this type of steel is controlled rolling. Controlled rolling is a thermomechanical treatment that consists of hot rolling in the austenite recrystallization area, cooling to the biphasic area and rolling, followed by the transformation of the austenite to a fine and uniform ferrite-pearlitic structure.

The final structure depends on the austenite grain size obtained after the different stages of controlled rolling.

After lamination, the sheet of steel was sent to the cooling beds, where the samples were taken (Fig. 1).

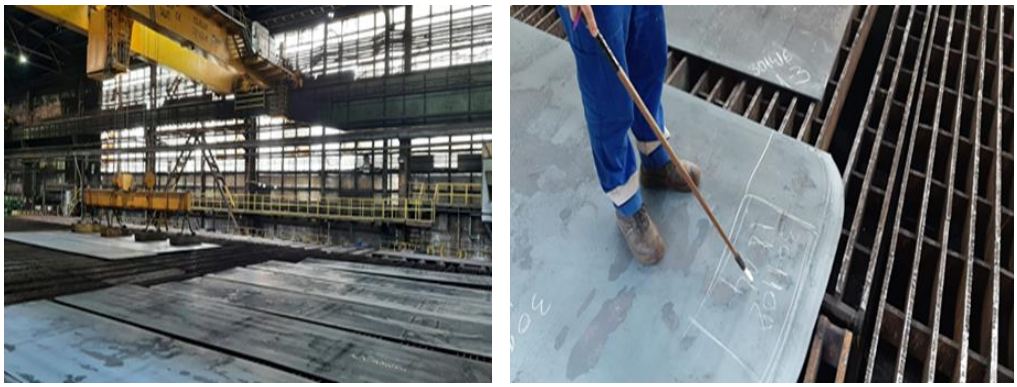

a) cooling beds b) sampling

Fig. 1. *Sampling*

a) placing the sample in the INSTRON machine b) obtaining the tested sample

Fig. 2. *Test results on the INSTRON mechanical testing machine*

THE ANNALS OF "DUNAREA DE JOS" UNIVERSITY OF GALATI
FASCICLE IX. METALLURGY AND MATERIALS SCIENCE
No. 4 - 2023, ISSN 2668-4748; e-ISSN 2668-4756
Article DOI: https://doi.org/10.35219/mms.2023.4.11

The sample presents a sufficient amount of material, for the execution of one or more samples, for the mechanical tests and the samples for achieving resilience.

The determinations were made in the Liberty Galati mechanical testing laboratory, on an X60M steel used in the manufacture of large-diameter welded pipes for the transportation of oil and natural gas products.

As part of the analysis of the structure, analyses were carried out for tensile, shock bending tests.

The tensile test was carried out using the "INSTRON" static testing machine. The stages are shown in Figure 2.

Establishing the breaking strength of the tested material is calculated with the following equations:

$$R_m = F_{max}/S_0 \text{ [MPa]}$$

The elongation at break is calculated using the relationship:

$$A = [(L_u - L_0)/L_0] \times 100 \text{ [\%]}$$

The results obtained for the mechanical tests were centralized in Table 5.

Table 5. *Mechanical test results*

Steel	Thickness [mm]	Width [mm]	Section [mm²]	FRm [kN]	FRc [kN]	Rm [Mpa]	Rc [Mpa]	A [%]
X60M	10	25	270.71	164.9	136.8	609	505	32

3. Shock bending test (resilience)

The cooling of the samples is carried out at a temperature of – 10 °C using dry ice as a cooling agent. This is done in a heat-insulating cooling container, which has a non-tight lid to prevent explosions due to the pressures of the released gases.

The test piece is inserted into the carbonic snow bath, kept for 5 min, then it is extracted and subjected to shock bending tests.

To carry out the shock bending test, is used the Charpy TINIUS OLSEN pendulum hammer.

The stages of carrying out the testing of the samples are shown in Fig. 3.

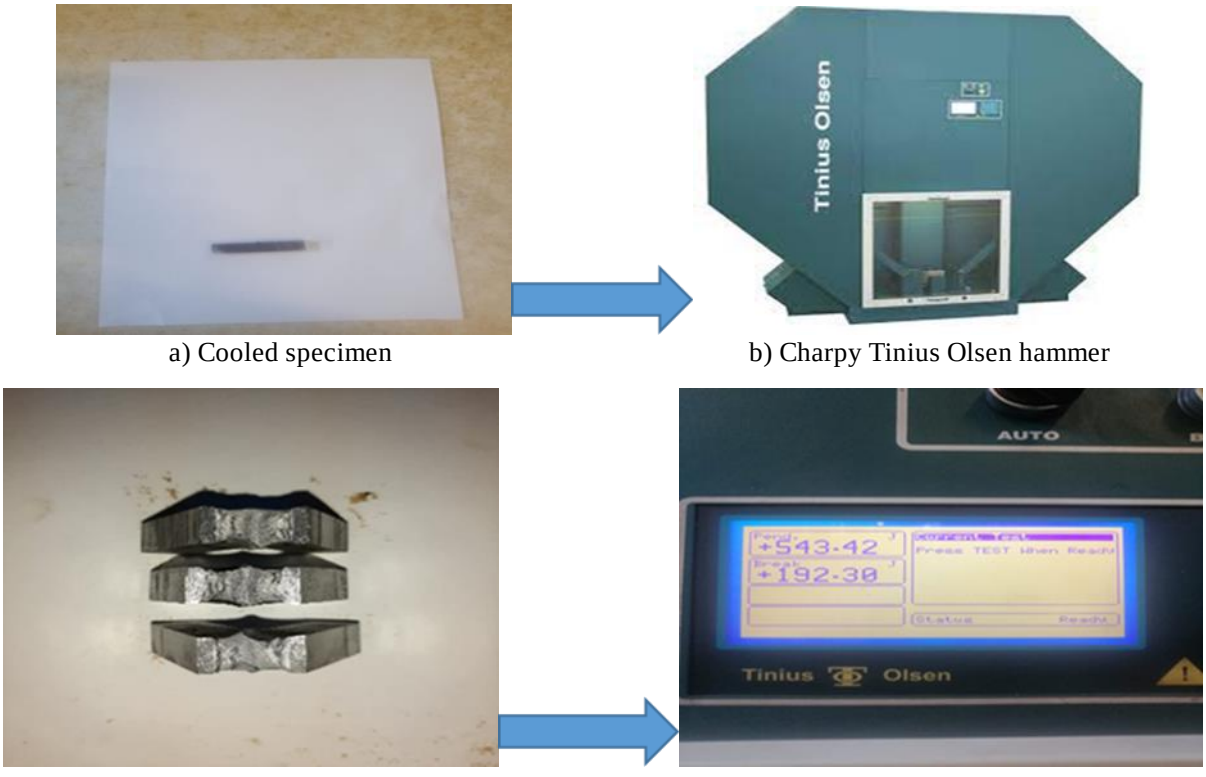

a) Cooled specimen b) Charpy Tinius Olsen hammer

Fig. 3. *Breaking of the specimens by the shock bending test*

THE ANNALS OF "DUNAREA DE JOS" UNIVERSITY OF GALATI
FASCICLE IX. METALLURGY AND MATERIALS SCIENCE
No. 4 - 2023, ISSN 2668-4748; e-ISSN 2668-4756
Article DOI: https://doi.org/10.35219/mms.2023.4.11

Results obtained from shock bending tests are presented in Table 6.

Table 6. *Shock bending test results*

Steel	Energie KV [J]	Test type [mm]	Tempure [°C]
X60M	61 – 60 – 58	KV 7.5	-10

4. Microscopic analysis

For the microscopic analysis, the sample was prepared by polishing the surfaces with the help of an automatic metallographic sample processing machine type LS2 – Remet (Fig. 4).

Fig. 4. *Automatic machine for processing metallographic samples type LS2 – Remet*

The polishing operation was performed mechanically and the metallographic attack was done with nital 2%.

The samples were analysed with the OLYMPUS PMG 3 microscope (Fig. 5).

By heating during thermal processing processes (heat treatments, plastic deformation, welding) a series of microstructural changes similar to those in non-alloyed steels can occur, which involve the change of pearlite morphology (from lamellar to semi-globalized pearlite). The extent of these phenomena depends on the value of the temperature and the holding time at that temperature [2, 5].

Fig. 5. *OLYMPUS PMG 3 metallographic optical microscope*

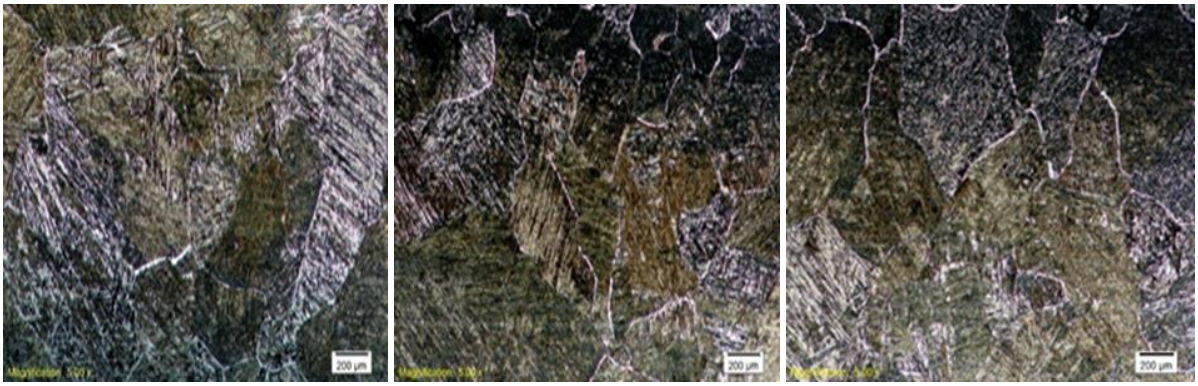

Fig. 6. *Magnified images: 200X*

5. Conclusions

The micro-alloyed steels used in the manufacture of longitudinally welded pipes under flux can be obtained by a combination between an appropriate chemical composition and a thermomechanical lamination at certain parameters of section reduction and temperature.

X60M steel, intended for the construction of pipes for the transport of gas and oil products, has very good resistance and plasticity.

X60M steels are among the materials most used in the construction of pipelines for the transport of natural gas and oil, due to an advantageous price/performance ratio.

THE ANNALS OF "DUNAREA DE JOS" UNIVERSITY OF GALATI
FASCICLE IX. METALLURGY AND MATERIALS SCIENCE
No. 4 - 2023, ISSN 2668-4748; e-ISSN 2668-4756
Article DOI: https://doi.org/10.35219/mms.2023.4.11

The role of the micro-alloy elements is to confer special properties of resistance and tenacity.

Microalloying only with niobium cannot ensure satisfactory tenacity properties for all pipe sizes and thicknesses, therefore microalloying with Ti is also done for a positive effect.

The improvement of the shock fracture energy depends on the purity of the steel and requires a low content of P and S, avoiding the formation and segregation of iron phosphide which gives a lot of brittleness to the steel.

The studied steel, X60M, intended for the construction of pipes for the transport of gas and petroleum products, has a very good resistance and plasticity.

References

[1]. Valentin Paul Tudorache, Nicolae Napoleon Antonescu, Lazăr Avram, Marius Stan, *Managementul integrității conductelor de transport țiței și gaze naturale*, Universitatea Petrol-Gaze din Ploiești.

[2]. Mitelea I., Budău V., *Materiale și tratamente termice pentru structuri sudate*, Editura de Vest, Timișoara, 1992.

[3]. Moldovan I., Crafti A., Zimbran P., *Procedee moderne de fabricare a țevilor sudate din oțel*, MIM - CPLIM, București, 1985.

[4]. Doniga A., Vasilescu E., *The influence of the termomechanical treatment condition on the structure and mechanical characteristics of the austenite hot deformation*, The Annals of "Dunarea de Jos" of Galati, 2002.

[5]. Vasilescu E., Doniga A., *The influence of the termomechanical treatment on the properties of steel plates for welded constructions*, Conf. BRAMAT, 2009.

THE ANNALS OF "DUNAREA DE JOS" UNIVERSITY OF GALATI
FASCICLE IX. METALLURGY AND MATERIALS SCIENCE
No. 4 - 2023, ISSN 2668-4748; e-ISSN 2668-4756
Article DOI: https://doi.org/10.35219/mms.2023.4.12

RESEARCH ON CORROSION UNDER TENSION A ALUMINUM ALLOY AlZn5.7MgCu

Marian-Iulian NEACȘU
"Dunarea de Jos" University of Galati, Romania
e-mail: mneacsu@ugal.ro

ABSTRACT

The paper presents the results of the research on the resistance to stress corrosion on some samples from the alloy. AlZn5.7MgCu which were previously subjected to various thermal and thermomechanical processing.

The gravimetric index or corrosion rate Vcr was used to evaluate the corrosion resistance under tension of the samples investigated in this regard.

KEYWORDS: aluminium alloy, heat treatment, corrosion, stress corrosion

1. Introduction

Aluminium is a very reactive metal, but it is also a passive metal. This contradictory nature is explainable, because it reacts with oxygen or water vapor and forms on the surface a compact and adherent oxide that prevents further reaction of aluminium with oxygen; for this reason, aluminium and most of its alloys have a very good resistance to corrosion [1-3].

Identifying the types of corrosion to which aluminium alloys are subject, as well as the way to achieve corrosion, are necessary to more easily find a solution to limit or eliminate this unwanted phenomenon.

The types of corrosion to which aluminium and its alloys are exposed are [3]: atmospheric corrosion, galvanic corrosion; corrosion in points (pitting); crevice corrosion; intercrystalline corrosion; exfoliation corrosion; fatigue corrosion; filiform corrosion; microbiological corrosion; stress corrosion.

Stress corrosion occurs if three conditions are met simultaneously [4]:

- the alloy should be sensitive to corrosion;
- the existence of a wet environment or water;
- the presence of a tensile stress, which will open the crack(s) and allow it(s) to propagate.

The corrosion resistance of Al-Zn-Mg alloys is comparable to that of Al-Mg-Si alloys, but when subjected to stresses, this property is greatly diminished. The formation of corrosion-sensitive zones at the weld boundaries is a general phenomenon in these alloys, regardless of whether they are rich or poor in zinc and magnesium [1, 4].

Aluminium alloys with a solid solution structure possess, due to their structural homogeneity, a good resistance to corrosion. Due to the fact that the precipitated phases during the aging and recovery of supersaturated solid solutions have a different structure and chemical composition from the base mass, they become sites with abnormal electrochemical activity as a result of different dissolution potentials. If the precipitate particle is anodic, it tends to dissolve in the presence of the electrolyte; if it is cathodic it is protected against corrosion, instead it will dissolve the base mass around it [5, 6].

Aluminium alloys from the Al-Zn-Mg-Cu system, both in cast and deformed state, due to the contents of Zn, Mg and Cu acquire very good mechanical properties following thermal and especially thermomechanical treatments.

Alloys of the Al-Zn system that do not contain Cu have a higher corrosion resistance than alloys of the same system, but that contain Cu.

Aluminium alloys that contain appreciable amounts of alloying elements soluble in aluminium, primarily copper, magnesium, silicon and zinc, are prone to stress corrosion.

Stress corrosion can occur in two ways [7]:

- corrosion under intergranular tension, which is the most common form;
- corrosion under transgranular stress.

Always corrosion under load was initiated by pitting corrosion and continued by intergranular attack at the grain boundary and then transgranular attack [8].

In the case of intergranular corrosion, the crack follows the grain boundaries. In transgranular stress

THE ANNALS OF "DUNAREA DE JOS" UNIVERSITY OF GALATI
FASCICLE IX. METALLURGY AND MATERIALS SCIENCE
No. 4 - 2023, ISSN 2668-4748; e-ISSN 2668-4756
Article DOI: https://doi.org/10.35219/mms.2023.4.12

corrosion, cracks appear by sectioning the grains [8], [9].

Stress corrosion represents the destruction of a metal or alloy that is subjected to the combined action of a corrosive environment and a static mechanical stress (elongation). It manifests itself through intercrystalline or transcrystalline cracks or even by breaking the part.

Stress corrosion cracking occurs when the stress value is close to the yield point, but it can also occur at lower stresses [8].

There are numerous chemical agents capable of causing stress corrosion but, in principle, chloride solutions are the most dangerous.

2. Experimental research

The investigation of the stress corrosion behavior of the studied alloy was carried out on samples that were previously subjected to various thermal and thermomechanical treatments according to Table 1.

Table 1. *The thermal / thermomechanical processing regime of the samples subjected to the stress corrosion test*

Proof coding	Thermal / thermomechanical processing regime
1	O + DPC + CPS + ÎN
2	O + DPC + CPS + ÎA
3	O + DPC + CPS + ÎA + DPR (ε = 10%) + ÎA
4	O + DPC + CPS + ÎA + DPR (ε = 20%) + ÎA
5	O + DPC + CPS + ÎA + DPR (ε = 30%) + ÎA

O – homogenization, CPS – solution hardening, ÎN – natural ageing
ÎA – artificial aging, DPC – hot plastic deformation,
DPR – cold plastic deformation with various degrees of deformation ε.

The tested samples have the dimensions of 60 x 30 x 3 mm and have the chemical composition presented in Table 2. The mechanical tension to which the samples were subjected (520N) resulted from the strength calculation. The test time was 20 days (480 hours) for each sample. The samples were weighed before corrosion, and after the corrosion test, they were weighed after carefully removing the corrosion products from their surface.

Table 2. *Chemical composition of the samples subjected to research*

Element / Alloy	Zn	Mg	Cu	Si	Fe	Pb	Cr	Mn	Al
AlZn5.7MgCu	5.76	2.61	1.55	0.15	0.19	0.021	0.19	0.10	rest

Test equipment and solution. Aluminium and aluminium alloys oxidize spontaneously, but in the presence of water molecules they form a hydrated oxide according to the reaction:

$$2Al + 6H_2O \rightarrow Al_2O_3\ 3H_2O + 3H_2$$

which can be dehydrated very easily by chlorine or sulphate ions, increasing the susceptibility to pitting corrosion.

The corrosive medium used in the experiments was a sodium chloride solution with a concentration of 3.5% NaCl.

Figure 1 shows the installation on which the stress corrosion tests were performed and which represents an original laboratory equipment designed and made based on resistance calculations.

THE ANNALS OF "DUNAREA DE JOS" UNIVERSITY OF GALATI
FASCICLE IX. METALLURGY AND MATERIALS SCIENCE
No. 4 - 2023, ISSN 2668-4748; e-ISSN 2668-4756
Article DOI: https://doi.org/10.35219/mms.2023.4.12

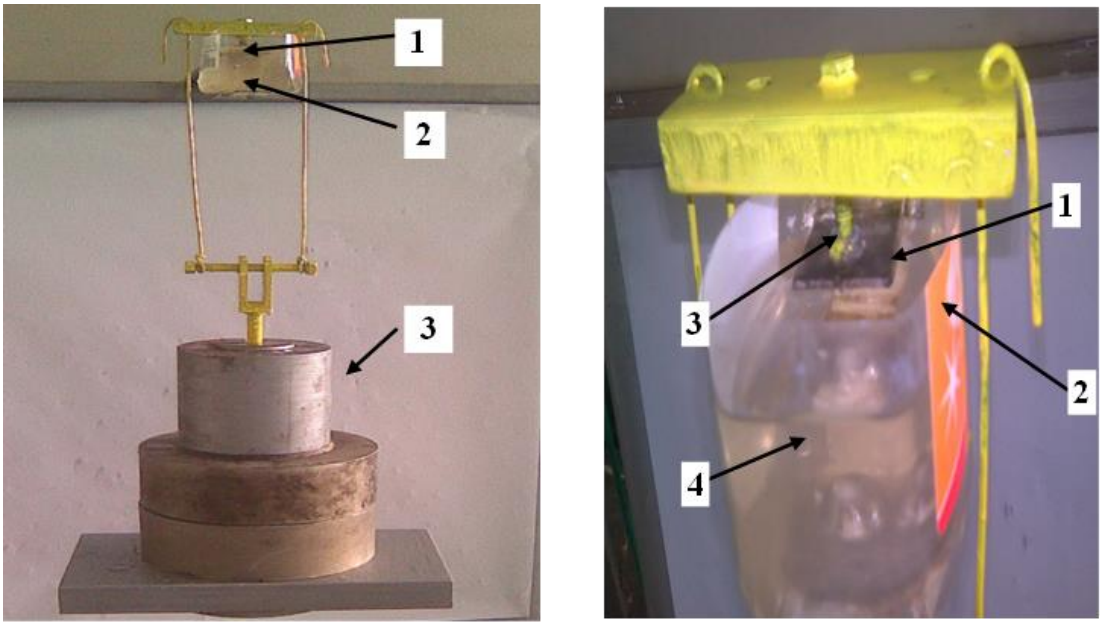

a b

Fig. 1. *a - The installation for testing the corrosion resistance under tension of the studied aluminium alloys: 1 - sample subject to corrosion; 2 - the container with the corrosion medium; 3 - mechanical voltage source. b - Detail image with the sample under tension in the corrosive environment: 1 - Al alloy sample; 2 - the container with the corrosive medium, 3.5% NaCl solution; 3 - the point of application of the force that generates the mechanical tension; 4 - the corrosive solution*

3. Results of experimental research

To assess the corrosion resistance of the samples that were subjected to the stress corrosion test, the gravimetric index or corrosion rate V_{cr} was used, which is calculated with the formula [4]:

$$V_{cr} = \frac{m_1 - m_2}{S \cdot t}, [g/m^2 h]$$

where: m_1 represents the mass of the sample before being subjected to corrosion, [g]; m_2 - is the mass of the corroded sample, [g]; S - the surface of the sample, [m^2]; t - the time in which corrosion has occurred, [h]. The data resulting from the calculations are given in Table 3.

Table 3. *Results obtained for the gravimetric index (corrosion rate V_{cr}) in the case of the samples subjected to the stress corrosion test*

Proof coding	m_1 [g]	m_2 [g]	Δm [g]	S [m^2]	Time [hours]	V_{cr} [$g/m^2 \cdot h$]	Observation
1	15	14.978	0.022	0.0027	480	0.0169	resistant
2	15	14.986	0.014	0.0027	480	0.0108	resistant
3	15	14.977	0.023	0.0027	480	0.0177	resistant
4	15	14.956	0.044	0.0027	480	0.0339	resistant
5	15	14.927	0.073	0.0027	480	0.0563	resistant

The values of the gravimetric index (corrosion rate) indicate that all samples subjected to the stress corrosion test fall into the corrosion resistance group as being corrosion resistant, for which V_{cr}. is between the values of 0.01 and 0.1 g/ m^2 h.

Among all the samples subjected to the stress corrosion test, the samples coded with number 5, with the degree of deformation of 30%, recorded the highest mass loss, but even these samples can be classified as resistant to corrosion.

THE ANNALS OF "DUNAREA DE JOS" UNIVERSITY OF GALATI
FASCICLE IX. METALLURGY AND MATERIALS SCIENCE
No. 4 - 2023, ISSN 2668-4748; e-ISSN 2668-4756
Article DOI: https://doi.org/10.35219/mms.2023.4.12

3.1. Macrostructural aspects of the surface of samples subjected to stress corrosion

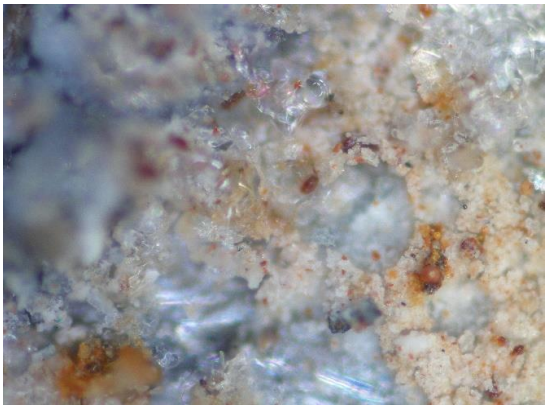

Fig. 2. *Sample 5 - Area near the place of maximum effort, Magnification: 400X*

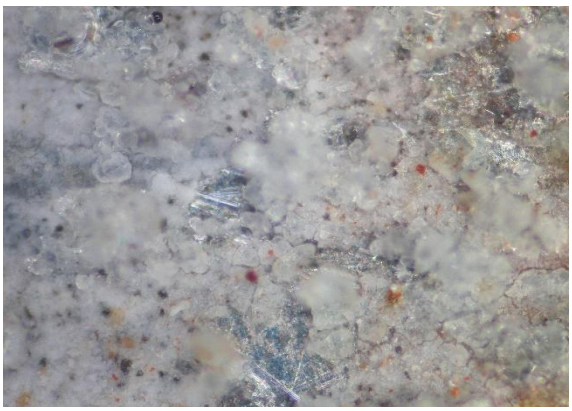

Fig. 3. *Sample 5 - Area near the force application point, Magnification: 400X*

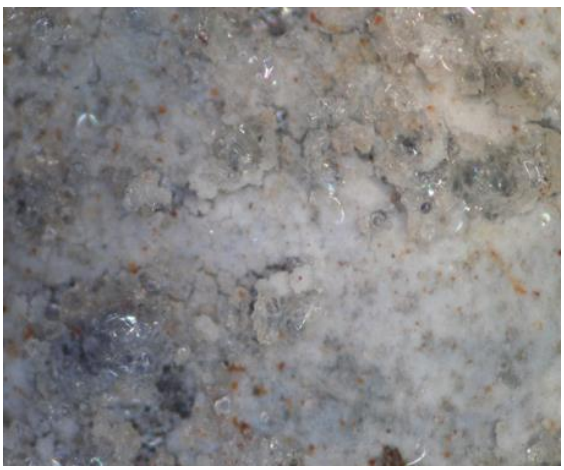

Fig. 4. *Sample 5. - Macro view of the stretched surface, Magnification: 100X*

Fig. 5. *Sample 5 - Macro aspect of the surface subjected to compression, Magnification: 100X*

4. Conclusions

The analysis of the surface of the corroded samples illustrates the point corrosion of the samples, as well as the exfoliation of the material, but without cracks or its breaking.

The amount of corrosion products decreases with the distance from the embedded area and the approach to the point of force application.

All the corrosion tests carried out in the work indicate that, near the place where the sample is embedded, i.e. in the place where the stretching effort was greater, the corrosion is more intense (expressed by the increase in the amount of corrosion products).

On an area equidistant from the end of the embedded sample, the amount of corrosion products is lower on the surface subjected to compression than on the surface subjected to tension.

Corrosion tests performed on samples 4 and 5 which were processed with a higher degree of plastic deformation, show a greater mass loss of the material, therefore a lower corrosion resistance.

Following the calculations of the corrosion rate V_{cr}, it can be stated that all samples subjected to this stress corrosion test can be rated as resistant.

For the alloys intended for the construction of airplanes with a low flight height, it is necessary to have a good resistance to corrosion because, due to the low flight height, they frequently come into contact with the humid atmosphere which negatively influences the phenomenon of corrosion by stress cracking.

References

[1]. ***, http://www.corrosionist.com/Materials_Aluminium_Alloys_Intro.htm.

THE ANNALS OF "DUNAREA DE JOS" UNIVERSITY OF GALATI
FASCICLE IX. METALLURGY AND MATERIALS SCIENCE
No. 4 - 2023, ISSN 2668-4748; e-ISSN 2668-4756
Article DOI: https://doi.org/10.35219/mms.2023.4.12

[2]. ***, http://www.scribd.com/doc/20150831/2/I-2-FORME-DE-ATAC-Coroziunea-in-puncte-pitting.
[3]. ***, http://www.scribd.com/doc/20150831/coroziunea-localizata.
[4]. Oniciu L., Constantinescu E., *Electrochimie şi coroziune*, Editura Didactică şi Pedagogică, Bucureşti, 1982.
[5]. Frankel G. S., *Corrosion: Fundamentals, Testing, and Protection*, ASM Handb., vol. 13A, p. 44073-2, 2003.
[6]. Uhlig's, *Uhlig'S Corrosion Handbook*, 2011.
[7]. Harb A. A., Ciuca I., Rahali B., *Investigation the Corrosion of Heat Transferring Unit in Hydrogen Peroxide & Sodium Chloride Solution Using Weight Loss*, vol. 79, 2017.
[8]. Beavers J., Bubenik T. A., *Stress corrosion cracking*, Elsevier Ltd, 2017.
[9]. Jones R. H., *Stress corrosion cracking*, ASM Handbook, 13A, ASM International, p. 346-366, 2003.

THE ANNALS OF "DUNAREA DE JOS" UNIVERSITY OF GALATI
FASCICLE IX. METALLURGY AND MATERIALS SCIENCE
No. 4 - 2023, ISSN 2668-4748; e-ISSN 2668-4756
Article DOI: https://doi.org/10.35219/mms.2023.4.13

POROSITY MEASUREMENTS AND ANALYSIS OF SINTERED AND THERMOCHEMICAL HEAT TREATED P/M COMPACTS

Mihaela MARIN, Florin Bogdan MARIN
"Dunarea de Jos" University of Galati, Romania
e-mail: mihaela.marin@ugal.ro

ABSTRACT

The objective of this paper was to examine the porosity in fluidized-bed carburizing on sintered alloys obtained by the powder metallurgy route using an image software analysis, and to compare the results with those obtained using the conventional porosity measuring technique. A material's porosity is a measurement of its vacancy percentage. The volume of empty space divided by the material's bulk volume, given as a percentage, determines the overall porosity of the material. The advancement of digital imaging and software has resulted in a novel and appropriate technique for figuring out the porosity of materials used in powder metallurgy.

KEYWORDS: powder metallurgy, fluidized bed carburizing, porosity, image software analysis

1. Introduction

Powder metallurgy (P/M) is a flexible manufacturing technique that involves the production of components from raw metal powders. A great degree of customization may be achieved, material waste can be minimized, and the technology can manufacture the indicated forms [1].

Understanding and controlling the porosity of the finished product is essential for guarantee its mechanical integrity and functional efficiency [2-5].

In sintered P/M alloys, porosity needs to be adjusted and balanced. Even when a certain level of porosity may be appropriate or even desired for some applications, excessive porosity can also have an impact on mechanical properties and performance. Therefore, process parameter modifications and careful consideration are necessary to attain the proper density and porosity balance [6-8]. Understanding and controlling porosity is essential in applications where sintered P/M alloys are often used, such as filters, cutting tools, bearings, and automotive components [9-11].

Understanding porosity is essential for knowing the mechanical properties and overall performance of materials, as sintering, a critical process in powder metallurgy, involves heating and compacting metal powders to produce solid structures [12-15]. Alloying elements can be added to sintered P/M alloys to improve their characteristics [16-18]. The most often added alloying elements in powder metallurgy include phosphorus, manganese, nickel, copper, and molybdenum. Because copper melts at 1083 °C during the sintering process, it fills the holes, increasing the toughness and density [19-24]. Due to the creation of Ni-rich areas during solid state sintering, nickel (Ni) boosts the sintered density and improves hardness and strength by promoting local ductility [25-27]. The hardenability of molybdenum (Mo) reacts well [28, 29].

Applying heat, thermochemical treatments, or mechanical treatments is another method to enhance the characteristics of these alloys. A thermochemical process that offers great heat and mass transfer is fluidized bed carburizing [30-36].

Porosity has an important effect in determining the success rate of fluidized-bed carburizing, a procedure frequently used to improve the surface hardness and wear resistance of P/M compacts. In carburizing, a material's surface is coated with carbon to increase its hardness and resistance to wear. In order to achieve uniform and controlled carburization, the fluidized-bed variation of this technique involves suspending the components in a fluidized bed of carburizing material.

The microstructure of sintered alloys may now be assessed non-destructively and with high accuracy using image software analysis, which has become a powerful and efficient technique for characterizing and measuring porosity in these materials. There are a number of benefits regarding employing picture

THE ANNALS OF "DUNAREA DE JOS" UNIVERSITY OF GALATI
FASCICLE IX. METALLURGY AND MATERIALS SCIENCE
No. 4 - 2023, ISSN 2668-4748; e-ISSN 2668-4756
Article DOI: https://doi.org/10.35219/mms.2023.4.13

software analysis for porosity measurement over more conventional techniques. With this method, big datasets may be evaluated quickly and automatically, leading to a deeper comprehension of the porosity distribution in the sintered alloy. It also reduces the subjectivity associated with manual approaches by providing accurate and quantitative results [37-39].

Obtaining high-resolution pictures of the microstructure of the sintered alloy is the initial stage in the image software analysis process. To get fine-grained pictures of the material, methods like optical microscopy, scanning electron microscopy (SEM), or micro-computed tomography (micro-CT) are frequently used. The input for the analysis that follows is these photographs.

Once the images are obtained, sophisticated image analysis software is employed to process and quantify the porosity. The software utilizes algorithms to identify and segment the pores within the microstructure, distinguishing them from the dense matrix of the alloy. Parameters such as pore size, shape, and distribution can be precisely measured, providing valuable insights into the material's characteristics.

The quantitative data generated through image software analysis can be used to assess the impact of various processing parameters on porosity levels in sintered alloys. Also, it can investigate the influence of sintering temperature, powder particle size, and compaction pressure on porosity formation, aiding in the optimization of manufacturing processes to achieve the desired material properties.

Moreover, image software analysis is instrumental in quality control and assurance during the production of sintered alloys. By implementing automated analyses, manufacturers can efficiently monitor and ensure consistency in porosity levels across batches, reducing the defects and enhancing the overall reliability of the final product.

This work aims to investigate the porosity in a fluidized bed carburizing sintered P/M materials using an image software tool, and then to compare the results with those obtained using a conventional approach to establish a correlation.

2. Experimental procedure

In this study, the samples were made from the Fe powder alloyed with 1.755% nickel, 1.50% Cu and 0.50% Mo. The second powder were made from Fe with 4.00% Ni, 1.50% Cu and 0.50 % Mo. As a solid lubricant, 1% zinc stearate was used. Lubricants are essential to the P/M process and are often added to mixes as an additive to lessen friction between powder particles and between powder compacts and the die-wall. The lubricant considerably increases the powder's compressibility. The green compacts were sintered for 60 minutes at 1150 °C in a laboratory furnace, after being obtained at 600 MPa pressure with a single die action. The obtained disc specimens have the dimensions of 8 6 mm. The samples were subjected to fluidized bed carburizing treatment at 930 °C during 90 minutes after cooling to room temperature the samples were. The sintered and carburized in fluidized bed density, porosity, and metallographic analysis were performed on the compacted samples. The sintered compacts' volumetric dimensional change was computed, and the specimens' overall porosity was assessed based on the variation between the measured and reference densities. One of the key advantages of image software analysis is its ability to perform three-dimensional (3D) reconstructions of the porosity within the sintered alloy. This allows for a more accurate representation of the spatial distribution of pores, enabling researchers and engineers to identify trends and patterns that might not be apparent in traditional two-dimensional analyses. Understanding the 3D porosity distribution is critical for predicting the material's mechanical behavior and structural integrity [40].

3. Results and discussions

3.1. Density results

Table 1 shows the results from conventional technique measurements of the density in sintered and carburized in fluidized bed state.

Table 1. *Sintered sintered and carburized in fluidized bed density for analysed specimens*

Powder type	Sintered density, (g/cm^3), ρs	Carburized in fluidized bed density, (g/cm^3), ρc
P_1	7.16	7.21
P_2	7.23	7.39

3.2. Microstructure analysis

The microstructures of fluidized bed carburized samples were observed by optical microscopy (Olympus BX 51M) at 100x are represented in Figure 2. The optical micrographs of the carburized in fluidized bed specimen P1 exhibit larger and irregular holes when compared to the pores in the sample with the maximum density, P_2, as can be seen by examining Figure 2.

THE ANNALS OF "DUNAREA DE JOS" UNIVERSITY OF GALATI
FASCICLE IX. METALLURGY AND MATERIALS SCIENCE
No. 4 - 2023, ISSN 2668-4748; e-ISSN 2668-4756
Article DOI: https://doi.org/10.35219/mms.2023.4.13

3.3. Porosity measurements

In Table 2 are presented the porosity measurements of P/M products calculated using the conventional method, using the density technique. Using the freeware application Fiji for image processing was another way to determine porosity. It may be used to identify porosity in images by applying filters, adjustments, and the threshold binary function. Using an optical microscope and a digital camera, pictures of non-etched materials were acquired. The application creates a separate picture with porosity by extrapolating the regions with pores using the Thresholding function, and it can compute the porosity in percents. Table 2 and Fig. 3 show the results of the porosity measurements of carburized in fluidized bed samples obtained by Fiji program. A few processing parameters, including temperature, sintering duration, powder size distribution, green and sintered density of compacts, and alloy type and quantity, influence porosity [6-8].

Table 2. *The porosity of analysed alloys in carburized in fluidized bed state*

Powder type	Porosity from convential method, (%)	Porosity from image analysis, (%)
P_1	8.61	9.76
P_2	7.82	8.44

The measurements of porosity resulted from density technique are ranging from 7.82% to 8.61%. The measurements of porosity resulted by using the Fiji software are ranging from 8.44 % for 7.21 g/cm^3 to 9.76% for 7.39 g/cm^3. A correlation between higher density and a decreasing in porosity was established. The sample P_2 had a lower porosity. Also, Fiji software can generate a plot profile of the surface for the carburized in fluidized bed samples presented in Fig. 4.

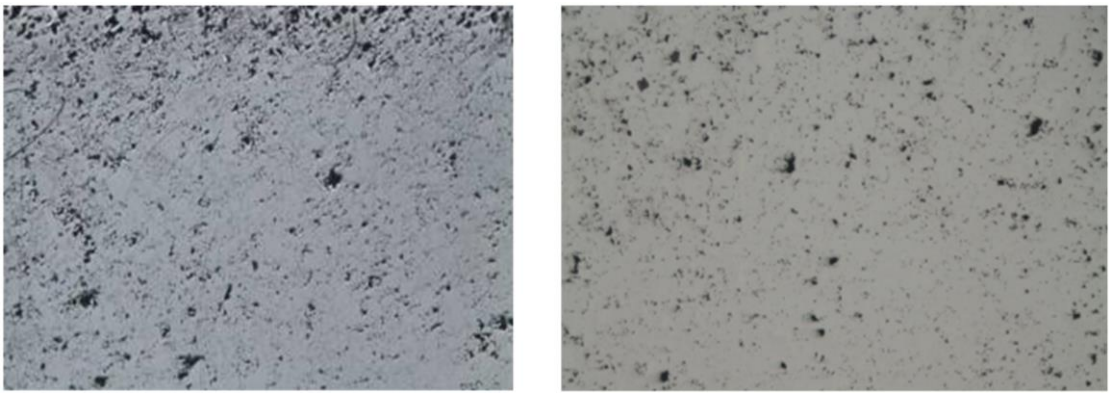

Fig. 2. *Micrographs of the non-etched carburized in fluidized bed samples a) P_1; b) P_2*

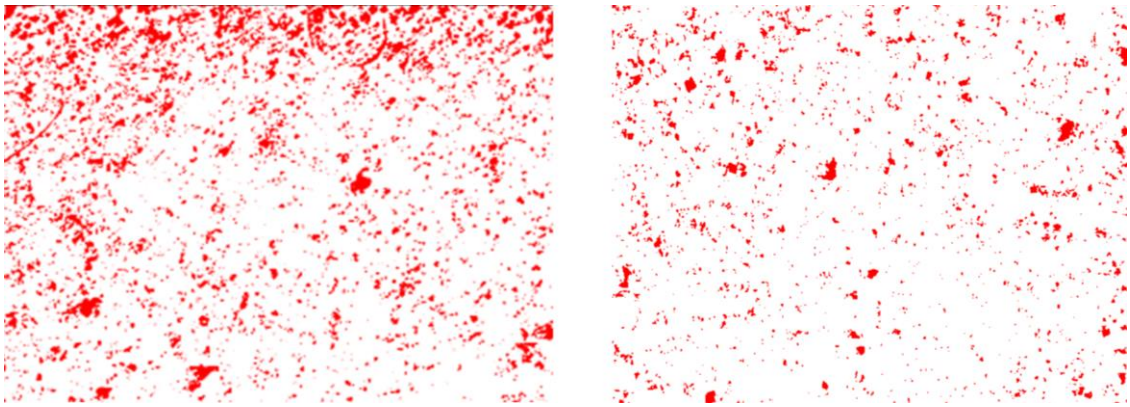

Fig. 3. *Processed images by using the image software for porosity measurements of carburized in fluidized bed samples: a) P_1; b) P_2*

THE ANNALS OF "DUNAREA DE JOS" UNIVERSITY OF GALATI
FASCICLE IX. METALLURGY AND MATERIALS SCIENCE
No. 4 - 2023, ISSN 2668-4748; e-ISSN 2668-4756
Article DOI: https://doi.org/10.35219/mms.2023.4.13

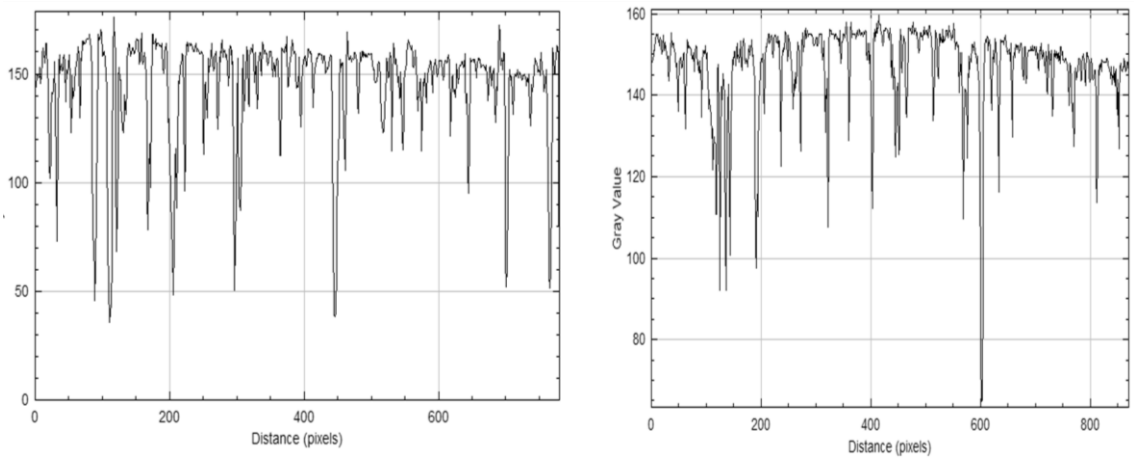

Fig. 4. *Plot profile of the surface for the carburized in fluidized bed samples, obtained using image software: a) P_1; b) P_2*

4. Conclusions

The density values obtained by the geometrical technique were linked with the measures of porosity in the fluidized bed carburized condition of the investigated materials using an image analysis program.

It was found that there was a relationship between increasing density and reducing porosity. The porosity of sample P_2 was lower.

There was a correlation found between the software data analysis and the experimental data analysis. The porosity measured from the image analysis technique was higher than the porosity measured from the density technique because the image analysis technique only accounts for open porosity; closed porosity is not taken into account. A decrease in porosity and a reduction in pore size was associated with an increase in sintered and carburizing in the samples' fluidized bed density.

The surface qualities and mechanical performance can be increased by optimizing the carburizing process settings by studying the porosity characteristics.

In conclusion, image software analysis has become an indispensable tool in the study of porosity in sintered alloys or subjected to a termochemical treatment, such as carburzing in fluidized bed, as presented in this paper. Its ability to provide accurate, quantitative, and three-dimensional insights into the material's microstructure empowers researchers and manufacturers to make informed decisions regarding process optimization, quality control, and the development of advanced materials with tailored properties.

Porosity measurements and analysis of fluidized-bed carburized P/M compacts are necessary to ensure the reliability and high quality of the final product.

As technology continues to advance, image software analysis will play an increasingly significant role in advancing our understanding of porosity in sintered alloys and optimizing their performance in various applications.

References

[1]. Jang G. B., Hur M. D., Kang S. S., *A study on the development of a substitution process by powder metallurgy in automobile parts*, J Mater Process Technol, p. 110-115, 2000.
[2]. Hamiuddin M., *Correlation between mechanical properties and porosity of sintered iron and steels-a review*, Powder Metall. Int. 18, p. 73-76, 1986.
[3]. Park J., Lee S., Kang S., Jeon J., Lee H., Kim H. –K., Choi H., *Complex effects of alloy composition and porosity on the phase transformations and mechanical properties of powder metallurgy steels*, Powder Technology, vol. 284, p. 459-466, 2015.
[4]. Lu Z., Wei D., Wei P., Liu H., Yan H., Yu S., Deng G., *Contact fatigue performance and failure mechanisms of Fe-based small-module gears fabricated using powder metallurgy technique*, Journal of Materials Research and Technology, vol. 26, p. 1412-1427, 2023.
[5]. Ehtemam-Haghighi S., Attar H., Ilya V. Okulov, Matthew S., Damon K., *Microstructural evolution and mechanical properties of bulk and porous low-cost Ti-Mo-Fe alloys produced by powder metallurgy*, Journal of Alloys and Compounds, vol. 853, 2021.
[6]. Narasimhan K. S., *Sintering of powder mixtures and the growth of ferrous powder metallurgy*, Materials Chemistry and Physics, vol. 67, p. 56-65, 2001.
[7]. Dyachkova N. L., Feldshtein E., *Microstructures, Strength Characteristics and Wear Behavior of the Fe-based P/M Composites after Sintering or Infiltration with Cu-Sn Alloy*, Journal of Materials Science & Technology, vol. 31, issue 12, p. 1226-1231, 2015.
[8]. Haynes R., *A study of effect of porosity content on ductility of sintered metals*, Powder Metall, vol. 20, p. 17-20, 1997.
[9]. Benkai L., Ding W., Li M., Zhang X., *Tool wear behavior of alumina abrasive wheels during grinding FGH96 powder metallurgy nickel-based superalloy*, Procedia CIRP, vol. 101, p. 182-185, 2021.

[10]. Konstanty J. S., *Applications of powder metallurgy to cutting tools*, Woodhead Publishing Series in Metals and Surface Engineering, Advances in Powder Metallurgy, Woodhead Publishing, p. 555-585, 2013.
[11]. Bhadeshia H. K. D. H., *Steels for bearings*, Progress in Materials Science, vol. 57, issue 2, p. 268-435, 2012.
[12]. Kulkarni H., Dabhade V. V., Blais C., *Analysis of machining green compacts of a sinter-hardenable powder metallurgy steel: A perspective of material removal mechanism*, CIRP Journal of Manufacturing Science and Technology, vol.41, p. 430-445, 2023.
[13]. Piotrowski A., Biallas G., *Influence of sintering temperature on pore morphology, Microstructure and Fatigue Behavior of Mo-Ni-Cu Alloyed Sintered Steel*, Powder Metallurgy, vol. 41, no. 2, p. 109-114, 1998.
[14]. Djohari H., Martínez-Herrera J., Derby J., *Transport mechanisms and densification during sintering: I. Viscous flow versus vacancy diffusion*, Department of Chemical Engineering and Materials Science, MN55455-0132.
[15]. Chagnon F., Trudel Y., *Effect of sintering parameters on mechanical properties of sinter hardened materials*, Advances in P/M & Particulate Materials, NJ, vol. 2, p 14-97/14-106, 1997.
[16]. Maheswari N., Ghosh Chowdhury S., Hari Kumar K. C., Sankaran S., *Influence of alloying elements on the microstructure evolution and mechanical properties in quenched and partitioned steels*, Materials Science and Engineering: A; 600, p. 12-20, 2014.
[17]. Wu M. W., Tsao L. C., Shu G. J., Lin B. H., *The effects of alloying elements and microstructure on the impact toughness of powder metal steels*, Materials Science and Engineering: vol. A 538, p. 135-144.
[18]. Trivedi S., Mehta Y., Chandra K., Mishra P. S., *Effect of carbon on the mechanical properties of powder-processed Fe-0.45 wt.% P alloys*, Indian Academy of Sciences, vol. 35, part 4, p. 481-492, 2010.
[19]. Angel W. D., Tellez L., Alcala J. F., Martinez E., Cedeno V. F., *Effect of copper on the mechanical properties of alloys formed by powder metallurgy*, Materials and Design, vol. 58, p. 12-18, 2014.
[20]. Marucci M. L., Hanejko F. G., *Effect of copper alloy addition method on the dimensional response of sintered Fe-Cu-C steels*, Advances in Powder Metallurgy and Particulate Materials, MPIF, p. 1-11, 2010.
[21]. Dong Y., Jun L., Wen J., Jie S., Kunyu Z., *Effect of Cu addition on microstructure and mechanical properties of 15%Cr super martensitic stainless steel*, Mater Des, vol. 41, p. 16-22, 2012.
[22]. Takaki S., Fujioka M., Aihara S., Nagataki Y., Yamashita Y., Sano N., Adachi Y., Nomura M., Yaguchi K., *Effect of Copper on Tensile Properties and Grain-Refinement of Steel and its Relation to Precipitation Behavior*, Mater Trans, vol. 45, p. 2239-2244, 2005.
[23]. Ramprabhu T., Sundar Sriram S., Boopathy K., Narasimhan K. S., Ramamurty U., *Effect of copper addition on the fatigue life of low alloy C-Mo powder metallurgy steel*, Metal Powder Report, vol. 66, issue 3, p. 28-34, 2011.
[24]. Yang X., Bai Y., Xu M., Guo S., *Effect of Additive Cu-10Sn on Sintering Behavior and Wear Resistance of 316L Stainless Steel*, Journal of Iron and Steel Research, International, vol. 20, issue 7, p. 84-88, 2013.
[25]. Chawla N., Babic D., Williams J. J., Polasik S. J., *Effect of copper and nickel alloying additions on the tensile and fatigue behavior of sintered steels*, Advances in powder metallurgy & particulate materials, part 5, 104, Princeton, NJ: MPIF, 2002.
[26]. Bernier F., Plamondon P., Bailon J. P., L.'Esperance G., *Microstructural characterisation of nickel rich areas and their influence on endurance limit of sintered steel*, Powder Metallurgy, vol. 54, issue 5, p. 559-565, 2011.
[27]. Sulowski M., *Structure and mechanical properties of sintered Ni free structural parts*, Powder Metallurgy, vol. 53, N. 2, p. 125-140, 2010.
[28]. Sanjay S. R., Milind M. S., Vikram V. D., *Effect of molybdenum addition on the mechanical properties of sinter-forged Fe Cu C alloys*, Journal of Alloys and Compounds 649, p. 988-995, 2015.
[29]. Li H., Cai Q., Li S., Xu H., *Effects of Mo equivalent on the phase constituent, microstructure and compressive mechanical properties of Ti-Nb-Mo-Ta alloys prepared by powder metallurgy*, Journal of Materials Research and Technology, vol. 16, p. 588-598, 2022.
[30]. Mansoorzadeh S., Ashrafizadeh F., *The effect of thermochemical treatments on case properties and impact behaviour of Astaloy CrM*, Surface and Coatings Technology, vol. 192, issues 2-3, p. 231-238, 2005.
[31]. Kazior J., Janczur C., Pieczonka T., Ploszczak J., *Thermochemical treatment of Fe–Cr–Mo alloys*, Surface and Coatings Technology, vol. 151-152, p. 333-337, 2002.
[32]. Radomyselsk I. D., Zhornyak A. F., Andreeva N. V., Negoda G. P., *The pack carburizing of dense parts from iron powder*, Powder metallurgy and metal ceramics, vol. 3, p. 204-211.
[33]. Askaria M., Khorsand H., Seyyed Aghamiric S. M., *Influence of case hardening on wear resistance of a sintered low alloy steel*, Journal of Alloys and Compounds, vol. 509, issue 24, p. 6800-6805, 2011.
[34]. Krauss G., *Microstructure residual stress and fatigue of carburized steels*, Proceedings of the Quenching and Carburizing, The Institute of Materials, p. 205-225, 1991.
[35]. Georgiev J., Pieczonka T., Stoytchev M., Teodosiev D., *Wear resistance improvement of sintered structural parts by C7H7 surface carburizing*, Surface and Coatings Technology, vol. 180-181, p. 90-96, 2004.
[36]. Sulowski M., *How processing variables influence mechanical properties of PM Mn steels*?, Powder Metallurgy Progress, vol.7, no. 2, 2007.
[37]. ***, *Fiji software*, https://fiji.sc/.
[38]. Marin M., Potecaşu F., Potecaşu O., Marin F. B., *Image Analysis Software for Porosity Measurements in Some Powder Metallurgy Alloys*, Advanced Materials Research, vol. 1143, p. 103-107, Trans Tech Publications, Ltd., 2017.
[39]. Dobrzanski L., Musztyfaga M., Actis Grande M., Rosso M., *Computer aided determination of porosity in sintered steels*, Archives of Materials Science and Engineering, vol. 38, no. 2., p. 103-11, 2009.
[40]. Dobrzanski L. A., Musztyfaga-Staszuk M., Luckos A., *The comparison of computer methods for porosity evaluation in sintered constructional steels*, Journal of Achievements in Materials and Manufacturing Engineering, vol. 61, no. 2, p. 395-402, 2013.

THE ANNALS OF "DUNAREA DE JOS" UNIVERSITY OF GALATI
FASCICLE IX. METALLURGY AND MATERIALS SCIENCE
No. 4 - 2023, ISSN 2668-4748; e-ISSN 2668-4756
Article DOI: https://doi.org/10.35219/mms.2023.4.14

CHAINSAW SOUND DETECTION USING DNN ALGORITHM

Florin Bogdan MARIN, Mihaela MARIN
"Dunarea de Jos" University of Galati, Romania
e-mail: florin.marin@ugal.ro

ABSTRACT

Deforestation and illegal logging stand as important environmental problems. In this paper we propose a DNN architecture for sound recognition of chainsaw detection. Various parameters need to be tuned in order to identify the sound of chainsaw but not to produce too much amounts of false positive detection. The task is challenging as different sound emerge in the forest.

KEYWORDS: sound processing, sound recognition, chainsaw sound detection

1. Introduction

Deforestation, the widespread cutting of forests, and illegal logging, the illicit harvesting of timber, stand as important environmental menaces with far-reaching consequences. These practices, driven by various factors including economic interests, agricultural expansion, and demand for timber, pose significant threats to biodiversity, climate stability, and the livelihoods of local communities. Illegal logging, a subset of deforestation, is perpetuated by the lure of financial gain. The demand for timber, often driven by the construction industry and global markets, creates lucrative opportunities for illegal loggers. Weak law enforcement, corruption, and inadequate governance in some regions exacerbate the problem, allowing illegal logging to persist [1-3].

The impact of deforestation and illegal logging on biodiversity is profound. Forests are home to a staggering array of plant and animal species, many of which are endemic and found nowhere else on Earth [4].

One solution to identify the use of chainsaw is to detect the specific sound using portable devices that are dedicated to this or to use cameras used for animal activity, as presented in Fig.1. The task to recognize the specific sound of chainsaw is quite challenging taking into account vast sound that emerge in forests. There are several algorithms commonly used for sound recognition.

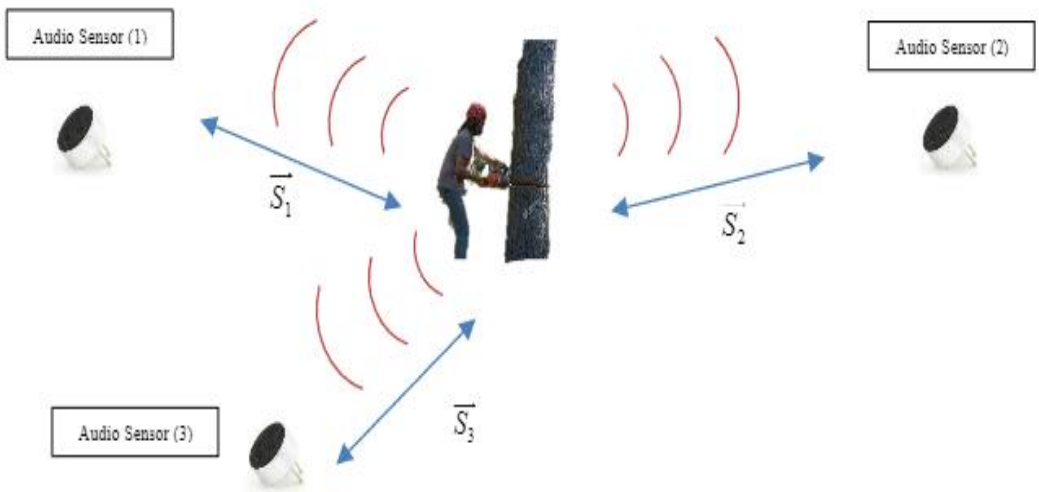

Fig. 1. *The concept of chainsaw sound detection* [1]

THE ANNALS OF "DUNAREA DE JOS" UNIVERSITY OF GALATI
FASCICLE IX. METALLURGY AND MATERIALS SCIENCE
No. 4 - 2023, ISSN 2668-4748; e-ISSN 2668-4756
Article DOI: https://doi.org/10.35219/mms.2023.4.14

Fast Fourier Transform (FFT) is a widely used algorithm for transforming a signal from the time domain to the frequency domain. It devises a signal into its constituent frequencies, allowing for the analysis of the spectral content of the sound.

Mel-Frequency Cepstral Coefficients (MFCC) is a feature extraction technique commonly used in speech and audio processing. It represents the short-term power spectrum of a sound and is widely used in sound recognition tasks. MFCCs capture the characteristics of the human auditory system.

Hidden Markov Models (HMMs) are used for modeling sequential data, making them suitable for tasks where the temporal dynamics of sound are important. HMMs have been applied in speech recognition and environmental sound classification.

Gaussian Mixture Models (GMMs) are probabilistic models that can be used for sound modeling and recognition. They are often applied to represent the statistical distribution of feature vectors extracted from sound signals.

Convolutional Neural Networks (CNNs), known for their success in image processing, have also been applied to sound recognition tasks. They can learn hierarchical representations of sound features by processing spectrogram or other time-frequency representations.

Recurrent Neural Networks (RNNs) and Long Short-Term Memory (LSTMs) are well-suited for tasks involving sequential data, making them applicable to sound recognition. They can capture temporal dependencies in sound sequences.

Support Vector Machines (SVMs) are used for classification tasks, including sound recognition. They work by finding the hyperplane that best separates different classes of sound based on their feature vectors.

Dynamic Time Warping (DTW) is a method for measuring the similarity between two temporal sequences that may vary in speed. It has been used in sound recognition to compare and align time series data.

Nearest Neighbor Algorithms, known as k-Nearest Neighbors (k-NN) and other nearest neighbour algorithms can be used for sound recognition by comparing the input sound features with those of known sound classes.

Ensemble methods, such as Random Forests or Gradient Boosting, combine the predictions of multiple base models. They are effective for improving the robustness and generalization of sound recognition systems.

Transfer learning involves leveraging pre-trained models on large datasets and fine-tuning them for specific sound recognition tasks. This approach is especially useful when limited labelled data is available.

These algorithms can be used individually or in combination, depending on the complexity of the sound recognition task and the characteristics of the data. The choice of algorithm often depends on factors such as the nature of the sound data, the available computational resources, and the specific requirements of the application. Chainsaw sound recognition using deep learning has practical applications in monitoring and combatting illegal logging activities, promoting conservation efforts, It showcases the potential of advanced technologies in addressing environmental challenges and promoting sustainable practices [5-10].

Deep learning algorithms excel at capturing complex patterns and dependencies in data, making them well-suited for tasks where distinguishing between subtle variations in sound is crucial [11, 12].

The models can adapt to variations in environmental conditions, such as changes in background noise, allowing for robust performance in diverse forest settings [13, 14].

2. Technique proposed

To train a deep learning model for chainsaw sound recognition, a dataset needs to be collected. This dataset should include audio recordings of various forest sounds, with a focus on capturing chainsaw sounds in different contexts and environmental conditions. We used own audio data consisting of 2 hours of recording.

The collected audio data is pre-processed to extract relevant features. This means converting the audio signals into a spectrogram, a visual representation of the spectrum of frequencies over time. Spectrograms provide a rich input for deep learning models to learn patterns associated with different sounds.

The deep learning model is designed to process the spectrogram data. Convolutional Neural Networks (CNNs) are used for sound recognition tasks. Recurrent Neural Networks (RNNs) or Long Short-Term Memory (LSTM) networks are other algorithm employed to capture temporal dependencies in the audio signals.

Training the Model is one important step in using CNN.

The model is trained using the pre-processed data, with chainsaw and non-chainsaw sounds labelled appropriately. During training, the deep learning algorithm adjusts its internal parameters based on the input data, learning to recognize features that distinguish chainsaw sounds from other sounds in the forest.

The trained model is evaluated on a separate dataset to assess its performance. Adjustments and fine-tuning are done based on the evaluation results to

THE ANNALS OF "DUNAREA DE JOS" UNIVERSITY OF GALATI
FASCICLE IX. METALLURGY AND MATERIALS SCIENCE
No. 4 - 2023, ISSN 2668-4748; e-ISSN 2668-4756
Article DOI: https://doi.org/10.35219/mms.2023.4.14

enhance the model's accuracy and generalization capabilities.

Once trained, the deep learning model can be used for chainsaw sound recognition in real-time. When deployed in the field, the model processes incoming audio signals and predicts whether the sound corresponds to a chainsaw.

The strengths of deep learning in this context include an important stage in learning, feature learning. Deep learning models automatically learn hierarchical representations of features from the raw audio data, eliminating the need for manual feature engineering.

In this study, we test several parameters for a deep learning algorithm to detect the presence of acoustic data of engine chainsaw. As chainsaw sound are rare events, we aimed to create a network architecture that maximises parameters in order to minimise false negatives and protecting forest ecosystems.

Using a Convolutional Neural Network (CNN) for audio recognition involves experimenting with various architectural elements and hyperparameters to achieve better performance.

Concerning convolutional layers, we experiment with the number of convolutional layers, kernel sizes, and the number of filters in each layer. Increasing the depth and width of the network capture more complex features. We tested the network for two convolutional layers with the size 3X3 and 6 layers with the size 3X3. The difference in accuracy to identify was very small, 0.5 percent, but the learning time increased by 30 percent.

Adjust the pooling layer's size and stride may produce improved results. Pooling helps reduce spatial dimensions and control overfitting. We tested using

Pool Size of (2,2) (4,4) and the identification rate drops from 98.2% to 90%. That is because the pool size defines the spatial extent over which the pooling operation is applied. A larger pool size reduces spatial dimensions and discard fine features.

Adjusting the learning rate (lr) with a too high learning rate can cause the model to converge too quickly or oscillate, while too low learning rate can lead to slow convergence. We experimented with optimizers Adam and SGD. For our own data set Adam predicted with 12% better results than SGD. The batch size can impact training speed and memory usage.

We experiment different size of 32,64,128. The best prediction rate was 94.2%, 95.2%, 92.3 % respectively. However, we note that false pozitive detection are higher in case of 64 dimensions.

3. Conclusions

Acoustic technology offers a multitude of opportunities for monitoring biodiversity, environmental health, and human disturbance such as gun hunting. However, there is currently a mismatch between the speed that affordable hardware is being developed and the ability of ecologists to process the vast amounts of data collected.

We have developed a deep learning technique that is able to classify sound information. Our algorithm achieve > 95% accuracy even we used relatively small training data sample size. Our algorithm is designed to work on low computational resources devices such as remotely processing units.

References

[1]. Wang S. F., Wang K. Y., Wang X. J., Liu Z. Q., *A Novel Illegal Logging Monitoring System Based on WSN*, Advanced Materials Research, p. 1417-142, 2012.

[2]. Tang Y., Han P., Wang Z., Hu L., Gao Y., Li H., *Based on intelligent voice recognition of forest illegal felling of detecting methods*, 2nd International Conference on Cloud Computing and Intelligent Systems, p. 1153-1156, 2012.

[3]. Soisoonthorn T., Rujipattanapong S., *Deforestation detection algorithm for wireless sensor networks*. 10.1109/ISCIT.2007.4392237, 2007.

[4]. Colonna J. G., Gatto B., Santos E. D., Nakamura E. F., *A framework for chainsaw detection using one-class kernel and wireless acoustic sensor networks into the amazon rainforest*, Mobile Data Management (MDM), 17th IEEE International Conference, vol. 2, p. 34-36, 2016.

[5]. Harvanova V., Vojtko M., Babis M., Duricek M., Pohronska M., *Detection of wood logging based on sound recognition using zigbee sensor network*, In Proceedings of the International Conference on Design and Architectures for Signal and Image Processing, Tampere, Finland, 2-4 November 2011.

[6]. Kalhara P. G., Jayasinghearachchd V. D., Dias A. H. A. T., Ratnayake V. C., Jayawardena C., Kuruwitaarachchi N., *TreeSpirit: Illegal logging detection and alerting system using audio identification over an IoT network*, In Proceedings of the 2017 11th International Conference on Software, Knowledge, Information Management and Applications (SKIMA), Malabe, Sri Lanka, 6–8 December 2017.

[7]. Prasetyo D. C., Mutiara G. A., Handayani R., *Chainsaw sound and vibration detector system for illegal logging*, In Proceedings of the 2018 International Conference on Control, Electronics, Renewable Energy and Communications (ICCEREC), Bali, Indonesia, 5–7 December 2018.

[8]. Jubjainai P., Pathomwong S., Siripujaka P., Chiengmai N., Chaiboot A., Wardkein P., *Chainsaw location finding based on travelling of sound wave in air and ground*, IOP Conf. Ser. Earth Environ. Sci. 2020.

[9]. Andrei V., Cucu H., Petrică L., *Considerations on developing a chainsaw intrusion detection and localization system for preventing unauthorized logging*, Journal of Electrical and Electronic Engineering, 3(6), p. 202-207, 2015.

[10]. Czuni L., Varga P. Z., *Time Domain Audio Features for Chainsaw Noise Detection Using WSNs*, IEEE Sens. J. 17, 1, 2017.

[11]. Meedeniya D., Ariyarathne I., Bandara M., Jayasundara R., Perera C., *A Survey on Deep Learning Based Forest Environment Sound Classification at the Edge*, ACM Computing Surveys, 56(3), p. 1-36, 2023.

[12]. Somwong B., Kumphet K., Massagram W., *Acoustic Monitoring System with AI Threat Detection System for Forest*

Protection, 20th International Joint Conference on Computer Science and Software Engineering (JCSSE), p. 253-257, IEEE, 2023.

[13]. Stefanakis N., Psaroulakis K., Simou N., Astaras C., *An Open-Access System for Long-Range Chainsaw Sound Detection*, 30th European Signal Processing Conference (EUSIPCO), p. 264-268, IEEE, 2022.

[14]. Prasetyo D. C., Mutiara G. A., Handayani R., *Chainsaw sound and vibration detector system for illegal logging*, International Conference on Control, Electronics, Renewable Energy and Communications (ICCEREC), p. 93-98, IEEE, 2018.

THE ANNALS OF "DUNAREA DE JOS" UNIVERSITY OF GALATI
FASCICLE IX. METALLURGY AND MATERIALS SCIENCE
No. 4 - 2023, ISSN 2668-4748; e-ISSN 2668-4756
Article DOI: https://doi.org/10.35219/mms.2023.4.15

SUPERVISED LEARNING PLASTIC DEFECT ALGORITHM DETECTION

Florin Bogdan MARIN, Mihaela MARIN
"Dunarea de Jos" University of Galati, Romania
e-mail: florin.marin@ugal.ro, mihaela.marin@ugal.ro

ABSTRACT

The goal of this research is to develop a supervised learning algorithm able to detect the defects of plastic's material. Finding patterns or examples in a dataset that differ from the norm is known as anomaly detection in plastic textures. Anomalies, in the context of plastic textures, can refer to imperfections' deviations, or anomalies in the material that may have an impact on the final product's overall quality. Conventional anomaly detection techniques frequently rely on rule-based systems or manual examination, which can be laborious, subjective, and unable to identify small anomalies.

KEYWORDS: computer vision, passenger fatigue detection, Advanced Driver Assistance System

1. Introduction

In recent years, the proliferation of plastic materials in various industries has raised concerns about the need for effective quality control and anomaly detection in the production process. Ensuring the quality and integrity of plastic textures is crucial for maintaining product standards and meeting consumer expectations.

The importance of product enclosure plastic components extends far beyond their structural role, encompassing crucial aspects that directly impact the user experience and satisfaction of clients. Two significant facets that contribute to this importance are the touch texture and design of these plastic components, touch texture and design [1].

The touch texture of plastic components plays a pivotal role in shaping the tactile experience of users interacting with a product. Clients often form their first impressions through the sense of touch, and the texture of plastic enclosures can greatly influence the perceived quality and premium feel of a product. A smooth and pleasing texture not only enhances the overall aesthetics but also conveys a sense of durability and sophistication [2].

The design of product enclosure plastic components is a key factor in determining the visual appeal and functionality of a product. A good design not only contributes to the product's aesthetic appeal but also influences its usability and ergonomics. Clients often seek products that not only perform their intended functions efficiently but also align with their personal preferences and lifestyle. The design of plastic components can significantly impact the user's overall satisfaction and willingness to engage with the product. Additionally, an aesthetically pleasing design enhances the marketability of the product, attracting potential customers and setting it apart from competitors. Thus, the design of plastic components within the product enclosure is integral to creating a holistic and desirable user experience.

One promising approach to address this challenge is supervised anomaly detection using transfer learning, a technique that leverages pre-trained models to enhance the performance of anomaly detection in specific domains.

Anomaly detection in plastic textures involves identifying patterns or instances that deviate from the norm within a given dataset. In the context of plastic textures, anomalies may include defects, irregularities, or abnormalities in the material that can affect the overall quality of the final product. Traditional anomaly detection methods often rely on manual inspection or rule-based systems, which can be time-consuming, subjective, and may not capture subtle anomalies.

Supervised learning is a machine learning paradigm where a model is trained on labelled data to make predictions or classifications [3, 4]. Transfer learning extends this concept by leveraging knowledge gained from pre-trained models on large datasets and applying it to a new, related task. In the context of plastic texture anomaly detection, transfer

THE ANNALS OF "DUNAREA DE JOS" UNIVERSITY OF GALATI
FASCICLE IX. METALLURGY AND MATERIALS SCIENCE
No. 4 - 2023, ISSN 2668-4748; e-ISSN 2668-4756
Article DOI: https://doi.org/10.35219/mms.2023.4.15

learning allows the model to benefit from patterns learned from diverse datasets, improving its ability to identify anomalies in specific plastic textures [5, 6].

There are many challenges in plastic texture anomaly detection [7]. Plastic textures exhibit a wide range of variations, making it challenging to develop a one-size-fits-all anomaly detection model [1, 8, 9-10]. Supervised learning may struggle when confronted with limited labelled data, as collecting a comprehensive dataset for every type of plastic texture anomaly is often impractical (Fig. 1). Transfer learning addresses this challenge by enabling the model to generalize well to new data by leveraging knowledge from broader domains. Transfer learning enables the model to extract relevant features from pre-trained models, which is particularly beneficial in cases where manual feature engineering is challenging.

Improved generalization is necessary because by learning from diverse datasets, the model can better generalize to various plastic textures, even those with limited labelled data, thereby enhancing its anomaly detection capabilities [11, 12]. Leveraging pre-trained models significantly reduces the time required for model training, allowing for more efficient development and deployment of anomaly detection systems. As the plastic industry evolves, new types of anomalies may emerge [13]. Transfer learning equips the model to adapt to these changes by incorporating knowledge from continuously updated pre-trained models [14].

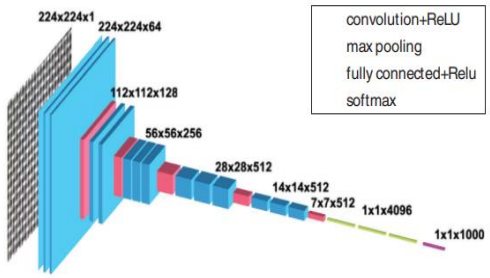

Fig. 1. *Architecture of the VGG19 network* [3]

Supervised anomaly detection using transfer learning presents a promising avenue for enhancing the detection of anomalies in plastic textures [15, 16]. By leveraging the power of pre-trained models and transferring knowledge across domains, this approach addresses the challenges posed by the diverse and evolving nature of plastic materials. As industries continue to prioritize quality control, the integration of transfer learning in anomaly detection systems holds great potential for ensuring the production of high-quality plastic products that meet the stringent demands of today's markets.

2. Technique proposed

Supervised anomaly detection in computer vision for detecting plastic texture defects often involves the use of deep learning algorithms. One commonly employed architecture for this task is the Convolutional Neural Network (CNN), which has proven effective in image classification and anomaly detection. Here is an outline of the architecture for supervised anomaly detection in the context of plastic texture defect detection.

We used several steps to identify defect in texture of plastic material. We used a pre-trained CNN architecture with ResNet. The supervised training is consisting of adding new layers to the modified CNN for the specific anomaly detection task.

We trained the model on the labelled dataset, using a binary cross-entropy loss function to distinguish between normal and defective textures. We used 200 images of samples with no defects and 40 with defects. During testing, pass new images through the trained model to obtain anomaly scores. The plastic component is of a hardware portable enclosure (Fig. 2).

Fig. 2. *Plastic enclosure pattern real size*

Anomaly scores can be calculated based on the difference between the predicted output and the ground truth labels.

Higher anomaly scores indicate a higher likelihood of a defect. To evaluate the performance of the model on a separate test dataset we used 20 with defects.

Fine-tune the model and adjust hyperparameters as needed for optimal performance is needed during using to introduce new data to the model.

Iterating on the model based on the evaluation results and, if necessary, incorporate additional data for further training is a must. We excluded techniques such as data augmentation to enhance the model's ability to generalize to different defect types, as will affect precision.

THE ANNALS OF "DUNAREA DE JOS" UNIVERSITY OF GALATI
FASCICLE IX. METALLURGY AND MATERIALS SCIENCE
No. 4 - 2023, ISSN 2668-4748; e-ISSN 2668-4756
Article DOI: https://doi.org/10.35219/mms.2023.4.15

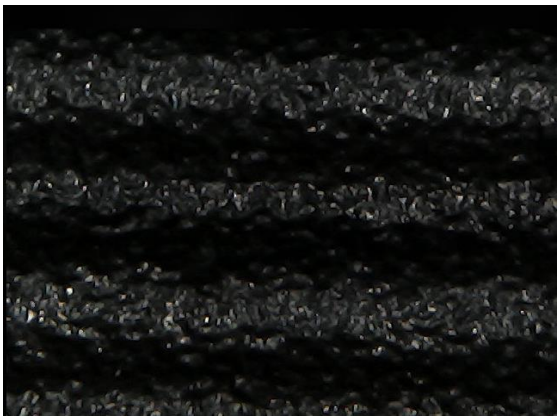

Fig. 3. *Pattern at 50X magnification*

As it may be noted the image at 50X magnification shows that no constant features can be detected such as lines. The pattern in the plastic enclosure exists but no direct detection using patterns of constant information can be used (Fig. 3 and Fig. 4). This algorithm provides a framework for implementing supervised anomaly detection in computer vision for plastic texture defect detection. We underline that the choice of the pre-trained model, architecture modifications and hyperparameter tuning may vary based on the specific plastic textures.

Accuracy learning rate shows a good learning rate though overfitting shows that the trained samples need more data for training. We used a network with 4 hidden layers, the input images are 128 X 128 pixels. We choose high learning rate (0.01) and we can see the model oscillate (Fig. 5). We chose too low a learning rate (0.001) but we obtained little or no convergence. Finally, we obtained a 93% rate detection.

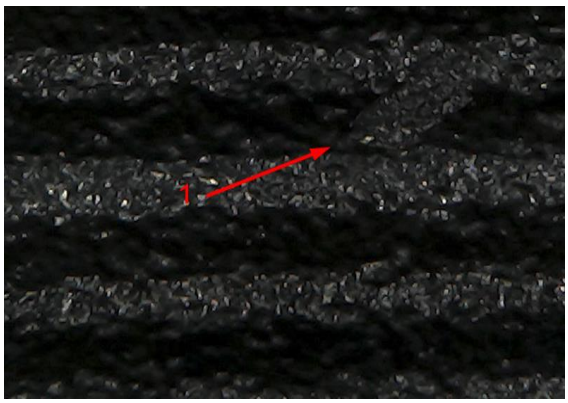

Fig. 4. *Defect present (1)*

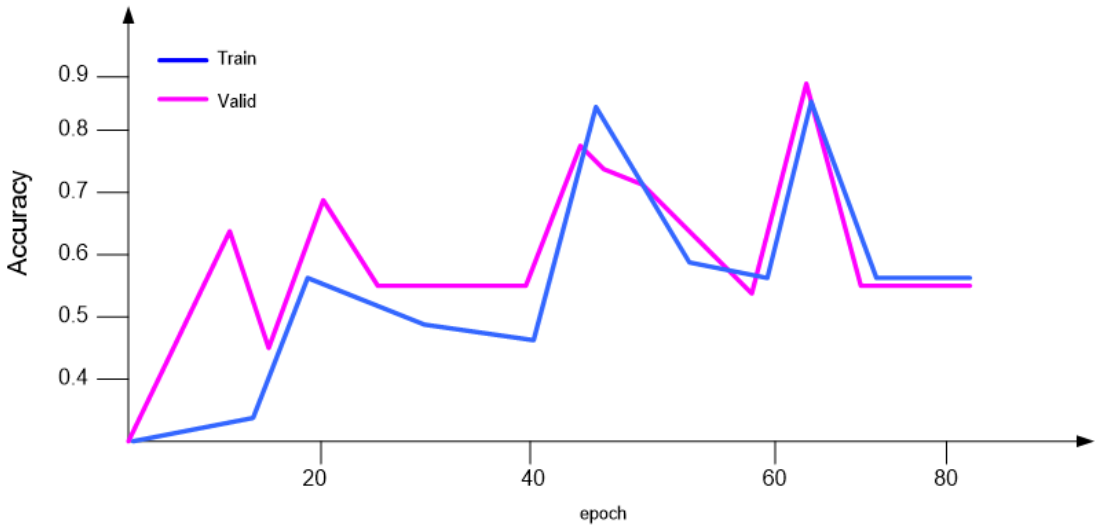

Fig. 5. *Accuracy learning rate*

3. Conclusions

Detecting defects in plastic enclosure is a challenging task when the patterns show hard to find patterns. Moreover, in case of images at magnification, the identification needs to be with high precision rate. The detection of defects allows to take measures to identify the source of defects.

The parameters of the network are causing the accuracy.

For our experiments choosing a high learning rate for Adam optimization parameter allows identification of defects. Also, the resolution of images for training translates into improved detection rate.

THE ANNALS OF "DUNAREA DE JOS" UNIVERSITY OF GALATI
FASCICLE IX. METALLURGY AND MATERIALS SCIENCE
No. 4 - 2023, ISSN 2668-4748; e-ISSN 2668-4756
Article DOI: https://doi.org/10.35219/mms.2023.4.15

References

[1]. Ai D., Jiang G., Siew Kei L., Li C., *Automatic Pixel-Level Pavement Crack Detection Using Information of Multi-Scale Neighborhoods*, IEEE Access, vol. 6, p. 24452-24463, 2018.

[2]. Yao H., Liu Y., Li X., You Z., Feng Y., Lu W., *A Detection Method for Pavement Cracks Combining Object Detection and Attention Mechanism*, IEEE Transactions on Intelligent Transportation Systems, vol. 23, no. 11, p. 22179-22189, Nov. 2022.

[3]. Velasquez R. A., Vanessa J., Lara M., *Automatic evaluation of cracks with semantic segmentation model with U-Net and an Efficient Net-b*, IEEE XXX International Conference on Electronics, Electrical Engineering and Computing (INTERCON), p. 1-7, 2023.

[4]. Dinh T. H. *et al.*, *Toward Vision-Based Concrete Crack Detection: Automatic Simulation of Real-World Cracks*, EEE Transactions on Instrumentation and Measurement, vol. 72, p. 1-15, art no. 5032015, 2023.

[5]. Park J., Chen Y. -C., Li Y. -J., Kitani K., *Crack Detection and Refinement Via Deep Reinforcement Learning*, IEEE International Conference on Image Processing (ICIP), Anchorage, AK, USA, 2021.

[6]. Akcay S., Abarghouei A. A., Breckon T. P., *GANomaly: Semi-supervised anomaly detection via adversarial training*, 2018.

[7]. Antipov G., Berrani S.-A., Ruchaud N., Dugelay J.-L., *Learned vs. hand-crafted features for pedestrian gender recognition*, Proceedings of the 23rd ACM International Conference on Multimedia, 2015.

[8]. Zhang J., Liang J., Zhang C., Zhao H., *Scale invariant texture representation based on frequency decomposition and gradient orientation*, Pattern Recognition Letters, vol. 51, p. 57-62, 2015.

[9]. Perepu P. K., *Deep learning for detection of text polarity in natural scene images*, Neurocomputing, vol. 431, 2021.

[10]. Zhu A., Wang G., Dong Y., *Detecting natural scenes text via auto image partition, two-stage grouping and two-layer classification*, Pattern Recognition Letters, vol. 67, Part 2, p. 153-162, 2015.

[11]. Do M. N., Vetterli M., *Wavelet-based texture retrieval using generalized Gaussian density and Kullback-Leibler distance*, IEEE Transactions on Image Processing, vol. 11, no. 2, p. 146-158, 2002.

[12]. Mathiassen J., Skavhaug A., Bo K., *Texture Similarity Measure Using Kullback-Leibler Divergence between Gamma Distributions*, ECCV 2002, LNCS 2352, p. 133-147, 2002.

[13]. Aiger D., Talbot H., *The phase only transform for unsupervised surface defect detection*, IEEE Computer Society Conference on Computer Vision and Pattern Recognition, p. 295-302, 2010.

[14]. Arivazhag S., Ganesan L., Bama S., *Fault segmentation in fabric images using Gabor wavelet transform*, Mach. Vis. Appl., vol. 16, p. 356-363, 2006.

[15]. Badrinarayanan V., Kendall A., Cipolla R., *Segnet: A deep convolutional encoder-decoder architecture for image segmentation*, IEEE transactions on pattern analysis and machine intelligence, 2017.

[16]. Maalej M., Cherif R., Yaddaden Y., Khoumsi A., *Automatic Crack Detection on Concrete Structure Using a Deep Convolutional Neural Network and Transfer Learning*, 2nd International Conference on Advanced Electrical Engineering (ICAEE), p. 1-6, 2022.

THE ANNALS OF "DUNAREA DE JOS" UNIVERSITY OF GALATI
FASCICLE IX. METALLURGY AND MATERIALS SCIENCE
No. 4 - 2023, ISSN 2668-4748; e-ISSN 2668-4756
Article DOI: https://doi.org/10.35219/mms.2023.4.16

MODELING AND SIMULATION OF AUXETIC MATERIALS FOR BALISTIC PROTECTION

Florin-Bogdan MARIN, Alexandru Andrei DOGARU, Mihaela MARIN
"Dunarea de Jos" University of Galati, Romania
e-mail: flmarin@ugal.ro

ABSTRACT

A type of structural metamaterials known as auxetics has a negative Poisson's ratio. Auxetic structurals have been found to possess a number of better qualities when compared to traditional ones, including: greater energy absorption, stronger indentation resistance, and enhanced mechanical properties. As a result, auxetic structures are becoming more known as a high-performance, lightweight defensive construction that can survive collisions and blasts.

KEYWORDS: modeling, simulation, auxetic materials, balistic protection

1. Introduction

Auxetic materials are of interest due to their counterintuitive behavior under deformation and enhanced properties due to negative values of Poisson's ratio. Auxetic materials' qualities must in some way correspond to the fundamental requirements of the application to be useful. Numerous elements and considerations must be taken into account when deciding which auxetic cell structure to use in a certain application [1-10].

An application's fundamental criteria must be identified first. For instance, auxetic structures are employed in some applications because of their capacity to enlarge under strain, with the size of the negative Poisson ratio (NPR) being the attribute to be focused on [11-15]. However, a minimal degree of stiffness might be necessary. Each unit cell's characteristics and constraints will reveal how well-suited it is. By altering the geometry of the unit cell, structural qualities can be changed, which will ultimately affect how the cell can be optimized for an application. If it is subjected to a stretch greater than a small one, some unit cells quickly lose their auxetic characteristics. Additionally, during the same stretch, some unit cells will suffer a localized maximum stress intensity in comparison to others. Some unit cells display auxetic activity for only one type of strain or are more restricted in that strain due to the geometry of their structure. It is crucial to take an application's required extents into account. The 2D or 3D nature of an auxetic unit cell is a crucial consideration [16-21].

2D geometry can be used to describe 2D unit cells. On the other hand, 3D unit cells require 3D geometry to be defined. While three-dimensional unit cells can display auxetic behavior in all three dimensions, two-dimensional unit cells can only do so in two of the four dimensions. As a result, 3D unit cells must be used in applications that call for an auxetic reaction in all three dimensions [22-24]. One such application is impact resistance, where the impact may be generated from an unknowable direction. The deformation mechanism of auxetic structures can be used to improve other qualities, whether through theory or practice.

In contrast to the characteristics and actions that may be seen at the cellular level, structural material attributes are the characteristics that an auxetic network displays at the macro level. There are several characteristics that are inherently auxetic, meaning they can be connected to a structure that exhibits an NPR and are not frequently observed in conventional structures. The performance is mostly determined by the geometry, not the material, because they directly depend on the special deformation mechanism of auxetic structures.

In this study, the ballistic impact behavior of auxetic sandwich composite armour was investigated.

2. Experimental procedure

In this research, a hybrid structure composed of an auxetic core was made sandwiched between front and back plates. We aim to simulate the effects of a projectile traveling at various speeds on composite auxetic sandwich armour. The Inventor Nastram

THE ANNALS OF "DUNAREA DE JOS" UNIVERSITY OF GALATI
FASCICLE IX. METALLURGY AND MATERIALS SCIENCE
No. 4 - 2023, ISSN 2668-4748; e-ISSN 2668-4756
Article DOI: https://doi.org/10.35219/mms.2023.4.16

program was used. The 3D model proposed is presented in Figure 1. The results were compared with monolithic armour under the same boundary conditions and speeds. The auxetic core was constructed from discrete re-entrant cellular units using 3D Inventor modeling software. The parametric geometry of the unit cell is presented in Figure 2. The Momentum and Kinetic Energy impulse of the model was converged with a fine mesh of solid tetrahedral and hexahedral elements for the auxetic armour models, with 463,835 elements and 418,512 nodes. The width of ballistic protection is 40 mm.

3. Results and discussions

Following the numerical experiments performed on the 3 D model proposed, the analysis demonstrates that the auxetic structure, as opposed to the monolithic panel, experiences a larger energy translation of a projectile's kinetic energy into elastic energy as a result of the elastic deformation of the unit cells. The auxetic structure outperforms the monolithic panel due to its better absorption capacity. Although the auxetic model experiences more deformation than the monolithic panel, the rear plate is unaffected by this deformation, elastic's dissipation. In the auxetic structure, elastic energy dissipation is stronger. The threat level is greatly decreased by the auxetic structure, which may be used at higher speeds and is secure up to 450 m/s.

The Figure 4 shows the projectile penetration and response behavior of the auxetic core. In the, the penetration is minimal and the energy absorption is mostly elastic, shown by deformation patterns in auxetic cells. It was noticed that the front face was slightly damaged after projectile impact. Auxetic cells could be observed vibrating frequently as the projectile was ricocheting.

It has been shown that due to the sufficient densification and indentation resistance provided by the auxetic core, the projectile cannot penetrate the rear face plate, up to a projectile velocity of 450 m/s.

The auxetic structure is safe up to 450 m/s and can be used at higher speed, significantly reducing the threat level. At 650 m/s, the rear face is damaged.

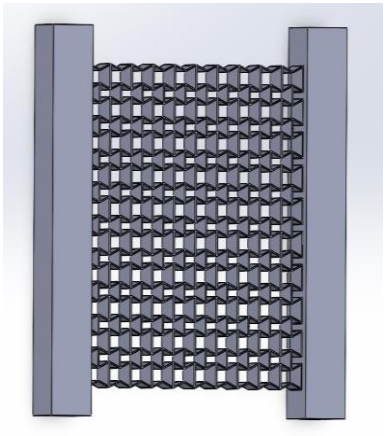

Fig. 1. *3D model proposed*

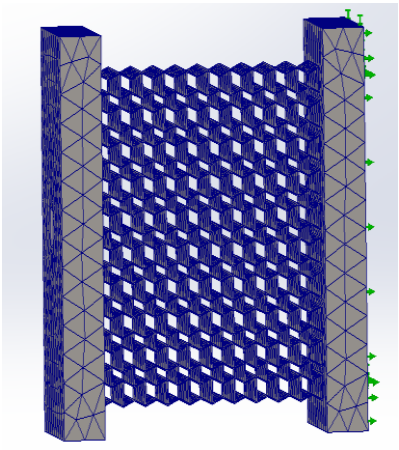

Fig. 2. *Mesh model for analyzed area*

THE ANNALS OF "DUNAREA DE JOS" UNIVERSITY OF GALATI
FASCICLE IX. METALLURGY AND MATERIALS SCIENCE
No. 4 - 2023, ISSN 2668-4748; e-ISSN 2668-4756
Article DOI: https://doi.org/10.35219/mms.2023.4.16

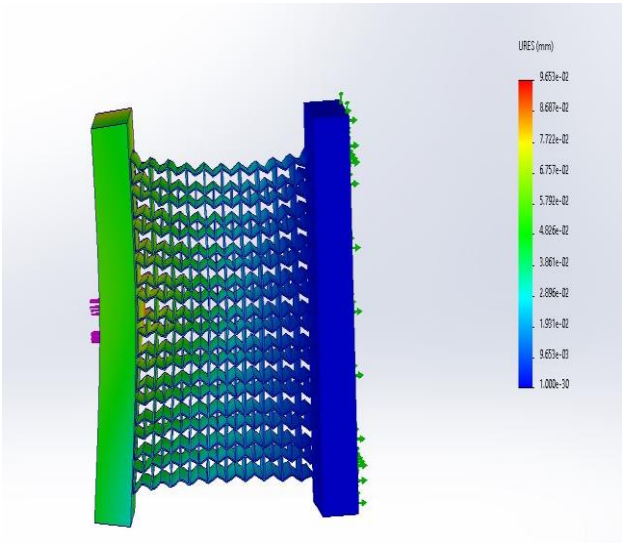

Fig. 3. *The deformed 3D model*

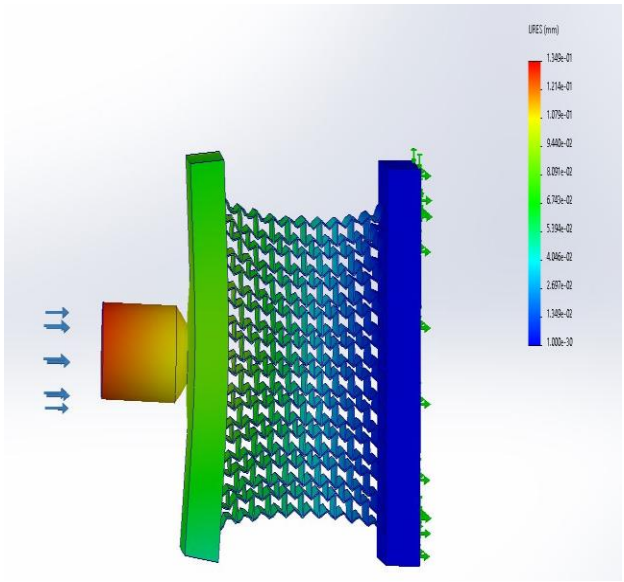

Fig. 4. *The projectile penetration and the response behavior of the auxetic core*

4. Conclusions

The ballistic impact behavior of composite armour was examined in this work using an auxetic sandwich. The Inventor Nastran program was used to simulate the effect of a projectile traveling at various speeds on composite auxetic sandwich armour. The results were compared with monolithic armour under the same boundary conditions and speeds. From the research, the following conclusions were drawn:

1. The auxetic structure outperforms the monolithic panel due to its better absorption capacity.

2. The threat level is greatly decreased by the auxetic structure, which may be used at higher speeds and is secure up to 450 m/s.

3. The auxetic method can be considered appropriate for the application if the advantages of auxetic structures satisfy the fundamental requirements of the application and the constraints are not of concern.

References

[1]. Anand P., Chandrakant R. K., Satish S. B., *Development of materials and structures for shielding applications against Blast and Ballistic impact: A Detailed Review*, Thin-Walled Structures, vol. 179, 2022.

[2]. Yongqiang L., Hualin F., Xin-Lin G., *Ballistic helmets: Recent advances in materials, protection mechanisms, performance, and head injury mitigation*, Composites Part B: Engineering, vol. 238, 2022.
[3]. Qian M., Pee D. L., *Development of spiral auxetic structures*, Composite Structures, vol. 192, p. 310-316, 2018.
[4]. Wu S., Sikdar P., Bhat G. S., *Recent progress in developing ballistic and anti-impact materials: Nanotechnology and main approaches*, Defence Technology, vol. 21, p. 33-61, 2023.
[5]. Rajendra P. B., Steven L., Tuan N., Abdallah G., Tuan N., *Anti-blast and -impact performances of auxetic structures: A review of structures, materials, methods, and fabrications*, Engineering Structures, 2023.
[6]. Zhenhua Z., Zhan Z., Xiufeng H., *Experimental study on the impact response of the polyurea-coated 3D auxetic lattice sandwich panels subjected to air explosion*, Composite Structures, vol. 323, 2023.
[7]. Xing C. T., Wei G. Z., Jiang X., Dong H., Xi H. N., Hang H., Jian H., Tong G., Yu F. W., Yi M. X., Xin R., *A stretchable sandwich panel metamaterial with auxetic rotating-square surface*, International Journal of Mechanical Sciences, vol. 251, 2023.
[8]. Feng J., Shu Y., Chang Q., Hai T. L., Alex R., Lian Z., *Blast response and multi-objective optimization of graded re-entrant circular auxetic cored sandwich panels*, Composite Structures, vol. 305, 2023.
[9]. Stefan B., Franziska H., Dirk B., Anne J., *Optimized design for modified auxetic structures based on a neural network approach*, Materials Today Communications, vol. 32, 2022.
[10]. Jianjun Z., Guoxing L., Zhong Y., *Large deformation and energy absorption of additively manufactured auxetic materials and structures: A review*, Composites Part B: Engineering, vol. 201, 2020.
[11]. Nejc N., Lovre K. O., Zoran R., Matej V., *Mechanical properties of hybrid metamaterial with auxetic chiral cellular structure and silicon filler*, Composite Structures, vol. 234, 2020.
[12]. Ying L., Zihao C., Dengbao X., Wenwang W., Daining F., *The Dynamic response of shallow sandwich arch with auxetic metallic honeycomb core under localized impulsive loading*, International Journal of Impact Engineering, vol. 137, 2020.
[13]. Qiang G., Xuan Z., Chenzhi W., Liangmo W., Zhengdong M., *Multi-objective crashworthiness optimization for an auxetic cylindrical structure under axial impact loading*, Materials & Design, vol 143, 2018.
[14]. Grujicic M., Galgalikar R., Snipes J. S., Yavari R., Ramaswami S., *Multi-physics modeling of the fabrication and dynamic performance of all-metal auxetic-hexagonal sandwich-structures*, Materials & Design, vol. 51, 2013.
[15]. Imbalzano G., Tran P., Ngo T. D., Lee V. S., *A numerical study of auxetic composite panels under blast loadings*, Composite Structures, vol. 135, 2016.
[16]. Chang Q., Feng J., Shu Y., Remennikov A., Shang C., Chen D., *Dynamic crushing response of novel re-entrant circular auxetic honeycombs: Numerical simulation and theoretical analysis*, Aerospace Science and Technology, vol. 124, 2022.
[17]. Nejc N., Biasetto L., Rebesan P., Zanini F., Carmignato S., Krstulovi-Opara L., Vesenjak M., Ren Z., *Experimental and computational evaluation of tensile properties of additively manufactured hexa- and tetrachiral auxetic cellular structures*, Additive Manufacturing, vol.45, 2021.
[18]. Ying L., Zihao C., Dengbao X., Wenwang W., Daining F., *The Dynamic response of shallow sandwich arch with auxetic metallic honeycomb core under localized impulsive loading*, International Journal of Impact Engineering, vol. 137, 2020.
[19]. Yuanlong W., Yi Y., Chunyan W., Guan Z., Aminreza K., Wanzhong Z., *On the out-of-plane ballistic performances of hexagonal, reentrant, square, triangular and circular honeycomb panels*, International Journal of Mechanical Sciences, vol. 173, 2020.
[20]. Chang Q., Remennikov A., Pei L., Yang S., Yu Z., Ngo D., *Impact and close-in blast response of auxetic honeycomb-cored sandwich panels: Experimental tests and numerical simulations*, Composite Structures, vol. 180, p. 161-178, 2017.
[21]. Jie M., Jiayi L., Mangong Z., Wei H., *Experimental and numerical study on the ballistic impact resistance of the CFRP sandwich panel with the X-frame cores*, International Journal of Mechanical Sciences, vol. 232,
[22]. Nejc N., Luka S., Matej V., Zoran R., *Blast response study of the sandwich composite panels with 3D chiral auxetic core*, Composite Structures, vol. 210, 2019.
[23]. Mehvesh I., Muhammad U., Ghulam H., Malik A. U., Wasim K., Asad H., *Development of mortar filled honeycomb sandwich panels for resistance against repeated ballistic impacts*, Journal of Materials Research and Technology, vol. 24, 2023.
[24]. Thawani V., Hazael R., Critchley R., *Numerical modelling study of a modified sandbag system for ballistic protection*, Journal of Computational Science, vol. 53, 2021.

THE ANNALS OF "DUNAREA DE JOS" UNIVERSITY OF GALATI
FASCICLE IX. METALLURGY AND MATERIALS SCIENCE
No. 4 - 2023, ISSN 2668-4748; e-ISSN 2668-4756
Article DOI: https://doi.org/10.35219/mms.2023.4.17

HYBRID NANOSTRUCTURES BASED OF Ta_2O_5-PMMA FOR ELECTRONIC APPLICATIONS

Elena Emanuela HERBEI[1]*, Claudiu-Ionuț VASILE[2,3]
[1]Interdisciplinary Research Centre in the Field of Eco-Nano Technology and Advance Materials CC-ITI,Faculty of Engineering, "Dunarea de Jos" University of Galati, 47 Domnească, 800008 Galati, Romania
[2]Clinical Medical Department, Faculty of Medicine and Pharmacy, "Dunarea de Jos" University, 800008, Galați, Romania,
[3]Department of Psychiatry, "Elisabeta Doamna" Psychiatric Hospital, 800179, Galați, Romania
e-mail: elena.herbei@ugal.ro

ABSTRACT

The scientific interest on hybrid materials is mainly related to understanding the types of interactions between inorganic and organic component and the effect of these interactions on the properties of the new material formed. Hybrid nanostructured materials and especially dielectrics are used for electronics (for gate layer) and especially those applicable in structure of different types of thin film transistors (TFTs).

In this paper is presented the research on thin film hybrid materials based on tantalum oxide (Ta_2O_5) starting with inorganic precursor - tantalum ethoxide and polymethylmethacrylate (PMMA). The chemical method sol-gel involves the precursor-tantalum ethoxide which is hydrolysed and functionalized (with special siloxane compound), and the organic methyl methacrylate monomer. The chemical reactions take place at low temperature below 160 ^oC. The sol is deposited as thin films by spin-coating to analyse intensity-voltage (I-V) and capacitance-voltage curves (C-V) to determine the electric properties. Metal-Insulator-Metal (MIM) structures were made-up for electric characterisation. The value of leakage currents was between 10^{-10} - 10^{-7} A at ± 40 V. The hybrid films were analysed by scanning electron microscopy (SEM) for thickness and morphology and for thermal stability the sol was investigated by TG and DSC.

The dielectric permittivity ranges between 3.5 and 4 at 1 MHz, depending on the tantalum alkoxide: MMA molar ratio, showing good behaviour for gate layer in future TFTs.

KEYWORDS: hybrid materials; spin-coating; tantalum oxide; PMMA

1. Introduction

The demand for new materials or materials with new properties is currently high. Hybrid materials have been developed to meet certain new performance requirements.

Inorganic-organic hybrids can be utilized in various fields of materials chemistry due to their simple processing and molecular design capabilities. One of the most used method is sol-gel. Currently, there are four major topics in the synthesis of inorganic–organic materials: (a) their molecular engineering, (b) their nanometer and micrometer-sized organization, (c) the transition from functional to multifunctional hybrids, and (d) their combination with bioactive components [1].

The purpose of these materials is to generate desirable properties and functionalities by combining both organic and inorganic components. The aim is to enhance or highlight beneficial traits while simultaneously minimizing or eliminating negative properties or effects. The process involves mixing a polymer with a metal alkoxide and then undergoing hydrolysis and condensation reactions, which are followed by gelification. The composition, processing, and physical properties of materials obtained by this method can vary significantly [2].

In order to use as a dielectric layer in TFTs and OTFT structure, the main requiremnts for materials as organic and inorganic species has to have a small

THE ANNALS OF "DUNAREA DE JOS" UNIVERSITY OF GALATI
FASCICLE IX. METALLURGY AND MATERIALS SCIENCE
No. 4 - 2023, ISSN 2668-4748; e-ISSN 2668-4756
Article DOI: https://doi.org/10.35219/mms.2023.4.17

number of charge traps, good processability, reproducibility and stability against degradation, small leakage current and high breakdown potential.

There are a lot of oxide nanoparticles that are considered promotors for dielectric properties such as SiO_2, ZrO_2, Ta_2O_5, HfO_2, etc [3-5].

The thermal and mechanical stability of PMMA, as well as its high resistivity, suitable dielectric constant, and thin film capability, make it an excellent choice [6].

Molas et al. used hafnium aluminium oxide as high k material for dielectric layer in electronic devices as non-volatile memories. They obtained very low current 10^{-7} to 10^{-14} A/cm^2 at an electric field ranges from 0 to -10 MV/cm [7]. Adjusting the zirconium alkoxide concentration in organosiloxane embedded in poly(4-vinylphenol) (PVP) determine the obtaining of dielectric layer for TFTs with higher on/off current ratio, and lower threshold voltage [8]. Based on the sol-gel reaction of SiO_2 and ZrO_2 nanoparticles in PMMA matrix were obtained thin layes for gate dielectrics. The dielectric constant values of 2.1, 3.4 and 5.4 have been obtained for PMMA, ZrO_2-PMMA and SiO_2-PMMA films, respectively [9]. Thermal silicon dioxide (SiO_2, 100 nm) was used as gate insulator [10] and ITO Sourse/Drain electrode (100 nm) was deposited using reactive sputter.

This work reports details of the preparation of hybrid materials based on tantalum ethoxide embedded in PMMA and presents also the chemical reactions that took place to obtain the sol for thin film. Here we investigated the electrical behaviour of thin films based on Ta_2O_5-PMMA.

2. Experimental

Reagents. Tantalum ethoxide, Ta(OEt)5, precursor (99.9%) was obtained from Cambridge Multivalent Ltd. (Cambridge, UK), Methylmethacrylate reagent grade 99% (MMA)-Sigma Aldrich, Ethanol 95%,were used without other processing steps.

Preparation of sols and thin films. Sols based on molecular precursors were obtained by mixing the metallic alkoxide of tantalum in an alcohol solution and the metallic oxide was generated in situ using tantalum ethoxide as a molecular precursor. For polymer was used the molecular monomer methylmethacrylate which was polymerised after the chemical reaction with the alkoxide (at a temperature and in UV light). For the production of Ta (Oet) 5-PMMA hybrid soil, tantalum ethoxide 99.99% (low Cl) was used. Hybrid films based on Ta_2O_5-PMMA were prepared in two molar ratios 1:1 and 6:1. The solutions were prepared by magnetically stirred at room temperature. First the solution was deposited on a glass substrate to have one and two layers of hybrid layers with 100-150 nm thickness. The deposition was done by spin-coating method at 2000 rpm for 30 seconds.

Thin films characterization. The thermogravimetric analysis-TGA and differential scanning calorimetry-DSC curves were registered in synthetic air (5.0 purity) at 5 K/min. heating rate, using Q 5000IR and Q20, respectively.

The prepared sols, deposited by spin-coating were investigated by scanning electron microscopy (SEM) using a JEOL JSM-7500F/FA microscope from Peabody, MA, JOEL Ltd. USA by top view and in cross section to determine the thickness of the layer.

For electrical characterization, were deposited by thermal evaporation, aluminium contacts (~100 nm in thickness) with different areas to have metal–insulator–metal (MIM). The structure of MIM was presented in an older work of author [3, 5, 9] The intensity–voltage (I-V), capacitance–voltage (C-V), were measured using an Agilent 4156 and HP 4277A Analysers, at 1 MHz, from Agilent Technologies.

3. Results and discussion

Chemical reactions. In the first step the precursor $Ta(OEt)_5$ and the siloxane agent are hydrolysed by the solvent and $Ta(OH)_5$ and $Si(OH)_2$ instable compounds are formed and immediately are condensed and form a complex compound with covalent bonds(-(Ta-O-Si)n-). The monomer reacts with the free chain from the siloxane agent and form new covalent bond as in Figure 1.

Thermal Analysis. The thermal decomposition of the as-prepared sols with different precursors ratios and corresponding aged sols, was done from room temperature-RT up to 600 ^oC, shown in Figure 2, was investigated for the optimization of the treatment of the as-deposed gel thin films. The TGA and DSC of the soil is presented for the molar concentration 1:1 and was carried out in air of purity 5.0 and with a heating speed of 5 K/min. The components were analysed in individual, binary and ternary systems to observe the points at which they modify certain properties. The data from the thermo-gravimetric analysis were analysed using the TA Analysis software and are presented in Figure 2 a(TGA) and b (DSC).

THE ANNALS OF "DUNAREA DE JOS" UNIVERSITY OF GALATI
FASCICLE IX. METALLURGY AND MATERIALS SCIENCE
No. 4 - 2023, ISSN 2668-4748; e-ISSN 2668-4756
Article DOI: https://doi.org/10.35219/mms.2023.4.17

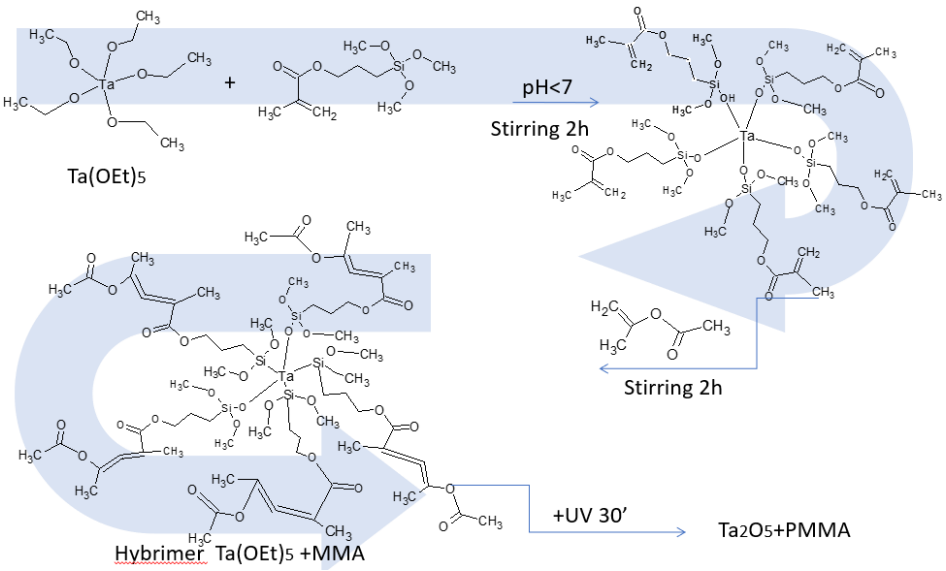

Fig. 1. *Chemical reactions by sol-gel method*

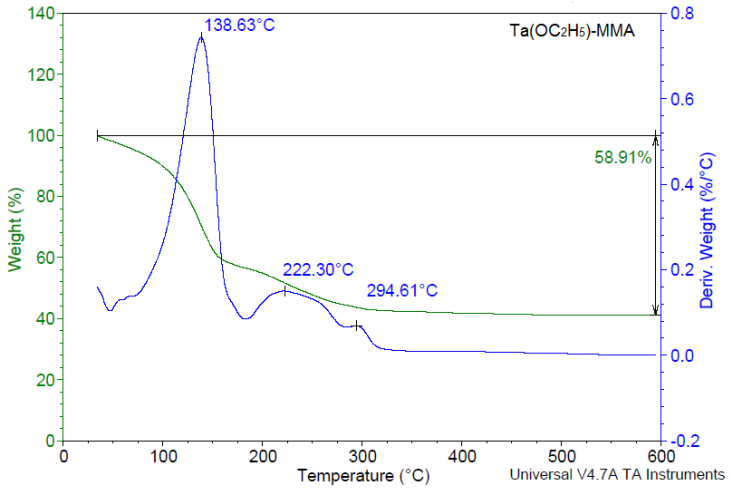

Fig. 2a. *TGA-DTG of Ta(OEt)4:PMMA*

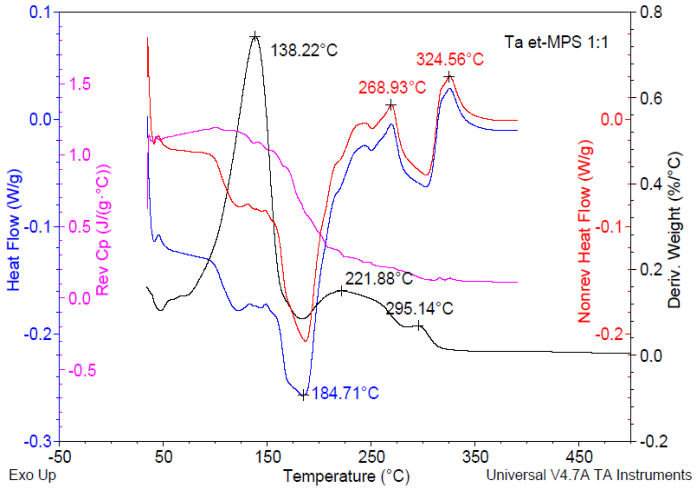

Fig. 2b. *DSC of Ta(OEt)4:PMMA*

THE ANNALS OF "DUNAREA DE JOS" UNIVERSITY OF GALATI
FASCICLE IX. METALLURGY AND MATERIALS SCIENCE
No. 4 - 2023, ISSN 2668-4748; e-ISSN 2668-4756
Article DOI: https://doi.org/10.35219/mms.2023.4.17

The tantalum ethoxide has two stages of decomposition with the maximum speed at 218 and 280 °C, the siloxane agent has the maximum decomposition speed at 143 °C, the MMA monomer shows a volatile behavior starting at room temperature up to 90 °C, while the PMMA shows the maximum decomposition at 106 °C, the decomposition ending at 125 °C. The thermal decomposition of the two-component system Ta $(OEt)_5$-MPS 1:1, shown in Figure 2a. The temperature for the tantalum ethoxide precursor is higher in the binary system than for individual systems. This leads us to the idea that in the binary system, new links were formed between the alkoxide precursor and the Si-O-Ta covalent bonding agent, bonds that are much stronger and breaking at higher temperatures.

From Figure 2b, we observe an endothermic peak at 187 °C and two exothermic peaks due to crystallization occurring between 270 and 330 °C. The temperature difference between the TG and DSC analysis is attributed to the type of crucible in which the analysis takes place. For TGA was used a crucible made of open Pt, and for the analysis DSC was used coated aluminium crucible.

SEM analysis. The SEM images (Figure 3) on both films display uniform morphology without phase separation between the organic and inorganic components. The very smooth interface between the Ta layer and the hybrid film, but the more irregular interface between the hybrid film and Al electrode can be observed, the latter reproducing the surface roughness of the hybrid polymer.

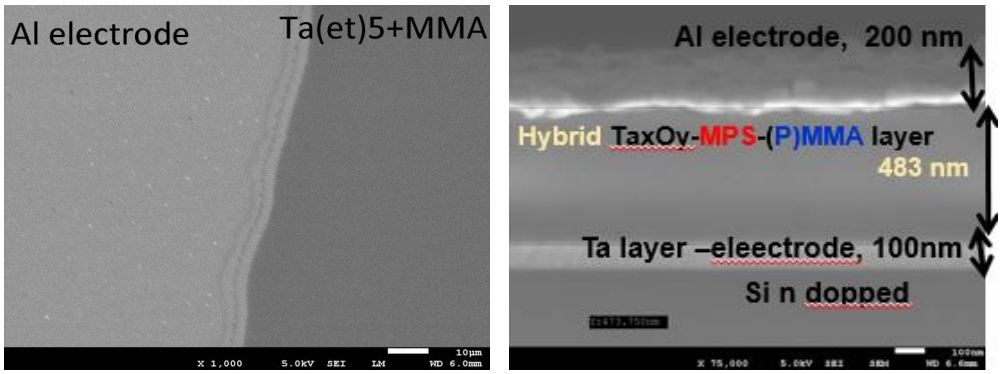

a b

Fig. 3. *Top view(a) and cross sections (b) SEM images of $Ta(OEt)_5$: PMMA 1:1 hybrid thin films*

Electrical properties of thin films. The I-V curves show leakage current densities of 10^{-10} to 10^{-7} A at electrical field strengths of 0.3 MV/cm and a constant capacitance in the bias range of ±40 V. There are some areas on the top of the sample where the electrode was breakdown, due to the pressing needle.

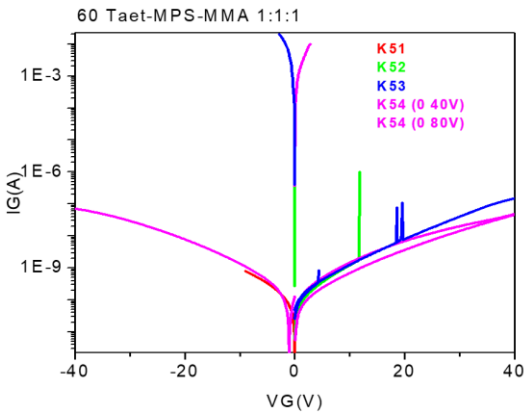

Fig. 4. *I-V characteristics for PMMA layer*

The C–V curves of the investigated films are presented in Fig. 5. The permittivity of the hybrid films were determined from C–V measurements at 1 MHz to be 3.5 for the 1:1 molar ratio of $Ta(OEt)_5$:MMA. The values were determined in the voltage range from -40 to +40 V, at 1 MHz. The dielectric permittivity of a material is proportional to its electronic polarization.

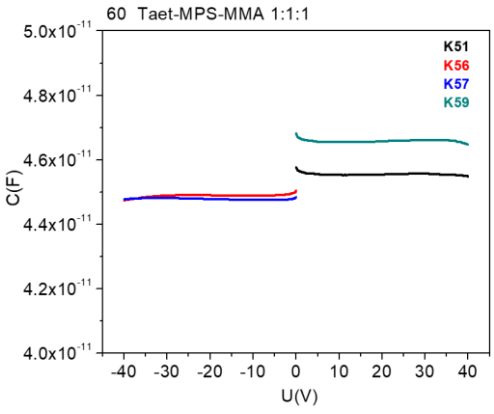

Fig. 5. *C-V characteristics for PMMA layer*

THE ANNALS OF "DUNAREA DE JOS" UNIVERSITY OF GALATI
FASCICLE IX. METALLURGY AND MATERIALS SCIENCE
No. 4 - 2023, ISSN 2668-4748; e-ISSN 2668-4756
Article DOI: https://doi.org/10.35219/mms.2023.4.17

The measurements showed a dielectric behaviour enough homogenous without breakdown leakage. The values of dielectric constant measured on different electrodes area varied from 3 to 4 as in Table 1.

Table 1. *Electrical capacitance and dielectric values of PMMA layer for different electrodes area*

Electrode area $*10^{-4}$ cm^2	Electrical capacitance C (F) $*10^{-11}$			ε_r	$\varepsilon_{r\ m}$
	Position 1	Position 2	Position 3		
2.054 (K1)	41.23	39.04	44.65	3	3.5
8.043 (K2)	2.135	2.765	1.904	3.7	
32.17 (K3)	4.312	4.657	4.281	3.3	
128.7 (K4)	0.1949	1.3435	0.3971	4	

4. Conclusions

The preparation of $Ta(OEt)_5$:PMMA hybrid dielectric thin films for transparent and flexible electronics was successfully done using sol-gel methods at 160 °C. Hybrid homogenous films that contain Ta_2O_5 and PMMA were made to function as dielectrics for MIM stacks with thickness around 400 nm. From CV electrical data, was determined the permittivity if thin layer between 3 and 4 at1MHz. The values for the leakage current are between 10^{-10} and to 10^{-7} A. The results measured lead us that we can use tantalum oxide in polymer matrix for electronic devices as thin film transistors with flexible and transparent properties.

References

[1]. Kickelbick G., *Introduction to Hybrid Materials. The Development of Hybrid Materials*, 2007.

[2]. Gomes S. R., Margaça F. M. A., Ferreira L. M., Salvado I. M. M., Falcão A. N., *Hybrid PDMS-Silica-Zirconia materials prepared by γ-irradiation*, Nucl. Instruments Methods Phys. Res. Sect. B Beam Interact. with Mater. Atoms, vol. 265, no. 1, p. 114-117, doi: 10.1016/j.nimb.2007.08.035, 2007.

[3]. Valcu E. E., Musat V., Oertel S., Jank M. P. M., Leedham T., *In situ formation of tantalum oxide-PMMA hybrid dielectric thin films for transparent electronic application*, Res. Artic. Adv. Mater. Lett, vol. 6, no. 6, p. 485-491, doi: 10.5185/amlett.2015.5785, 2015.

[4]. Muşat V., *et al.*, *Low-Temperature and UV Irradiation Effect on Transformation of Zirconia-MPS nBBs-Based Gels into Hybrid Transparent Dielectric Thin Films*, Gels, vol. 8, no. 2, doi: 10.3390/gels8020068, 2022.

[5]. Valcu E. E., Musat V., Jank M., Oertel S., *Sol-gel preparation of ZrO2-PMMA for thin films transistors*, Rev. Chim., vol. 65, no. 5, p. 574-577, 2014.

[6]. Na M., Rhee S. W., *Electronic characterization of Al/PMMA[poly(methyl methacrylate)]/p-Si and Al/CEP(cyanoethyl pullulan)/p-Si structures*, Org. Electron., vol. 7, no. 4, p. 205-212, doi: 10.1016/j.orgel.2006.02.003, 2006.

[7]. Molas G., *et al.*, *Evaluation of HfAlO high-k materials for control dielectric applications in non-volatile memories*, Microelectron. Eng., vol. 85, no. 12, p. 2393-2399, doi: 10.1016/j.mee.2008.09.008, 2008.

[8]. Lee S. H., Jeong S., Moon J., *Nanoparticle-dispersed high-k organic-inorganic hybrid dielectrics for organic thin-film transistors*, Org. Electron., vol. 10, no. 5, p. 982-989, doi: 10.1016/j.orgel.2009.05.009, 2009.

[9]. Emanuela E., Herbei V., Musat V., Oertel S., Jank M., High-k dielectric inorganic-organic hybrid thin films for field effect transistors (FETFT), p. 64-68, 2013.

[10]. Lee S. H., Jeong H. J., Han K. L., Baek G., Park J. S., *An organic-inorganic hybrid semiconductor for flexible thin film transistors using molecular layer deposition*, J. Mater. Chem. C, vol. 9, no. 12, p. 4322-4329, doi: 10.1039/d0tc05281g, 2021.

MANUSCRISELE, CĂRŢILE ŞI REVISTELE PENTRU SCHIMB, PRECUM ŞI ORICE CORESPONDENŢE SE VOR TRIMITE PE ADRESA:

MANUSCRIPTS, REVIEWS AND BOOKS FOR EXCHANGE COOPERATION, AS WELL AS ANY CORRESPONDANCE WILL BE MAILED TO:

LES MANUSCRIPTS, LES REVUES ET LES LIVRES POUR L'ECHANGE, TOUT AUSSI QUE LA CORRESPONDANCE SERONT ENVOYES A L'ADRESSE:

MANUSCKRIPTEN, ZIETSCHRITFTEN UND BUCHER FUR AUSTAUCH SOWIE DIE KORRESPONDENZ SID AN FOLGENDE ANSCHRIFT ZU SEDEN:

After the latest evaluation of the journals by the National Center for Science Policy and Scientometrics (**CENAPOSS**), in recognition of its quality and impact at national level, the journal will be included in the B^+ category, 215 code (http://cncsis.gov.ro/userfiles/file/CENAPOSS/Bplus_2011.pdf).

The journal is already indexed in:

DOAJ: https://doaj.org/

SCIPIO-RO: http://www.scipio.ro/web/182206

EBSCO: http://www.ebscohost.com/titleLists/a9h-journals.pdf

Google Academic: https://scholar.google.ro

Index Copernicus: https://journals.indexcopernicus.com

Crossref: https://search.crossref.org/

The papers published in this journal can be viewed on the website: http://www.gup.ugal.ro/ugaljournals/index.php/mms

Name and Address of Publisher:
Contact person: Prof. Dr. Eng. Elena MEREUȚĂ
Galati University Press - GUP
47 Domneasca St., 800008 - Galati, Romania
Phone: +40 336 130139
Fax: +40 236 461353
Email: gup@ugal.ro

Name and Address of Editor:
Ș. L. Dr. Eng. Marius BODOR
"Dunarea de Jos" University of Galati, Faculty of Engineering
111 Domneasca St., 800201 - Galati, Romania
Phone: +40 336 130208
Phone/Fax: +40 336 130283
Email: marius.bodor@ugal.ro

AFFILIATED WITH:

- THE ROMANIAN SOCIETY FOR METALLURGY
- THE ROMANIAN SOCIETY FOR CHEMISTRY
- THE ROMANIAN SOCIETY FOR BIOMATERIALS
- THE ROMANIAN TECHNICAL FOUNDRY SOCIETY
- THE MATERIALS INFORMATION SOCIETY (ASM INTERNATIONAL)

Edited under the care of the FACULTY OF ENGINEERING

Annual subscription (4 issues per year)

Fascicle DOI: https://doi.org/10.35219/mms

Volume DOI: https://doi.org/10.35219/mms.2023.4

Editing date: 15.12.2023
Number of issues: 200
Printed by Galati University Press (accredited by CNCSIS)
47 Domneasca Street, 800008, Galati, Romania